Shear Behaviour of Engineered Cement-based Composites

By

Qinjiang Shang

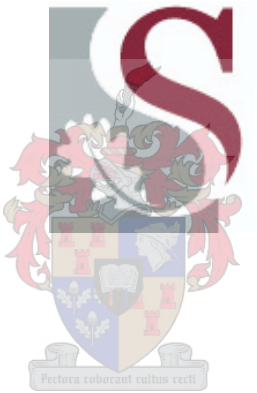

Thesis presented in partial fulfillment of the requirements for the degree Master of Engineering at the University of Stellenbosch

Study leader: Prof G.P.A.G. van Zijl

December 2006

Synopsis

Some experiments utilizing the shear capacity of Engineered Cement-based Composites (ECC) have suggested that elimination of shear reinforcement is feasible when the concrete matrix is replaced by ECC. However, actual application and more rigorous cost analysis are prevented by the fact that the shear stress and strain properties of ECC have not yet been characterized as accurately as the tensile properties. This study focuses on the investigation of the shear property of ECC.

The study starts with a survey and comparison of existing shear tests for composite materials. The Iosipescu shear test concept is chosen as the most objective method for ECC, and subsequently, modified for specific application on ECC by simple analytical design and finite element refinement.

The modified Iosipescu shear test method is applied on, four types of ECC specimens with different fibre content (0%, 1%, 2%, 2.5% by volume), which have been cast in specially designed moulds and cured in laboratory conditions. Three phases of shear measurements are used to check the shear test appropriateness and study the shear mechanical properties of ECC. The failure mode is verified in the first phase, detailed measurement of the shear strain and shear stress is performed and recorded in the second phase, and in the third phase more information about the ductility of diagonal cracking is obtained by measurement of the tensile principal deformation. By also conducting direct tensile tests on specimens of the exact same mix, information of both uniaxial tension and shear behaviour is available, from which elastic and shear moduli, as well as Poisson's ratio of ECC are computed.

A first step toward application of this knowledge of the shear behaviour of ECC is taken by studying the response of shear-dominated beams and beam-columns of reinforced concrete and reinforced concrete combined with ECC as the outer crusts. These beams were prepared and tested by other members of the research group of the Division for Structural Engineering of the University of Stellenbosch. It is shown that ECC can indeed successfully replace shear reinforcing steel, due to its shear capacity.

Sinopsis

Die gebruik van Engineered Cement-based Composites (ECC) tydens eksperimente wat die skuif weerstand van strukturele eenhede toets, dui aan dat die weglating van skuif bewapening moontlik is wanneer die beton matriks vervang word met ECC. Die praktiese toepassing en meer akkurate koste analise word verhoed deur die feit dat die skuifgedrag van ECC nog nie akkuraat genoeg gekarakteriseer is nie, soos vir die geval van die trek eienskappe. Hierdie studie fokus op die ondersoek na die skuif eienskappe van ECC.

Hierdie studie begin met die ondersoek en vergelyking van bestaande skuif toets metodes vir saamgestelde materiale. Die Iosipescu skuiftoets konsep is gekies as die mees objektiewe metode vir ECC. Hierdie metode is deurentyd verbeter vir die spesifieke toepassing van ECC deur middel van analitiese ontwerp en eindige element verfyning.

Die aangepaste Iosipescu shuiftoets metode is toegepas op vier tipes ECC monsters met verskillende veselinhoud (0%, 1%, 2%, 2.5% by volume), wat gegiet was in spesiale ontwerpte vorms en gevolg is deur nabehandeling in beheerde laboratorium omstandighede. Drie fases van skuif metings word gebruik om die skuiftoets se toepaslikheid te bepaal en sodoende die skuif meganiese eienskappe van ECC te bestudeer. Die falings mode word bepaal in die eerste fase, gedetaileerde metings van skuifspanning en –vervorming word gedoen en vasgel**e** in die tweede fase. Die derde fase behels die meet van diagonale trekdeformasie tydens die trektoets om inligting oor die duktiliteit van skuifgedrag te bekom, wat nie met rekstrokies gemeet kan word nie. Direkte trektoetse is op toetsmonsters van dieselfde meng gedoen om ook inligting van die aksiale trekgedrag te verkry. Met inligting oor beide trek- en skuifgedrag, kan die elastisiteitsmodulus en die skuifmodulus van ECC bepaal word en ’n aanduiding van die dwarskontraksie, of die verhouding van Poisson, verkry word.

Die eerste stap wat lei tot die toepassing van hierdie kennis oor die skuif gedrag van ECC, is geneem deur die gedrag te meet van balke en kolomme wat aan oorheersend skuif gedrewe toetse onderwerp is. Sodoende is ’n vergelyking getref tussen gewone staalbewapende beton elemente en elemente wat bestaan uit staalbewapende beton waarvan die buitenste kors deur ECC vervang is. Hierde balke was voorberei en getoets deur ander lede van die navorsingsgroep van die Afdeling Struktuuringenieurswese van die Departement van Siviele Ingenieurswese, Universiteit van Stellenbosch. Dit word aangedui dat ECC, op ’n suksesvolle wyse, die skuifbewapening kan vervang as gevolg van die skuifweerstandsvermoë van die materiaal.

Declaration

I, the undersigned, hereby declare that the work contained in this thesis is my own original work，

except where specifically acknowledged in the text, and that I have not previously in its entirety or in part submitted it at any university for a degree.

Signature…….

Date…….

Acknowledgement

The experience of my master's study at University of Stellenbosch in South Africa, from January of 2004 – April of 2006, was unforgettable and enriching.

I would like to thank the following people:

Prof. G.P.A.G. Van Zijl for the supervision of my study and thesis. I really appreciate that Prof. Van Zijl leaded me into this academics field and let me be the member of the ECC research group, as well as for his trust and understanding with regard to the difficulties and frustration attached to the completion of my thesis. Many ideas of this thesis sourced from the meet with Prof. Van zijl.. I appreciate all the trouble Prof. Van zijl went thought in organising the experimental programme.

Prof. J.V. Retief for his lecture and kindly help of my thesis when I meet the frustration in the experimental data treatment.

Dr. P. Maincon for his lecture and elicitations for my study. It is pleasant to discuss with Maincon since his erudition.

Mr. W. P. Boshoff for his work to design the set of the test system and kindly help when I meet the difficulties in the research project. Boshoff also lead me go through Stellenbosch make me homefelt to stay in Stellenbosch.

Mrs. Mary lotter for her many meticulous helps during my two years study in Stellenbosch.

A. Layman for his many helps in the experimental projects from serving the sand to weight most materials and preparing my experiments.

Table of Content

List of Figures

List of Tables

Chapter 1
Introduction

Concrete is one of the most important materials in the construction industry. Remaining weaknesses of concrete materials are the inherent brittleness and low tensile strength, which always cause a brittle shear failure that can be catastrophic in the concrete structure. Therefore, the traditional concrete structures are always reinforced by a number of shear reinforcement bars to avoid unsafe shear failure, but rather ensure that a safer, ductile failure mechanism, like bending, will occur. It is a continued goal for engineers to reduce or replace traditional shear reinforcement by enhancing the inherent mechanical properties of concrete structures, to avoid costly, time consuming placement of steel for shear reinforcement.

The development of modern fibre reinforced concrete and mortar (FRC) since the 1960's, gives the engineer an opportunity to accomplish this aim. The proper addition of fibres to concrete ensures that they are uniformly distributed and randomly oriented throughout the volume of concrete. Thus, reinforcement that is uniformly effective is automatically established. A significant consequence of fibre addition is a substantial improvement in the resistance to the formation and growth of cracks. In addition, a marginal improvement in tensile strength may also results in the case of moderate fibre quantities (Narayanan, and Darwish, 1987). The addition of fibres also aids in converting the brittle characteristic of normal concrete to ductility.

Many different types of fibre can be used in concrete. Steel fibre reinforced concrete (SFRC) as most popular one has been extensively studied to replace the shear reinforcement in concrete structures. There are considerable laboratory data indicating that fibres substantially increase the shear capacity of concrete and mortar (Batson et al.1972, Paul and Sinnamon, 1975, Swamy et al., 1979).

With the rapid development of FRC in the last decade, a new group of FRC, namely Engineered Cementitious Composite (ECC), a class of microstructurally tailored FRC, has been developed. This class of FRC exhibits tough, pseudo strain-hardening behaviour in tension, despite containing low volumes of fibre. These performances were brought about by developments in fibre, matrix and processing technology. The mechanical properties

of ECC have been shown to be strongly superiour to FRC (Li, 2002).

Due to the excellent mechanical properties, a number of investigations into the use of ECC in enhancing structural performance have also been conducted in recent years. These include the repair and retrofit of pavements or bridge decks (Lim and Li, 1997), the retrofit of building walls to withstand strong seismic loading (Kesner and Billington, 2001); and the design of new framing systems (Parra-Montesinos and Weight, 2000). Some tests results also indicate the ECC has superiour shear capacity, and suggest that elimination of shear reinforcement is feasible when the concrete matrix is replaced by ECC (Li and Wang, 2002).

However, actual application and more rigorous cost analysis are prevented by the fact that the shear stress and strain properties of ECC have not yet been characterized as accurately as the tensile properties. The main reason is a lack of appropriate shear test methods. Therefore, the present work is focused on development of shear test method to characterise the shear properties of ECC.

In Chapter2, the mechanisms of shear failure in concrete without and with shear reinforcement are introduced. FRC used as shear reinforcement is presented subsequently. Finally, ECC as a new type of FRC is introduced in the last section. Chapter3 discusses the status of composite material shear test methods at present. The applicability of these methods on ECC shear testing is discussed and the modified Iosipescu shear test method is chosen finally for further modification and adaptation for ECC.

Chapter 4 presents the design of the modified Iosipescu shear test method for ECC, which involves the simple analytical design of the test setup and specimen geometry and finite element analysis for further refinement. Chapter 5 describes an experimental program devised for validation of the proposed shear test method, as well as characterisation of the shear behaviour of ECC. A locally developed new ECC type containing high levels of fly ash, as well as ground granulated Corex slagment was used in the experimental work. The experimental set up and procedure are also presented.

Chapter 6 presents the experimental results of three phases. The first phase identifies the failure modes of specimens. In the second phase detailed measurements of the shear stress and strain by strain gages are reported. The third phase predicts the development of shear strain by LVDT measurement to quantify shear deformation in the post elastic regime. Uniaxial tensile results are also presented to compare with shear result.

Chapter 7 presents a simple case study of concrete partly replaced by ECC. The case involves two beams-columns consisting of RC effectively without traditional shear reinforcement, but with an ECC crust, or outer tube. The responses of these beam-columns are compared to that of two identical RC beams with traditional steel shear reinforcement. The study subsequently uses different methods to calculate the structural shear resistance of RC as well as ECC, based on the shear properties of the pure ECC characterised in chapter 6. This is done to introduce a design and prediction methodology for the use of ECC structurally, in this case for shear replacement. A simple relationship of decomposed shear resistance, including shear contributions by the concrete, flexural steel and the ECC is presented.

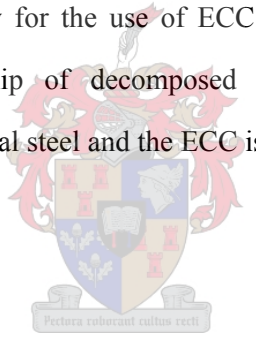

Chapter 2
Background study

2.1 Introduction

Concrete as a structural material has been developed over centuries. Excellent structural behaviour and mature production technologies have made that concrete is established as the most popular structural material. However, the low tensile strain capacity causes a brittle shear failure that can be catastrophic in the structures.

Therefore, shear reinforcement is always used to improve the shear capacity of concrete structures. With the development of fibre reinforced concrete (FRC), it is found that the shear reinforcement in the structures can be reduced and may even be eliminated by using the fibre reinforced concrete.

In this chapter, the mechanisms of shear failure in concrete without and with shear reinforcement are introduced in the first and second section. Fibre reinforced concrete used as shear reinforcement is presented subsequently. Engineered Cementitious Composite (ECC) as a new kind of fibre reinforced cementitious composite is introduced in the last section.

2.2 Shear failure in members without shear reinforcement

2.2.1 Failure mode

Shear distress and failures have been reported in beams, columns, walls, slabs, and other members. Shear failure involves cracking or crushing of concrete under complex states of stress, for example in the form of diagonal cracking, shear-compression failure, splitting, or web crushing. Several shear failure theories for concrete members have been developed. In the 1960's the Canadian researcher Kani defined a shear failure as a failure where a diagonal tension crack caused failure of a structural element, calling it a diagonal tension failure (Kani, 1966). This theory was accepted extensively in the engineering field.

The diagonal tension theory can be indicated as in figure 2.1, which shows half of a symmetrical reinforced concrete beam acted on by a shear force V. an element in the beam

would be subjected to shear stresses v, see in figure 2.1(b). The bending stresses are comparatively small and can be neglected if the element is near the neutral axis or within a flexurally cracked region. The pure shear stress situation, figure 2.1(b), is equivalent to the principal stress situation shown in figure 2.1(c), in which the principal tensile stress is traditionally called the diagonal tension stress. If the diagonal tension stress reaches the tensile strength of the concrete, a diagonal crack will form.

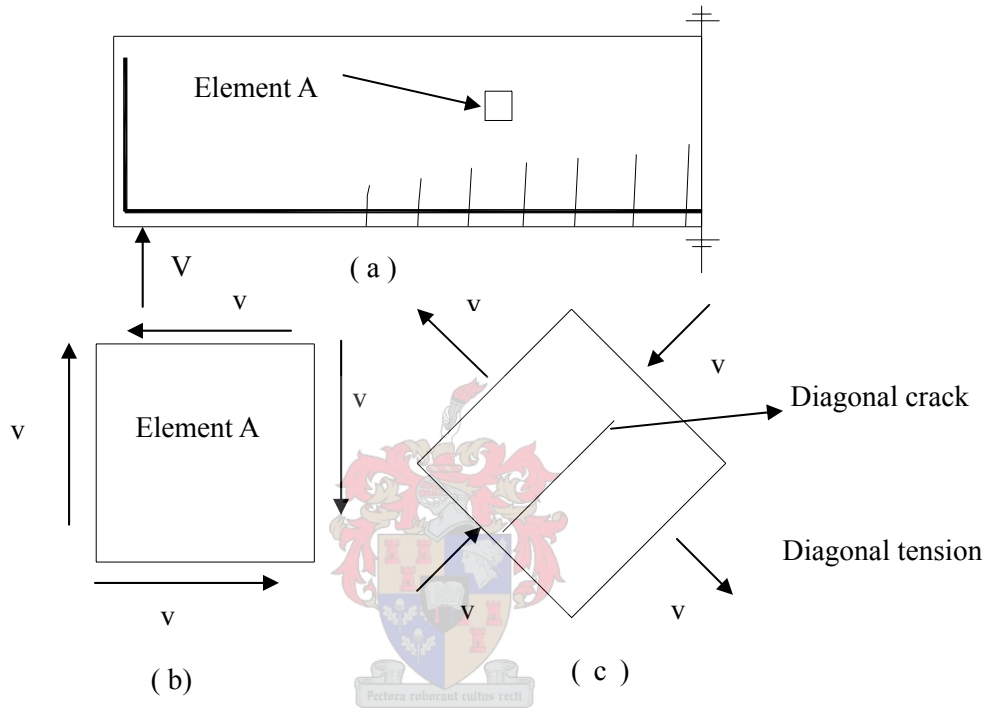

Figure 2.1 Illustration of concepts of shear diagonal tension

2.2.2 Shear resistance of concrete members without shear reinforcement

In general, the mechanism of the shear is transmitted from one plane to another within the members is similar. The main types of shear transfer have been well known for quit some time and have been reported in the ASCE-ACI Task Committee 426 (1973). These are

a) Shear stress in uncracked concrete

b) Interface shear transfer

c) Dowel action

d) Arch reinforcement

e) Shear reinforcement

The shear resistance of concrete members without shear reinforcement can be studied in a RC (reinforced concrete) beam at the location of a diagonal crack, as show in figure 2.2. V_{cz} is the shear force carried by the uncracked concrete in the flexural compression zone, V_d is a dowel force that develops where the longitudinal tension reinforcement crosses the diagonal tension cracks and V_{ay} is the vertical component of the frictional force that develops along the crack interface.

The total shear resistance is comprised of the sum of these components:

$$V_R = V_{ay} + V_{cz} + V_d \tag{2.1}$$

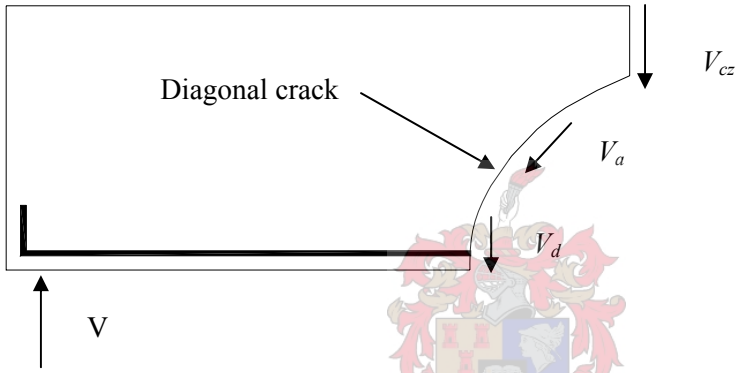

Figure 2.2 Mechanisms of shear transfer in RC members without shear reinforcement

(Kong and Evans 1987)

a) Shear transfer by concrete shear stress

The simplest method of shear transfer is by shearing stresses. This occurs in uncracked members or in the uncracked portions of structural members. The interaction of shear stresses with tensile and compressive stresses produces principal stresses which cause inclined cracking failure of the concrete.

b) Interface shear transfer

A diagonal tensile crack forms when the principal tensile stress in the concrete members exceeds the tensile capacity of the concrete. Shear force is transferred along the crack by interface shear transfer. Aggregate particles protruding from the diagonal tension crack provides "aggregate interlock", the vertical component of which contributes to shear resistance. In high strength concrete and in concretes made with light weight aggregates the

diagonal tension crack breaks through the aggregate, and shear transfer is then due to a frictional force instead of aggregate interlock, hence the term " interface shear transfer" is preferred in shear literature. However aggregate interlock has a higher shearing capacity than crack friction. The capacity of these two mechanisms depends on the width of the crack, crack slip, aggregate size and the stresses applied to the crack. Interface shear transfer is the controlling shear mechanism in reinforced members containing no shear reinforcement.

c) Dowel action

If longitudinal reinforcing bars cross a crack, shearing displacements along the crack will be resisted by a dowelling force in the bars. The dowel force gives rise to stresses in the surrounding concrete and these in combination with wedging action of the bar deformations produce splitting cracks along the reinforcement. This in turn decreases the stiffness of the concrete around the bar and therefore the dowel force. Following splitting, the dowelling force is a function of the stiffness of the concrete directly under the bars and the distance from the point where the dowelling shear is applied and the first stirrups supporting the dowel.

d) Arch action

In relatively deep beams with short spans, the load is transmitted to the supports by arch action. This is not a shear mechanism in the sense that it does not transmit a force to a nearby parallel plane. However, arch action does permit the transfer of a vertical concentrated force to a reaction in a deep member and thereby reduces the contribution of the other types of shear transfer. For arch action to develop, a horizontal reaction component is required at the base of the arch. In beams this is usually provided by the tie action of the longitudinal bars and failure may occur due to loss of the anchorage of these bars.

The ASCE-ACI Task committee 426 reports list some values on the relative importance of the shear resistance mechanisms in concrete, obtained from experiments on rectangular members without shear reinforcement, near failure load. Percentages of the total shear resistance are as follows:

20%-40% concrete shear stress

15%-20% dowel action

25%-50% interface shear transfer

According to the study by Taylor (1974), when the external shear force is increased beyond the initiation of shear cracks, i.e. the concrete shear stress is exceeded; the dowel action is the first to reach its capacity. Then shear is transferred to aggregate interlock. The aggregate interlock mechanism is the next to reach its capacity. Subsequently, a large shear force transfers to the concrete compression zone rapidly, which is why the shear failure of structural members is abrupt and explosive. The failures of the concrete members without shear reinforcement always indicate a brittle behaviour with a low shear capacity. There is msotly little warning before failure occurs, and this makes shear failures particularly dangerous.

2.3 Shear failure in members with shear reinforcement

To prevent catastrophic failure, conventional design procedure has been developed to provide vertical or inclined stirrup reinforcements to arrest diagonal cracks and substantially increase the shear capacity of the structural members. The mechanism of shear resistance of reinforced concrete can be presented by a reinforced concrete beam as shown in figure 2.3.

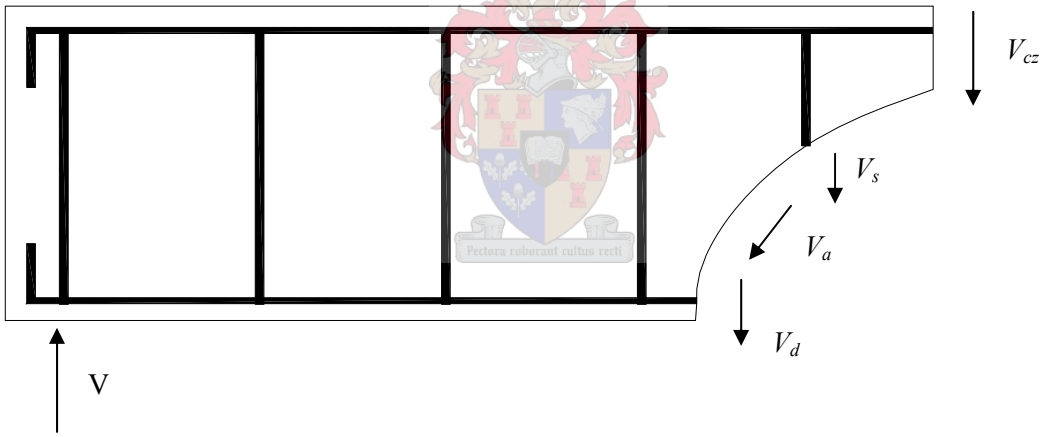

Figure 2.3 Mechanisms of shear transfer in RC members with shear reinforcement

(Kong and Evans 1987)

Before the concrete cracks, the external shear force V produces no stress in the web reinforcement. When the diagonal crack forms, the web bar intercepts the diagonal crack and carries a proportion of shear force V. The mechanism of shear transfer is shown in figure 2.3, V_S represents the shear force carried by the web bars crossed by the diagonal crack. Thus

$$V = V_{cz} + V_a + V_d + V_S \tag{2.2}$$

$$Vc = V_{cz} + V_a + V_d \tag{2.3}$$

$$V = V_c + V_s \tag{2.4}$$

Conventionally V_c is referred to as the shear carried by the concrete and V_s as the shear carried by the (web) steel. As the diagonal crack widens, the aggregate interlock becomes less effective and V_a reduces. The influence of V_{cz} and V_d increase because the shear reinforcement prevents the development the cracks. The mechanism of shear resistance in the beam can be understood originally by the so-called truss analogy (TA).

2.3.1 The introduction of the truss model (TA)

The truss model was first used to explain the flow of shear forces in a cracked reinforced concrete beam by Ritter in 1899. The truss analogy can be illustrated as in figure 2.4, in which the web bars are assumed to form the tension members of an imaginary truss, while the thrusts in the concrete constitute the compression members. The shear reinforcement and the concrete are shown inclined at the general angles α and β, respectively, to the beam axis. A line A-A parallel to the concrete 'strut' is used to derive design equations.

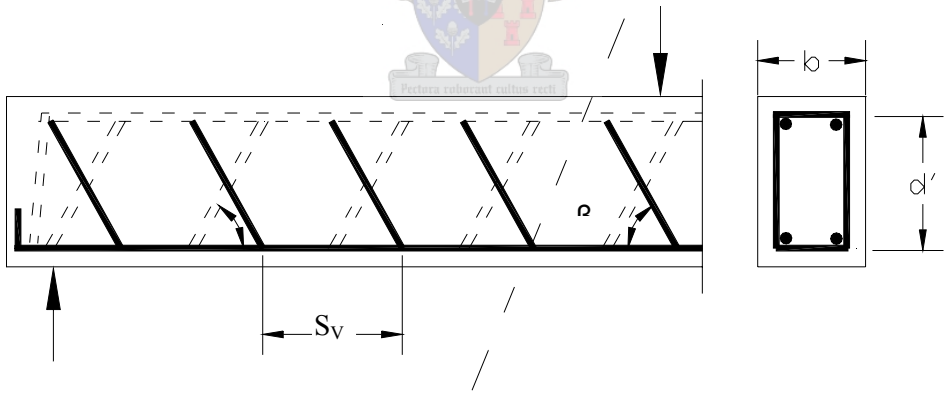

Figure 2.4 Truss analogy (Kong and Evans, 2001)

Consider the vertical equilibrium of the free body to the left of the line A-A. The web steel resistance V_s, which is contributed by the vertical components of the tension in the individual links that are crossed by A-A , is expressed as follows:

$$V_s = A_{sv} \cdot f_{vy} \cdot \sin\alpha \left[\frac{d'(\cot\alpha + \cot\beta)}{S_v} \right]$$

$$= A_{sv} \cdot f_{vy} \cdot [\cos\alpha + \sin\alpha \cot\beta] \cdot \left[\frac{d'}{S_v} \right] \quad (2.5)$$

where A_{sv} is the area of both legs of each link and f_{vy} is the characteristic yield stress of the links. For traditional stirrups, $\alpha = 90^0$. It is always assumed that after cracking the diagonal compression stress would remain at 45^0, therefore, $\beta = 45^0$, so that

$$V_s = A_{sv} \cdot f_{yv} \cdot \frac{d'}{S_v} \quad (2.6)$$

It can be seen that only the shear resistance from shear reinforcement is computed. The total shear resistance from beams is

$$V = V_C + V_S \quad (2.7)$$

However, the calculation of shear resistance of concrete (V_c) is complicated. In order to account for the contribution of the shear resistance of the concrete (V_c), different national codes give different experiential formula. For example, the British Code (BS 8110) and the South African Code (SANS10100-1) give tables for the design concrete shear stress (V_c). This value depends on the concrete strength, but also on the amount of flexural (longitudinal) steel reinforcement, which enhances the concrete shear resistance by dowel action.

2.3.2 The introduction of the modified compression field theory (MCFT)

To improve the traditional truss model, a new theory termed modified compression field theory (MCFT) was derived by Collins and Mitchell at the University of Toronto (1987). MCFT considers the variable angle of the compression strut inclination and tensile stress in the concrete, which can predict the shear resistance of concrete more accurate.

The MCFT assumes that the reinforcement is anchored to the concrete, this means that there is no slip between the reinforcement and the surrounding concrete. A compatibility condition

can be obtained by the Mohr's strain circle as:

$$\tan^2\theta = \frac{\varepsilon_x - \varepsilon_2}{\varepsilon_t - \varepsilon_2} \tag{2.8}$$

Where ε_x = longitudinal strain at mid-depth of web, (tension positive)

ε_t = transverse strain, (tension positive)

ε_2 = principal compressive strain, (negative)

If strains in three directions are known, then the strain in any other direction can be found from the Mohr's circle of strains. For cracked concrete these compatibility relationships are expressed in terms of the "average" strains. This is, strain measured over base lengths long enough to average out the local effects of the cracks. Also from the strain transformation as visualised by Mohr, the principle tensile strain can be expressed as:

$$\varepsilon_1 = \varepsilon_x + \varepsilon_t - \varepsilon_2 \tag{2.9}$$

The MCFT also accounts for the contribution of the tensile stresses in the concrete between the cracks. The tensile stresses in the diagonally cracked concrete vary in magnitude from zero at the crack locations to peak values between the cracks (see figure 2.5). The equilibrium conditions for the modified compression field theory are introduced using the symmetrical cross section subjected to pure shear shown in figure 2.5. The shear on this section is resisted by the diagonal compressive stresses, f_2, together with the diagonal tensile stresses, f_1. By stress transformation, for instance as by Mohr's stress circle, the relationship between the principal compressive stress (f_2) and principal tensile stress (f_1) can be expressed as :

$$f_2 = (\tan\theta + \cot\theta)\cdot v - f_1 \tag{2.10}$$

where the shear stress is given by

$$v = \frac{V}{b \cdot d'} \tag{2.11}$$

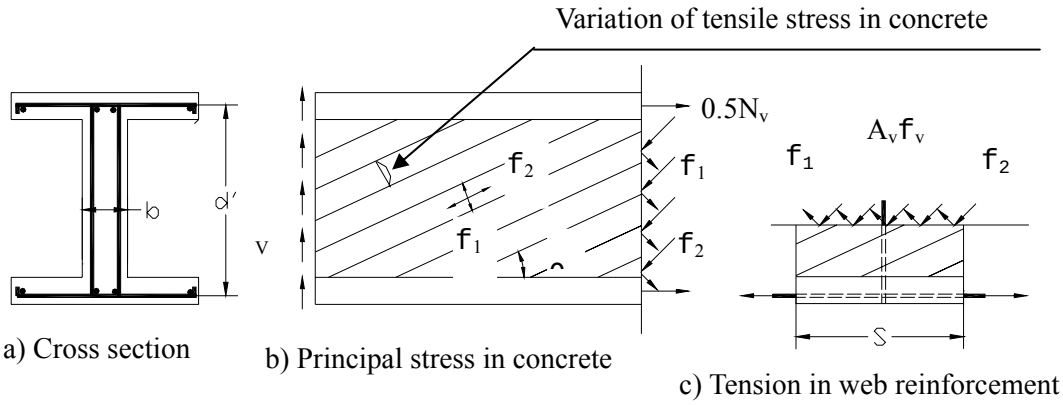

Figure 2.5 Equilibrium conditions of MCFT
(Collins and Mitchell, 1991)

By considering vertical force equilibrium of the section shown in Figure 2.5(c), the following expression is found:

$$A_v f_v = (f_2 \cdot \sin^2\theta - f_1 \cdot \cos^2\theta) \cdot b \cdot s \tag{2.12}$$

where f_v is the average stress in the stirrups. Substituting for f_2 from equation (2.10) gives:

$$V = f_1 \cdot b \cdot d' \cot\theta + \frac{A_v \cdot f_v}{s} \cdot d' \cdot \cot\theta \tag{2.13}$$

Equation (2.13) expresses the shear resistance of a member as the sum of a concrete contribution, which depends on tensile stresses in the concrete, and the steel contribution, which depends on tensile stresses in the stirrups. That is, it has the same form as the traditional "$V_c + V_s$" approach.

If the axial load (N_v) on the member is zero, the unbalanced longitudinal component of the diagonal concrete stresses must be equilibrated by tensile stresses in the longitudinal reinforcement, this longitudinal equilibrium requirement can be expressed as

$$A_{sx} \cdot f_{sx} = (f_2 \cdot \cos^2\theta - f_1 \cdot \sin^2\theta) \cdot b \cdot d' \tag{2.14}$$

where f_{sx} is the average stress in the longitudinal reinforcing bars. Substituting for f_2 from equation (2.10) gives:

$$A_{sx} = V \cdot \cot\theta - f_1 \cdot b \cdot d' \tag{2.15}$$

Based on the tests of reinforced concrete panels in pure shear, Vecchio and Collins (1986) recommended the average tensile stress vs. average tensile strain relationship:

If $\varepsilon_1 \le \varepsilon_{cr}$ then $f_1 = E_c \cdot \varepsilon_1$ (2.16)

$\varepsilon_1 > \varepsilon_{cr}$ then $f_1 = \dfrac{\alpha_1 \cdot \alpha_2 \cdot f_{cr}}{1 + \sqrt{500 \cdot \varepsilon_1}}$ (2.17)

Where α_1 and α_2 are factors accounting for the bond characteristics of the reinforcement and type of load (Collins and Mitchell, 1991), and ε_{cr} is the cracking strain of concrete.

In the treatment above, the average stresses and average strains are considered and not local variations. The stresses that occur at a crack location are different from the calculated average value (see figure 2.6).

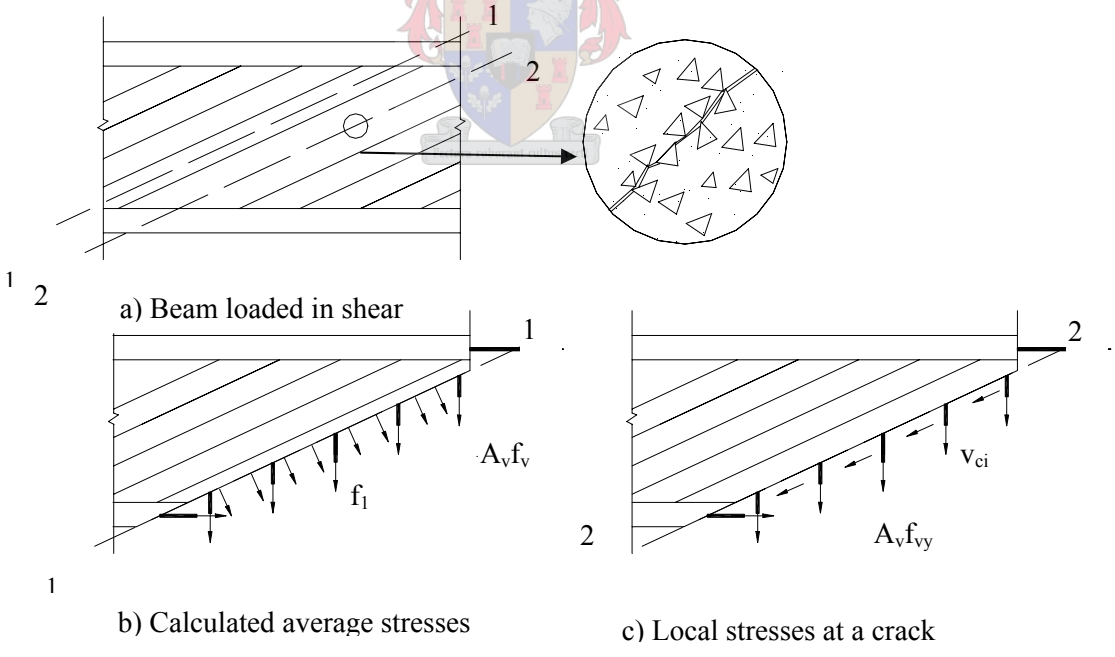

Figure 2.6 Transmitting forces at cracks
(Redrawn from Collins and Mitchell, 1991)

The ability of the crack interface to transmit these shear stresses depends on the crack width, w, the maximum aggregate size, a, and the concrete strength f_c. It is suggested that the

limiting value of v_{ci} be taken as :

$$v_{ci} = \frac{0.18 \cdot \sqrt{f_c}}{0.3 + \frac{24 \cdot w}{a + 16}} \tag{2.18}$$

The two sets of stresses shown in figure (2.6 b, c) must be statically equivalent, expressed as follows:

$$A_v \cdot f_v \cdot (\frac{d'}{s \cdot \tan\theta}) + f_1 \cdot \frac{b \cdot d'}{\sin\theta} = A_v \cdot f_{yv} \cdot (\frac{d'}{s \cdot \tan\theta}) + v_{ci} \cdot b \cdot d' \tag{2.19}$$

and to maintain this equality, f_1 must be limited to

$$f_1 = v_{ci} \cdot \tan\theta + \frac{A_V}{s \cdot b} \cdot (f_{vy} - f_v) \tag{2.20}$$

Yielding of the longitudinal reinforcement at a crack may also limit the magnitude of concrete tension that can be transmitted. The requirement that the two sets of stresses in figure (2.6) produce the same horizontal force will be satisfied if

$$A_{sx} \cdot f_y \geq A_{sx} \cdot f_{sx} + f_1 \cdot b \cdot d' + \left[f_1 - \frac{A_V}{b \cdot s} \cdot (f_{vy} - f_{v)} \right] \cdot b \cdot d' \cdot \cot^2\theta \tag{2.21}$$

All of the relationships needed to predict the response of a beam load in shear have been discussed above. For detailed discussion of an algorithm to use these equations to compute the shear resistance of RC beams, refer to Collins and Mitchell (1991). The method is complicated, and the nonlinearities require an iterative approach. It is further complicated in cases where both shear and axial load exist, and even more when bending moment acts in addition. The detailed discussion falls outside the scope of this thesis. However, the theory has been implemented in a program RESPONSE (Bentz, 2001) by the research group of Prof. Collins at Toronto. This program is employed in the computation of the RC beam and beam-column resistances for comparison with the experimentally measured values of van Dyk (2004) and Avenant (2005) in chapter 7.

By introducing the TA and the MCFT, it can be seen that sufficient shear reinforcement is

usually provided to increase the shear capacity to ensure that the failure of a RC structure is due to yielding of the longitudinal steel, which provides adequate warning of imminent collapse. Even if the shear reinforcement is insufficient in the concrete structure, the development of diagonal cracks is slower and the amount of diagonal cracks are much more than in concrete without shear reinforcement.

The above discussion suggests that the shear performance of concrete can be enhanced by adding shear reinforcement. However, some disadvantages are:

1) Due to the relative wider cracks in the concrete structure at these high shear loads, the reinforcement is exposed and may corrode so that the durability of structures is reduced.

2) The weak plane can occur under multiaxial loading conductions in concrete structure due to the reinforcement that is always arranged in a specified plane, especially in earthquake and wind loading conditions.

3) Conventional stirrups require relatively high labour input to bend and fix in place.

Therefore, it would be beneficial to design structures subjected to high shear loads using material, which has enhanced inherent strength, strain, and fracture energy. Unfortunately, plain and conventionally reinforced concrete cannot meet any of these criteria. High strength concrete can reach higher tensile and compression strength, but their strain capacity and fracture energy remains low.

2.4 Steel fibre reinforced concrete (SFRC) as shear reinforcement

The development of modern fibre-reinforced concrete gives the engineer a new way to improve the structural performance of normal concrete since the early 1900s. Fibres of various shapes and sizes produced from steel, plastic, glass, and natural materials are used in concrete. However, for most structural and non-structural purposes, steel fibre is the most commonly used of all fibres.

Steel fibre reinforced concrete (SFRC) is made of hydraulic cements, fine or fine and coarse aggregate, along with discontinuous discrete steel fibres. The mechanical properties of SFRC are influenced by the type of fibre; length- to- diameter ratio (aspect ratio); the amount of fibre; the strength of the matrix; the size, shape, and method of mixture of the specimen.

SFRC mixtures that can be mixed and placed with normal equipment and procedures use

from 0.5 to 1.5 volume percent fibres. However, higher percentages of fibres (from 2 to 10 volume percent) have been used with special fibre addition techniques and placement procedures (Lankard 1984).

Fibres influence the mechanical properties of concrete in all failure modes (Gopalaratnam and Shah 1987), especially those that induce fatigue and tensile stress. The strengthening mechanism of fibres involves transfer of stress from the matrix to the fibre by interfacial shear, or by interlock between the fibre and matrix if the fibre surface is deformed. The fibre thus shares stress and matrix in tension until the matrix cracks, and then the total stress is progressively transferred to the fibres.

The fibre efficiency and fibre content (percentage of fibre by volume) are the most important factors governing the properties of steel fibre reinforced concrete. Fibre efficiency is controlled by the resistance of the fibre to pullout, which depends on the bond strength at the fibre-matrix interface. For fibres with uniform section, pullout resistance increases with an increase in fibre length; the longer the fibre the greater its effect in improving the properties of the composite.

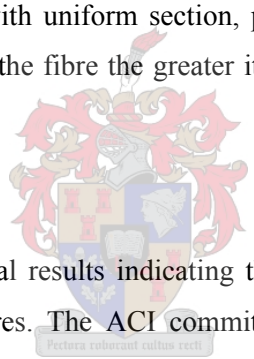

There are a number of experimental results indicating that fibres substantially increase the shear capacity of concrete structures. The ACI committee 544 (1998) report lists several potential advantages when steel fibres is used to supplement or replace vertical stirrups. These advantages are

1) The fibres are randomly distributed through the volume of the concrete at much closer spacing than can be obtained with reinforcing bars.

2) The first-crack tensile strength and the ultimate tensile strength are increased by the fibre pullout function.

3) The shear –friction strength is increased.

These advantages are also verified by several experiments in which the shear reinforcements are supplemented or replaced (Batson et al.1972), using 100 x 150 x 2000 mm beams, conducted a series of tests to determine the effectiveness of straight steel fibres as shear reinforcement in beams with conventional flexural reinforcement. In tests of 96 beams, the fibre size, type and volume content were varied, along with the shear span to depth ratio a/d, where a = shear span (distance between concentration load and face of support) and d = the

depth to centroid of reinforcing bars. Third –point loading was used throughout the test program.

It was found that, for a shear span to depth ratio of 4.8, the nonfibre beams failed in shear and developed a shear stress at failure of 1.91 MPa. For V_f = 0.88%, the average shearing stress at failure was 2.14 MPa with a moment-shear failure; for V_f= 1.76%, 2.28 MPa with a moment failure; and for V_f = 2.66%, 2.43 MPa, also with a moment failure. The latter value represents an increase of 27% over the nonfibre beams. Paul and Sinnamon (1975) studied the effect of straight steel fibres on the shear capacity of concrete in a series of seven tests similar to those of Batson et al (1972).

The influence of steel fibre reinforcement on the shear strength of reinforced concrete flat plates was investigated by Swamy et al. (1979) in a test series on four slabs with various fibre contents (V_f= 0, 0.6, 0.9, and 1.2 %). The slabs were 1830 x 1830 x 125mm with load applied through a square column stub (150 x150 x 250 mm). All slabs had identical tension and compression reinforcement, and the steel fibres had crimped ends and were 0.5 x 50 mm long. The shear strength increases were 22%, 35%, and 42% for the V_f= 0.6%, 0.9%, and 1.2% by volume fibre contents, respectively.

From these cases, it can be found that the shear capacity of SFRC can reach or exceed the normal shear reinforced concrete capacity. However, due to the lack of a shear testing method, the real shear behaviour of SFRC cannot be determined to enable the accurate calculation of shear resistance of SFRC. Some disadvantages also exist in the practical application of the SFRC, especially with large amount of fibres (Li, 2002), for example, the special processing techniques requirements, high cost and high weight.

2.5 ECC as shear reinforcement

Before describing the shear characteristics of ECC and the potential shear reinforcing it offer for RC elements, the classification of modern FRC of which ECC is a class, some terminology and the micromechanics of these materials are discussed first.

2.5.1 The classification of fibre reinforced cementitious composites (FRCC)

With the rapid development of composites material technology in the last decade, many types of fibre reinforced cementitious composites (FRCC) have been developed. There are various systems of classification of FRCC. For example, based on the performance in dealing with

crack localization, FRCC is divided into two categories by Shah. These are: conventional cast materials and High Performance Fibre Reinforced Cementitious Composites (HPFRCC). The former is a kind of material with a low fibre volume, less than V_f = 2%, and improved post-crack ductility. HPFRCC is produced by specialized techniques based on analysis and characterized by elasticity, strain hardening, and post-peak softening (Shah et al., 2004).

FRCC is classified into three groups by Li (2002). FRCC employing low fibre volume fractions (V_f<1%) utilize the fibre for reducing shrinkage cracking. FRC with moderate fibre volume fractions (between 1% and 2%) exhibit improved mechanical properties including modulus of rupture (MOR), fracture toughness, and impact resistance. The fibres in this class of FRC could be used as secondary reinforcement in structural members, such as in partial replacement of shear steel stirrups, or for crack width control in structures. A third class of FRCs, generally labelled as high performance FRC, or simply HPFRCC, has been introduced. HPFRCC exhibits apparent strain- hardening behaviour by employing high fibre contents. These HPFRCs include SIFCON (slurry infiltrated 5% -20% of steel fibres (JCI-DFRCC Committee, 2003)), SIMCO (slurry infiltrated 6% steel fibre), and CRC matrix (using 5%-10% finer steel fibres). The tensile strain capacity of HPFRCC is typical about 1.55% or less.

Recently, a new type of fibre reinforced cementitious composite, known as Engineered Cementitious Composite (ECC) has been developed. ECC exhibits tensile strain-hardening behaviour with strain capacity in the range of 3-7%, yet the fibre content is typically 2% by volume. The ultra-high ductility is achieved by optimising the microstructure of the mechanical interaction between the fibre, matrix and interface. These models provide guidance to tailoring of these three phases synergistically so that high composite performance can be achieved with only a moderate amount of fibres. ECC may be regarded as an optimised HPFRCC. The difference between ECC, FRC and common HPFRCC are summarized in table 2.1.

As a kind of new material, ECC materials are characterized by various properties for various application purposes. So there are actually various definitions of ECC property requirements

and mix design, such as fibre content less than 2% or 3%(JCI-DFRCC Committee, 2003), with ductility ranging from 3% to 6%.

For processibility and economic reasons, a particular PVA-ECC has be developed in the concrete laboratory of structural Engineering Division, Stellenbosch University. (Gao & Van Zijl, 2004). Some specific ECC materials are also defined, including FA-ECC, Slag-ECC and FA & Slag-ECC, which are series ECC mixes with a large fraction by mass of Fly Ash (FA), Ground Granulated Corex Slag (GGCS), and the combination of FA and GGCS as cement replacements respectively.

Table 2.1 Comparisons between FRC, HPFRCC and ECC (Li, 2002)

	FRC	Common HPFRC	ECC
Composite Design Methodology	NA	Use high V_f	Micromechanics based, minimized V_f for cost and processibility
Fibre	Any type V_f usually< 2%; d_f (steel) about 500um	Mostly steel, V_f usually > 5%; d_f About 150um	Tailored, polymer fibre most suitable; V_f usually < 2%; d_f < 50um
Matrix	Coarse aggregates used	Fine aggregates used	Controlled for matrix toughness and initial flaw size; fine sand used
Interface	Not controlled	Not controlled	G and τ controlled
Tensile behaviour	Strain softening	Strain hardening	Strain hardening
Tensile strain capacity	0.1%	<1.5%	>3%; 8% demonstrated
Crack width	Unlimited	Typically several hundred um, unlimited for ε >1.5%	Typically <100um during strain-hardening
Processing	Self-compaction demonstrated; Extrudability demonstrated	Self-compaction impossible due to high V_f often requiring high frequency vibration Extrudability demonstrated	Self-compaction demonstrated; Extrudability demonstrated

2.5.2 Characteristics of ECC

ECC exhibits some unique characteristics, which need some specific terminology to define it. The specific terminology are described as following:

Strain hardening/pseudo strain hardening and strain softening: strain hardening/ pseudo strain hardening describes a phenomenon where under uniaxial tension, transmitted tensile stress increases successively even after first cracking, with continued tensile straining. However, because the strain-hardening property of ECC is different from metallic materials, pseudo strain hardening may also be used instead. If the transmitted tensile stress reduces after first crack, it is described as strain softening.

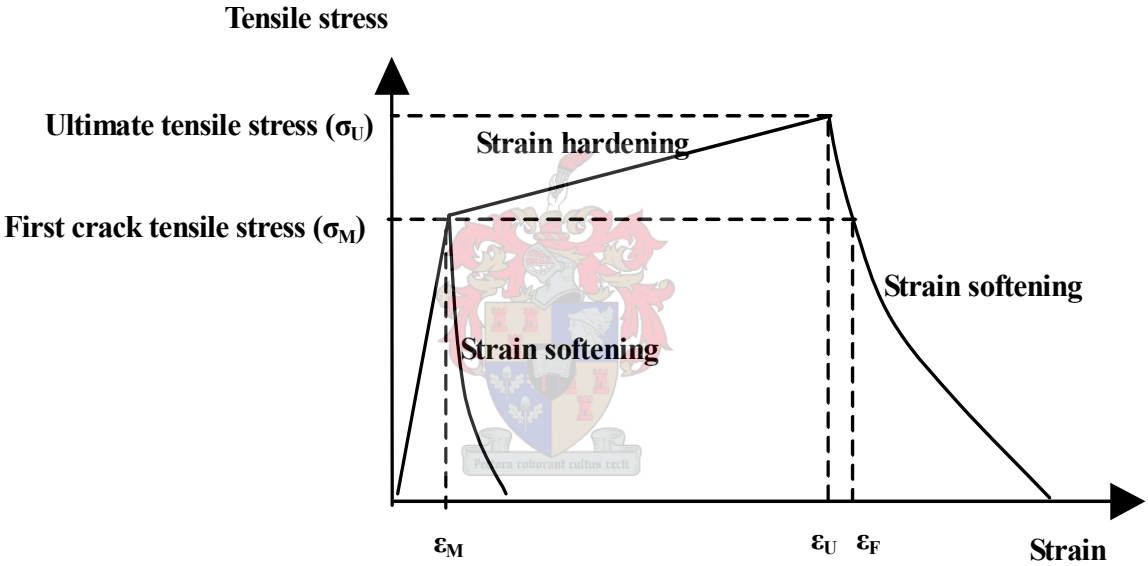

Figure 2.7 Definition of first cracking stress σ_M & strain ε_M, ultimate stress σ_U & strain ε_U, strain softening, and strain hardening

Multiple cracks: Cracks are consecutively formed after first cracking under direct tension , and ultimately become evenly and closely spaced in parallel. Deformation is often expressed in terms of strain instead of crack opening displacement. Multiple cracking results in the improvement in composite properties such as "ductility, toughness, fracture energy, strain hardening, strain capacity, and deformation capacity under either tension, compression, or bending" (JCI-DFRCC Committee, 2003). Multiple cracking in direct tension is also used to distinguish HPFRCC and normal DFRCC. Normal DFRCC does not show multiple cracking in direct tension but in bending tests.

First cracking strength: First cracking strength σ_M is the stress stage where the first crack is formed under direct tension, and first cracking strain ε_M is the corresponding strain.

Ultimate tensile strength and strain: Ultimate tensile strength σ_U is the maximum stress achievable under direct tension after first crack, and the ultimate tensile strain (ε_u) is the corresponding strain. The ultimate tensile strain ε_U is a direct measurement of material ductility. The tensile strain capacity ε_F is defined as the tensile strain when the corresponding tensile stress reaches the first crack stress again in the strain softening stage.

Tension toughness, compression toughness, and flexure toughness: Toughness portrays energy absorption of the composite, which is given by the area below the stress-strain curve or load displacement curve either in tension, compression, or flexure. In practice, toughness is calculated based on the area up to a prescribed strain or displacement.

Fibre bridging function: this is a composite property, which describe that the load is transmitted by fibre across a crack. When a crack occurs, bridging fibre carry load previously carried by the matrix in the crack zone and the matrix at the end of the crack becomes stress free, which means composite stress is transmitted through matrix and/or fibres. The bridging function is a basic parameter that governs ECC strain hardening/softening behaviour in tension, compression, or flexure.

Critical fibre volume fraction: this is the minimum fibre content with which strain hardening is achieved for a particular matrix. Critical fibre volume fraction is associated with fibre, matrix, and interfacial properties. Under the critical fibre volume fraction, composites cannot form multiple cracking and strain hardening in direct tension.

Snubbing factor: this is a parameter to describe the fibre snubbing pitch. Snubbing is a phenomenon of enhancing the bond properties when a fibre is embedded in matrix with an angle other than 90^0 to the crack.

This is normally given by equation:

$$g = \frac{2}{4 + f^2}\left(1 + e^{\pi f/2}\right), \tag{2.22}$$

where f is the snubbing coefficient (Li & Maalej,1996), which has to be established experimentally for a specific mix. The snubbing factor increases with the interfacial bond and fibre aspect ratio.

2.5.3 Micromechanism theory of ECC

The micromechanics of the strain–hardening for cementitious composites reinforced with randomly oriented short fibres have been extensively studied. The distinguishing phenomena of the composite performance of ECC are the high tensile ductility and strain hardening. The requirement to attain strain hardening is multiple-cracks and steady state cracking. Kanda and Li (1998) suggested two important complementary requirements, which are:

ι) Cracking stress criterion

The first crack stress criterion requires that the tensile stress at first crack must exceed the strength of matrix, but must not exceed the maximum bridging stress available from fibre bridging of a matrix crack. If this criterion is not satisfied, either the first crack cannot occur or immediate stress drop will accompany the first crack with bridging fibres being pulled out or ruptured. This first crack will continue to open with no new cracks created, which is the common behaviour of brittle or quasi-brittle fibre reinforced brittle matrix composites.

ii) Steady state cracking criterion.

Steady state cracking is the cracks opening keep a constant tempo and most fibres in the crack zone remain unbroken as the crack propagates under a constant, steady state stress. This means that tensile stress can be transferred to another weak zone, resulting in the multiple cracking (Li, 2003). These two criteria are both necessary for multiple cracking. If either of these criteria is not satisfied, no multiple cracking can exist, and the material fails with a

single crack.

In ECC, matrix cracks open with fibre bridging across the crack edges. During the cracking, the tensile stress increases when the fibre and matrix interface debond (fibre adhesive failure type) or crushing of the transition zone with fibres stretching (the fibre cohesive failure type). The maximum fibre bridging stress σ_0 is the stress at the peak in Figure 2.8, where a single fibre pull-out response is shown. Maximum fibre bridging stress σ_0 is equal to ultimate direct tensile stress σu in tensile stress-strain curve if two criteria are met. Because the ultimate tensile stress occurs at the stage when the matrix is divided into several segments by parallel cracks, all tensile loads are carried by bridging fibres at the ultimate crack zone. Thus, fibre in this zone will be supported by ultimate frictional force.

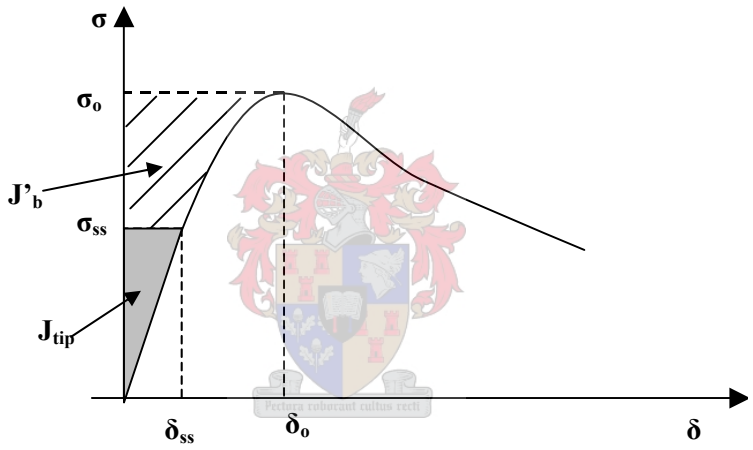

Figure 2.8 The single fibre pull-out bridging stress-displacement curve of ECC

The first requirement for multiple-cracking, namely the first crack limit, can be expressed as the first matrix crack stress $\sigma_{fc} < \sigma_o$. Note the difference between matrix first crack stress σ_{fc} and matrix crack stress σ_M. The latter typically (σ_M) is the apparent first crack stress obtained from experiments, which is higher than σ_{fc} because first cracking can not clearly be distinguished.

With the matrix cracking, to the amount of applied load, the crack edges crush flatly to a state of cracking stress and then the steady cracking occurs. The second requirement for multiple cracking formation is steady state cracking. Marshall and Cox (1988) provide an inference of steady state stress σ_{ss} from the equation (2.23) to (2.28).

$$J_{tip} = \sigma_{ss}\delta_{ss} - \int_0^{\delta_{ss}} \sigma(\delta)d\delta \tag{2.23}$$

where σ_{ss} = matrix steady state cracking stress, δ_{ss} = strain corresponding to σ_{ss} and J_{tip} is the composite crack tip toughness.

Certainly, σ_{ss} is less than σ_o. Then the composite crack tip toughness should also be smaller than the complementary bridging energy J'_b (figure 2.8), which also can be named complementary energy and can be defined with the following equation (2.24):

$$J_b^{'} = \sigma_0\delta_0 - \int_0^{\delta_0} \sigma(\delta)d\delta \tag{2.24}$$

Equation (2.24) interprets the external energy supply that is dissipated by the deformation during the inelastic processes of fibre deformation/rupture and interface debond and slippage of the bridging fibres across the crack (Li, 2002). The relationship of J_{tip} and J'_b is illustrated in Figure 2.5. The second requirement can be described with the following equation (2.25)

$$J_{tip} < J_b^{'} \tag{2.25}$$

It is clear that the method to achieve steady state cracking, and thus multiple cracking is to keep a sufficient margin between complementary energy J'_b and crack tip toughness J_{tip}. This can be achieved by reducing the crack tip toughness J_{tip} or increasing the complementary energy J'_b. J_{tip} can be approximated as the matrix toughness when the fibre bulk is less than 3% (Li, 1997 and 2002). That is

$$J_{tip} = K_m/E_m \tag{2.26}$$

K_m is the fracture toughness and E_m the elastic modulus of the matrix. So the equation (2.23) can also be expressed as equation (2.27), which indeed is based on energy balance.

$$\frac{K_m^2}{E_m} \le \sigma_0\delta_0 - \int_0^{\delta_0} \sigma(\delta)d\delta \tag{2.27}$$

It can be see from equation (2.27) that successful design of ECC requires the tailoring of fibre,

matrix, and interface properties. The fibre and interface properties control the shape of $\sigma(\delta)$ curve and therefore the dominant factor governing J_b'. ECC design for strain- hardening requires the tailoring of the fibre/matrix interface to maximize the value of J_b'. Similarly the matrix composition must be designed so that the value of $J_{tip} = K_m/E_m$ is not excessive. The shape of the $\sigma(\delta)$ curve and especially the rising branch associated with J_b' shown in figure 2.8 is related to a number of fibre/matrix interaction mechanisms. In the simplest case when fibres and matrix are in frictional contact only, the slope of the rising branch of the $\sigma(\delta)$ curve is mainly governed by the fibre content V_f, diameter d_f, length L_f and stiffness E_f, and the interface friction bond τ. Furthermore, the relationship between the composite performance in terms of the ultimate tensile stress (σ_u) and these factors has been modelled as follows (Soroushian & Lee, 1990):

$$\sigma_u = 0.405\, V_f\, g\, \tau \frac{L_f}{d_f} \tag{2.28}$$

In equation (2.28), it is assumed that the snubbing factor is equal for the same fibre in the various matrices used in present research, produced by normal casting and vibration. The interface friction bond τ is solely responsible for variations in the composite ultimate bridging strength σ_u, found through direct tensile testing of the various specimens. However, the interface friction bond τ is only the ultimate frictional bond but not the only parameter to describe the fibre/matrix interfacial properties. The present study only involved one kind of fibre with various fibres content.

2.5.4 Application of the shear behaviour of ECC

A number of investigations into the use of ECC for improving structural performance have been conducted in recent years. These include the repair and retrofit of pavements or bridge decks (Lim and Li, 1997); the retrofit of building walls to withstand strong seismic loading (Kesner and Billington, 2001); and the design of new framing systems (Parra-Montesinos and Weight, 2000). Some unique characteristics of ECC are often revealed in a structural context.

These include high damage tolerance, resistance to shear load, energy absorption, delamination and spall resistance, and high deformability and tight crack width control for durability. Within these unique structural behaviours, the excellent shear capacity is most attractive and studied extensively.

Mostly, the purpose of application of ECC in shear resistance is the reduction or elimination of conventional shear reinforcement in structural members. Under shear, ECC develops multiple cracking with cracks normal to the principal tensile direction. Because the tensile behaviour of ECC is ductile, the shear response is correspondingly ductile. As a result, the conventional steel shear reinforcement of R/ECC elements can be decreased or eliminated in some cases. For example, test result by Fischer and Li (2002) indicate that flexural members subjected to cyclic loading confirm that the load carrying capacity and the energy absorption of steel bar reinforced ECC (R/ECC) without shear stirrups exceed those of a standard R/C with stirrups. An experiment utilizing the shear capacity of ECC material to reduce or even eliminate the shear reinforcement indicated that ECC beams without shear reinforcement demonstrate superior performance to high strength concrete (HSC) beams with closely spaced steel stirrups, and suggest that elimination of shear reinforcement is feasible when the concrete matrix is replaced by ECC (Li and Wang, 2002).

The cost of ECC is higher than that of normal concrete due to the use of fibres and higher cement content. This motivated a recent study of the combined use of ECC and RC to reduce overall cost of standard RC element (van Dyk, 2004, Avenant, 2005). Two beams-columns consisting of RC with an ECC crust were tested in the concrete laboratory of structural Engineering Division, Stellenbosch University. The result of these two group indicated that the shear capacity of RC with a thin ECC crust without shear reinforcement is similar to that of the RC alone, but with standard steel stirrup shear reinforcement. To predict the shear capacity of ECC in these two cases, the more detail discussion will be perform in chapter 7.

2.6 Conclusion

In the introduction to this chapter the shear mechanics capacities of normal RC, SFRC, and

ECC have been presented. It is possible to replace the conventional shear reinforcement by using SFRC and ECC. Due to its unique structural behaviour and low fibre content, ECC exhibits more promising application in structures than SFRC. However, due to the lack of shear testing, the excellent shear behaviour of ECC only can be exhibits in the structural application. The excellent shear behaviour of ECC cannot yet be exploited in design and construction. Therefore, this research project sets out to study and test the shear behaviour of ECC and attempt to formulate design equations for the structural use of ECC, with particular focus on shear resistance.

Chapter 3
The status of composite material shear test methods

3.1 Introduction

The properties of ECC in tension and flexure have been studied extensively by uniaxial tensile tests and three-point or four point flexure tests. However, it is still a problem to accurately describe the true shear behaviour of ECC due to a lack of an accurate test method. The determination of shear properties has been regarded as one of the more difficult tasks in composite materials.

Many experimental and analytical efforts have been conducted in the development of shear test methods for determination of shear stress and strain of composite materials. One of the principal difficulties in the development of a test method for the measurement of shear properties is the provision of a pure shear stress state in the specimen. Two ideal conditions for accurate determination the shear property of composite materials were defined by W.R.Broughton (Hodgkinson, 2000).

1) For quantitative shear measurements, the shear test method should provide a region of pure and uniform shear stress in the test section of the specimen throughout the linear and non-linear response regimes.

2) A unique relationship should exist between the applied load and the magnitude of the shear in the test section.

In addition, the test should be reproducible, require no special test equipment, and provide the entire stress-strain response to failure from a single specimen. Although many and varied test methods have been developed for use with composite material over the years, none completely satisfies all of these criteria. Thus, there remains considerable confusion as to which shear test method to use.

Although the development of shear test is a complex and difficult task in composite materials, there are many shear test methods have been reported in the literature. These include short beam shear test (ASTM Standard D-2344), torsion of a thin-walled tube (Wall, 1971), plate twist (Whitney, 1968), off-axis tensile shear test (Richards, 1969), Ohno shear beam (Arakawa, and Ohno, 1957), shear panel (Collins, 1986), and Iosipescu shear beam test (Iosipescu 1967).

Within these shear test methods, the short beam shear test is the most popular and simplest method as used in the past. Torsion of a thin-walled tube is a method of directly applying shear stress to specimen, but special test equipment and complex specimen configuration make it difficult to conduct. Off-axial tensile shear test method is commonly employed for shear characterization of laminate and only suitable for continuous aligned fibre materials. Ohno shear beam method and shear panel method were originally developed for reinforced concrete, and were used for testing HPFRC later. Iosipescu shear beam test originally developed for characterizing the shear properties of metals was subsequently adapted for use with fibre-reinforced plastic composites.

For investigating the shear behaviour of ECC, a more accurate shear test will be selected in this chapter. Torsion of a thin-walled tube should not be used due to complex specimen configuration and special test equipment. The Off-axial tensile shear test method is not suitable obviously due to short and randomly distribution of fibres in ECC. So, short beam shear test, Ohno shear beam test, shear panel method, and Iossipescu shear beam test will be discussed in detail in this chapter.

3.2 Short beam shear test

The short beam method is one of the simplest tests and is used widely for measuring the fabric-reinforced composites, which was defined by ASTM Standard D-2344. The test consists of a short beam specimen of rectangular cross-section loaded in three-point bending so that a shear failure occurs. Two cylindrical rollers support the specimen, and the load is applied through a central roller located at the specimen mid-length, the configuration as shown in figure 3.1.

According to classical beam theory, the shear stress distribution in short beams loaded in three-point flexure is distributed parabolically through the specimen thickness. The stress is a maximum at the mid-plane and zero at the upper and lower surfaces. The maximum transverse shear is:

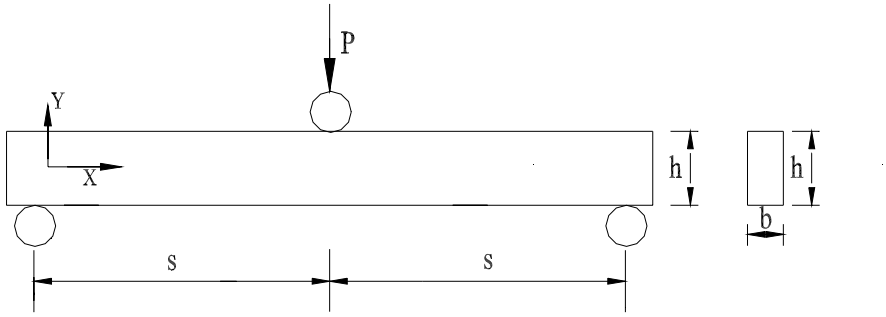

Figure 3.1 Short beam shear test method

$$\tau^{\max} = \frac{V \cdot Q}{I_Z \cdot b} = \frac{3 \cdot P}{4 \cdot A} \qquad (2.1)$$

V: transverse shear force

Q: area moment

I_z: moment of inertia

b: beam width

P: applied force

A: cross-section area of the beam (i.e., A=b*h)

It can be found from Equation (1) that the shear stress is independent of span length. On the other hand, bending moment is directly proportional to span length. Thus, a short support span minimizes bending stress, allowing the transverse shear stresses to dominate. Therefore, for small s/h ratios, classical beam theory becomes valid. However, finite element analysis has shown that the shear stress distribution is severely skewed near the load and support

points and varies along the beam length. The maximum shear stress is in fact positioned between the mid-plane and the upper surface, close to the loading zone, and is larger than predicted by classical beam theory. Figure3.2 shows the difference of result between the elastic solution and classical beam theory by Whitney (1985).

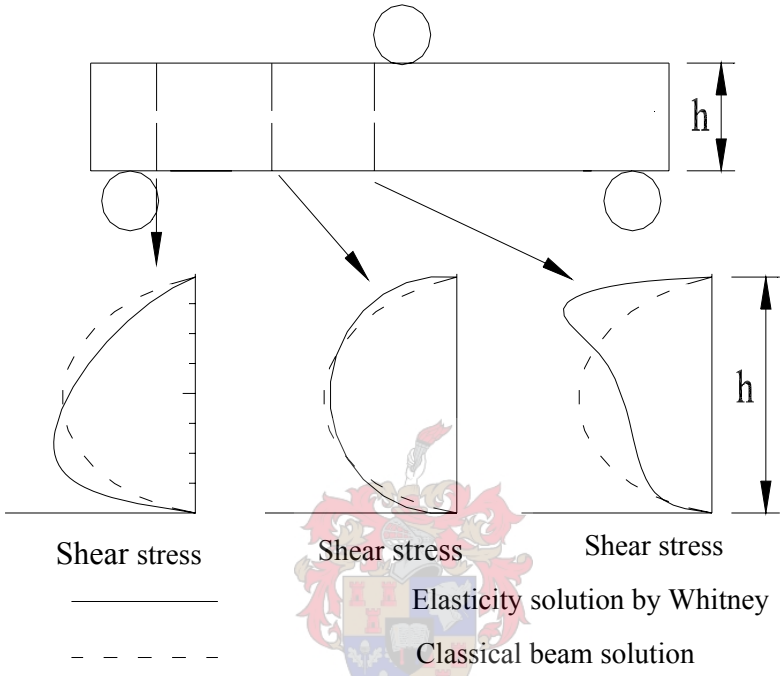

Figure 3.2 Shear stress distributions at three locations (Whitney, 1985)

This deviation from classical beam theory is due to the classical beam theory assumption that the bending stresses vary linearly and the shear stresses vary parabolically through the specimen thickness.

Therefore, The short beam method appears to be inadequate in describing the uniform stress state in the specimens. It can also found that the failure patterns of a normal three-point bending beam is not under pure shear state in despite of a short support span minimize bending stress. To a short span beam, the failure frequently results from a combination of high shear and compression present in the upper portion of beams, near the concentrated central load. The surface under the central loading zone is subjected to compression, and the composite may undergo localized buckling.

It is obvious that the shear strain corresponding to the shear stress is difficult to measure by short beam shear test. Most of the short beams shear tests use the relationship between the shear stress and middle line deflection to describe the shear characterize of material simply under a defined s/h ratio.

In conclusion, the short beam test cannot give results, which are acceptable as the absolute material shear strength due to non-uniform shear stress distribution and the presence of normal flexural stress. However, the simplicity of the test, combined with economic costs, has ensured its popular use for quality control and as a materials screening tool. In the FRC field, this method is always used to compare the shear behaviour within different kinds of materials. During the test, the shear strength and mid-span displacement can be obtained under a fixed s/h ratio. The failure modes of specimens from different kind of materials are also observed.

3.3 Ohno shear beam test

The Ohno shear beam test method was originally developed to test reinforced concrete beams by Ohno of Japan (Arakawa, and Ohno, 1957). The method was extensively used to assess the shear behaviour of R/HPFRCC (Li et al., 1994, Kanda et al., 1998, Fukuyama et al., 1999, Shimizu et al., 2003). The Ohno shear beam concept is shown in figure 3.3.a. Two cylindrical rollers support the specimen; a vertical load is translated to two loads to apply on the specimen top by a load beam. The stiffness of the load beam should be much more than that of the specimen.

The mechanism of Ohno shear beam is shown in figure3.3 b-d. As can be observed from the accompanying shear force and bending moment diagrams (figure 3.3 c, d), a state of pure shear exists at the center of the beam where the bending moment is zero. The existence of this pure shear state gives the engineer a chance to study the shear property of materials more accurately.

It will be also noted that the bending moment varies along the beam with the maximum and minimum values at the two inner loading points. Thus, the failure patterns of beam specimens

become uncertain; shear failure, flexural failure or combined shear and flexural may also occur. For solve this problem, some new versions Ohno shear beam test have been addressed to estimate the shear behaviour of HPFRCC.

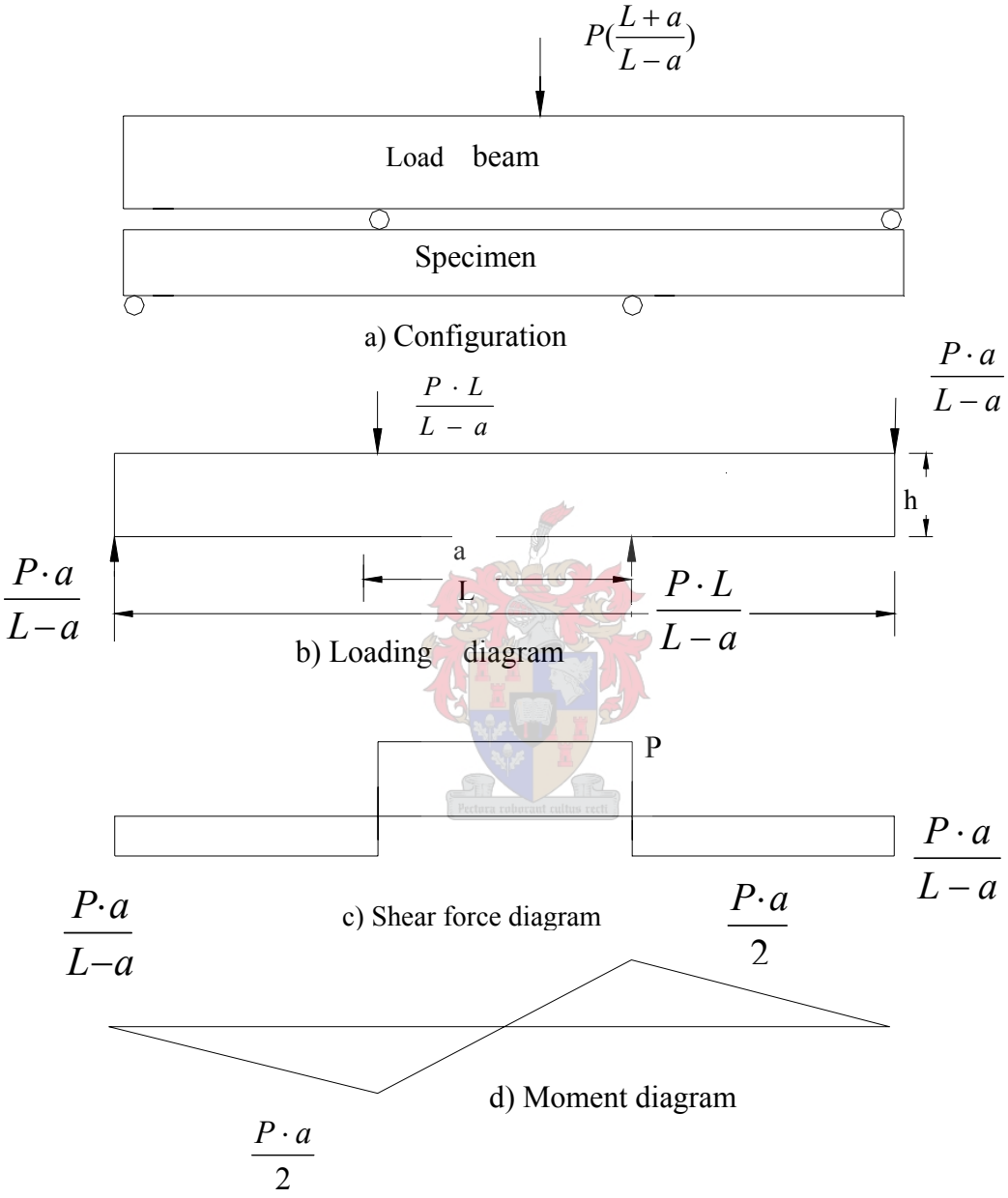

Figure 3.3 a) configuration b) loading diagram c) shear force diagram d) moment diagram

In 1994, an Ohno shear test was conducted to compare the shear property of Engineered Cementitious Composites (ECC) with different strength and ductility

(DRECC, an ECC mix with 7% by volume of Dramix steel fibres; SPECC, an ECC mix with 2% by volume of Spectra fibres) and three control specimens: ordinary concrete without shear reinforcement (PC), ordinary concrete reinforced by wire mesh (RC), and quasi-brittle steel fibre reinforced concrete (FRC) (Li et al., 1994).

The flexural steel has been designed to prevent flexural failure in the shear panel and ensure a shear mode of failure; the specimen configuration and the flexural reinforcement layout is shown schematically in figure 3.4. The amount and position of the flexural reinforcement bars were calculated by considering clear cover requirement, adequate bar development length and maximum flexural stress at failure of the beam. The tips of the bars were tapered to reduce stress concentration.

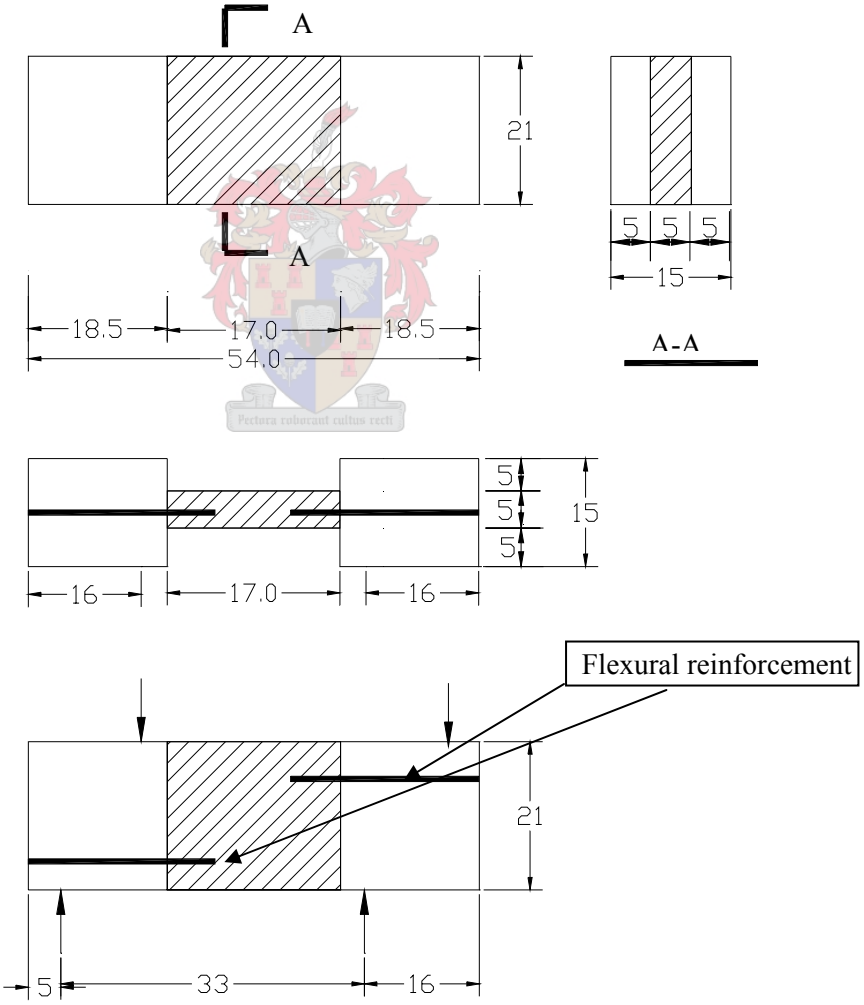

Figure 3.4 Ohno shear beam geometry, dimension (All dimensions are in centimetres) (Li et al., 1994)

The average shear strength in the Ohno shear beams was estimated as the shear force at the beam center line at failure divided by the cross-sectional area resisting the shear force. An auxiliary surface bonded strain gage rosette and infrared system were used to determine deformation in the region of pure shear near the center of the specimen. A reasonable result was obtained from this, which the shear strength and strain capacity of ECC materials were shown to be higher than ordinary concrete and fibre reinforced concrete materials. It is also noted that after the first crack, ECC allowed continued straining with increase in load capacity, whereas FRC and the PC exhibited rapid load drop. After first crack the RC system also showed macroscopically comparatively good strength and ductility by the wire mesh, but a single opening large crack occurred suddenly in the plastically deformation range.

This test can be regarded as the first one to evaluate the shear behaviour of ECC in more detail under a pure shear state. However, some disadvantages were also found later.

1) The shear distribution along the section is still parabolical so that the average shear strength was inaccurate as shear strength of materials.
2) It is considered as tensile stress concentration at the end of the bars caused initiation of cracks near the beam top and bottom surface. These cracks propagated diagonally into the mid-section at the peak load (Kabele, 2005).

Therefore, the test used the Ohno shear test method and later added some experimental parameters; shear-span to depth ratio, longitudinal and transversal reinforcement ratios (Kanda et al., 1998, Fukumy et al., 1999). The failure mode usually also was reported in the experimental studies which can be shear-tension or shear-compression. Therefore, a theoretical pure shear failure cannot be implemented in the Ohno shear beam test, so it cannot objectively determine the shear behaviour.

3.4 Pure shear panel test

This test method was first developed by Collins (1986) to measure the relationship between the principal strength and the principal strain at the University of Toronto. A simplified testing machine was used to study the shear behaviour of fibre reinforced concrete later, which is

modified from the Collins machine (Nobuhiro et al., 2005). This method is shown in figure 3.5. These machines apply several loading jacks in two directions to transfer a vertical load to pure shear force directly on the specimens as show in the figure 3.6.

The pure shear strength can be obtained by a simple calculation, whereas the result is not accurate. The reason is the transfer of axial load through a complex mechanism, which will disperse some force. It is obvious that the shear stress distribution in the specimen is not uniform. The shear stress at each surface has a maximum value and decreases along the diagonal, and minimum values occur at the centre. The measurement of strain in this test is more difficult, so the displacements in the center along the two resultant direction of pure shear force are used to evaluate behaviour before and after crack occurrence.

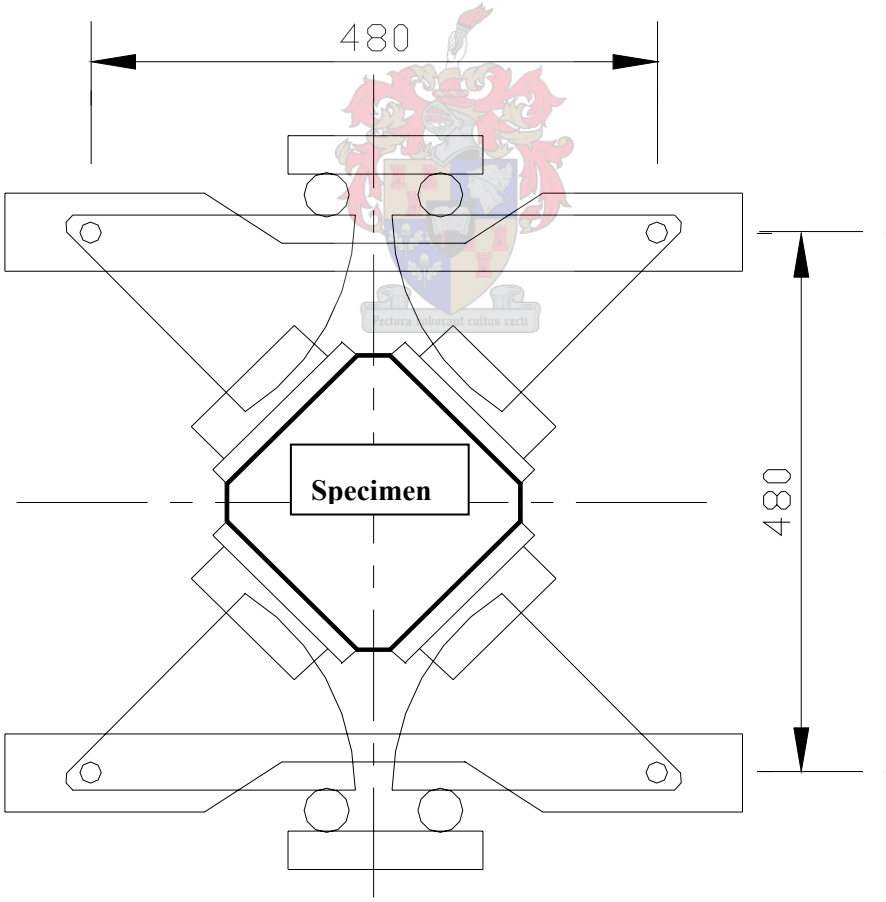

Figure 3.5 Simplified pure shearing machine
(Nobuhiro et al., 2005)

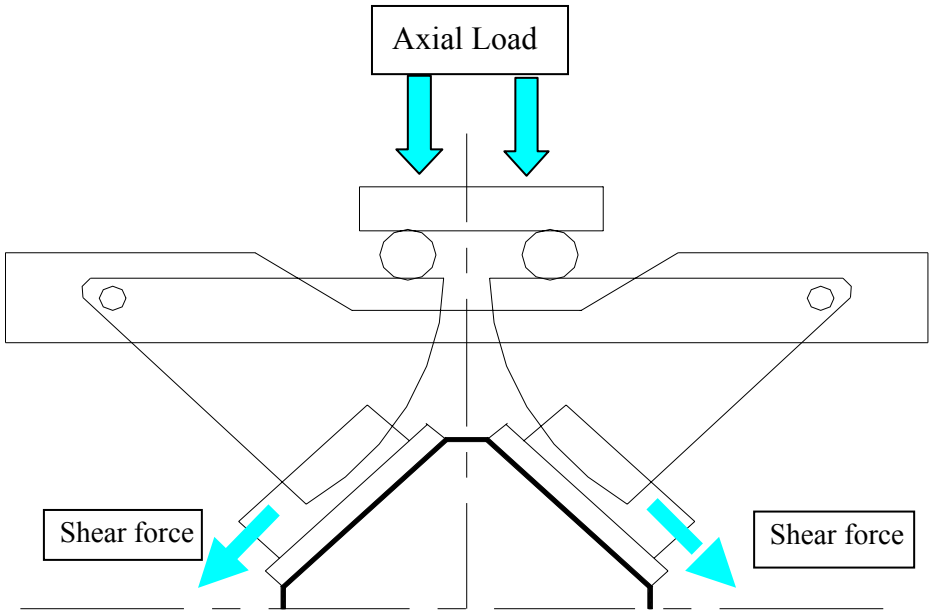

Figure 3.6 Transfer of axial load
(Nobuhiro et al., 2005)

With this test method only shear forces act on the test specimen, thus ensuring that pure shear failure takes place. Therefore, failure modes and strength of test specimens were used to describe the shear behaviour of materials. A test applying the pure shear panel test method was used to indicate the different shear modes of plain concrete, FRC, and lightweight aggregate concrete (Nobuhiro et al., 2005).

3.5 Iosipescu (V-notched) shear beam test method

This test method was originally developed for characterizing the shear properties of metals by Nicolai Iosipescu of Bucharest, Romania in the early 1960's. His only English-language publication was in 1967 (Iosipescu, 1967). The method was later extensively adapted for use with fibre-reinforced plastic composites. It has been adopted as ASTM Standard D-5379 in 1993 for this material.

The mechanism of the Iosipescu shear beam test method is similar to the Ohno shear beam method (see figure 2.3). The two methods have the same loading arrangement and introduce the same shear and moment distribution on the beam, but use a different specimen

configuration. The Iosipescu shear test method is shown in figure 3.7.

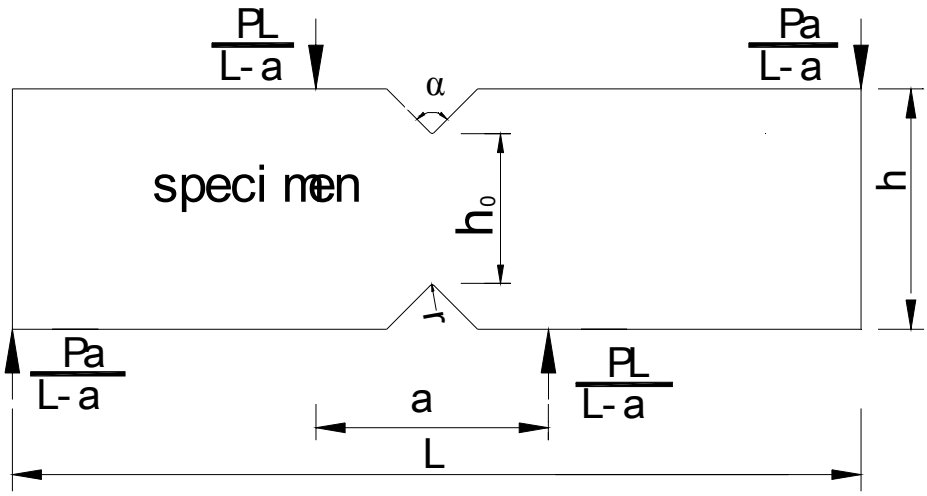

Figure 3.7 Configuration of Iosipescu specimen

It will be noted that Iosipescu specimens consist of a double edge-notch with small beam height h_0, angle α, and tip radius r at the pure shear section. The small beam height was regarded to make sure that a shear failure occurred, the angle α can cause a comparatively uniform shear distribution, and the tip radius can minimize the stress concentration. Many experimental and analytical studies were conducted concerning the influence between specimen shape and the stress-strain state in the Iosipescu shear test specimen.

A detailed study to determine the configuration of Iosipescu specimen has been conducted by Walrath and Adams at the University of Wyoming U.S (Walrath and Adams, 1985). An optimum specimen was found to be one with two 90^0 angle notches with a notch root radius of 1.3 mm that are made at the edge mid-length with faces orientated at (ϕ)45^0 to the longitudinal axis, to a depth of 20% of the specimen height. The specimen length and width are 76mm and 20mm, respectively. Eventually, this configuration was accepted in the ASTM Standard.

The expression of an average shear stress in the Iosipescu shear beam test is reasonable due to a more uniform shear stress distribution. The average shear strength τ can be calculated using :

$$\tau = \frac{P_{max}}{W \cdot h_0} \tag{3.2}$$

Where P_{max} is the ultimate failure load, h_0 is the distance between the notches and W is the specimen thickness. The shear strain usually is measured by an auxiliary surface bonded strain gage. Some time Moir interferometry is also used to measure the shear strain and to compare it with strain gauge results.

The failure modes of Iosipescu specimens are different for different fibre reinforced plastic material compositions. Three fibre orientation arrangements in the composite material are commonly used, causing anisotropy of these materials, which can be describe as following:

a) The fibres are parallel to the specimen longitudinal (x) axis. Such specimens are designated 0^0 specimens.

b) The fibres are parallel to the specimen transverse (y) axis. Such specimens are designed 90^0 specimens.

c) The fibres are parallel to both the specimen longitudinal (x) axis and transverse (y) axis. Such specimens are designed 0^0 /90^0 specimens.

Of these three specimens types, a) and b) can be regarded as anisotropic, while c) can be regarded as close to isotropic. Tests have been conducted to study the differences in shear failure of these three specimens types (Morton et al., 1992). Graphite-epoxy composite specimens were used in Iosipescu tests. The results show that:

i) The strength of the 90^0 specimens is much less than those of the other two cases. The 90^0 specimens failed through the propagation of a single vertical crack between the notches, parallel to the fibres. The failure location did not occur at the minimum section but at the intersection of the notch root and the notch flank.

ii) The shear strength of the 0^0 specimens is the highest in these three specimens. The 0^0 specimen failed with two longitudinal cracks propagating parallel to the fibres

and emanating from the intersection of the notch root and the notch flank. Cracks appeared on opposite side of the upper and lower notches.

iii) The strength of the 0^0 /90^0 specimens lies between the other two cases. The specimens failed through a network of cracks developing in both fibre directions.

These three kinds of failure modes have been regarded as typical, acceptable failure modes in the ASTM Standard D-5379. However, the 90^0 specimens were suggested not to be used in the test due to the invariable failure at significantly lower stresses than those measured for the corresponding 0^0 specimens (Hodgkinson, 2000). In addition, failure modes initiated at loading points were regarded as unacceptable failure modes in ASTM Standard D-5379.

Aditional disadvantages exist with the Iosipescu shear beam test. Firstly for orthotropic material it does not produce a uniform elastic shear stress distribution across the shear section (Walrath and Adams, 1985). Secondly, an experimental error will be caused by twisting effects if the specimen preparation or some irregularity of the fixture is improper (Morton et al., 1992). In addition, the test cannot be used under cyclic loading conditions.

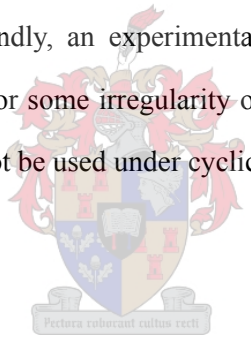

3.6 Conclusion

Four shear test methods have been described in this chapter. All of these shear test methods are intended to measure the same material properties, and have been in existence for some time. However, each test method obviously has advantages and disadvantages.

The short shear beam method is simple to implement and the most inexpensive, but it cannot produce pure shear state. The pure shear panel test method can produce pure shear, but is complicated and expensive. The Ohno shear beam test method has been used to investigate the shear behaviour of ECC, but it is not possible to prevent other failure mechanics than shear. The Iosipescu shear beam test method as an accurate and convenient method has been adopted as ASTM Standard. Therefore, the Iosipescu shear beam test method is chosen for further development and applied to reveal the characteristics of ECC.

However, the Iosipescu shear beam test method has never been used for cement-based materials. As mentioned in the previous chapter, ECC belong to a class of short random fibre reinforced cement based materials. The specimen recommended in the ASTM Standard is suitable for continuous-fibre composites and the specimen size is so small that it is difficult to be casted in the concrete laboratory. The design of a new specimen is discussed.

Chapter 4
Iosipescu shear test specimen design

4.1 Introduction

From the evaluation of shear test methods for the shear characterisation of ECC (engineered cementitious composites) in the previous chapter the Iosipescu shear test was found to be the best. However, it was also recognized that the test specimen from ASTM Standard D-5379 was not suitable for ECC. So, a new Iosipescu shear test specimen which is developed for ECC is presented in this chapter.

In this chapter, an approximate configuration of the specimen is obtained by simple analytical experimental design in the first section. Then, the finite element analysis method is used to refine the specimen in the second section. Eventually, the geometry of the specimen in detail will be set up.

4.2 Simple analytical experiment design

An approximate configuration of the Iosipescu shear specimen is found before detailed finite element analysis is applied for refinement. It can be seen from figure 4.1 that a specimen is controlled by seven parameters: two inner load points distance (a), two outside load points distance (L), the height of beam (h), the distance between inner load point and notch edge (d), the depth between two notch roots (h_0), the notch angle (α), and the notch radius (r). As mentioned in the previous chapter, a small depth between two notch roots (h_0) can produce a weak pure shear section in the specimen, the notch angle α can influence the shear stress distribution along the notch section, and the notch radius (r) can change the stress concentration at the notch tip roots. However, it is difficult to use simple mechanics theory to evaluate the stress distribution and stress concentration. So, a preliminary geometry of the specimen in term of the remaining parameters will be established by comparing the failure modes of the specimen in this section.

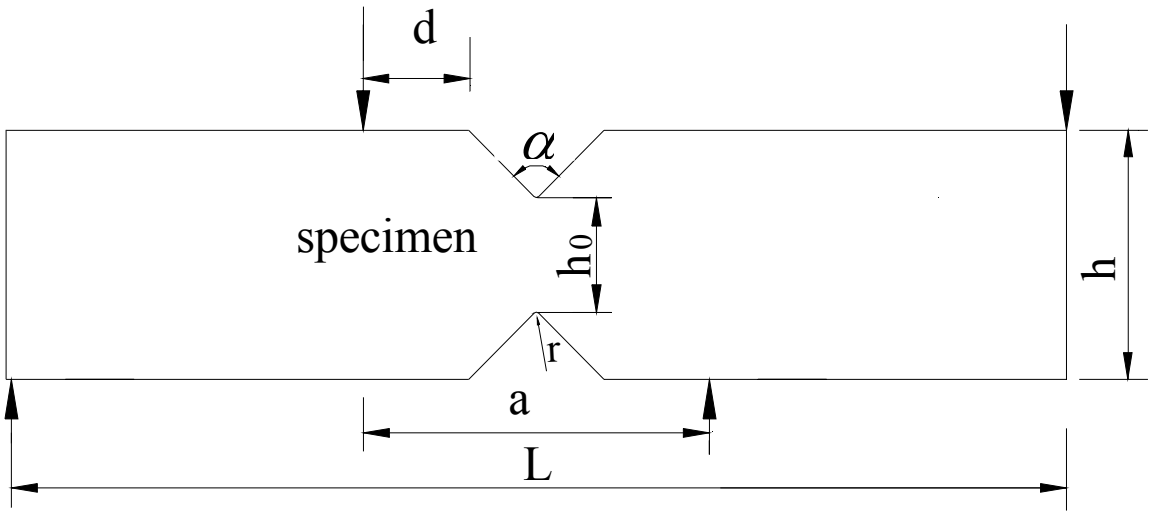

Figure 4.1 The configuration of specimen with seven parameters

According to the Iosipescu shear test mechanism, as shown in the previous chapter in figure 3.3, there are three types of failure modes that can occur in the specimen:

1) Shear dominated failure mode, which occurs at the mid-length at the position of zero bending moment.
2) Bending dominated failure mode, which occurs at two inner loads point at the maximum bending moment.
3) Shear-flexure combined failure mode, which occurs from the mid-length to two inner load points with the constant shear force and linear varying bending moment.

The relationship is more complex in the shear-flexure combined failure mode due to the varying depth along the notch edges. Therefore, the shear dominated failure mode and bending dominated failure mode will be used to evaluate the relationship between the parameters simply.

To ensure that the failure mode is the shear-dominated failure mode, and the failure of the specimen occurs at the notch section, two simple relationships between the specimen resistance property and external force should be considered:

1) The bending moment of resistance (M_r) at the maximum bending moment point has

to be more than the internal bending moment (M_m) at that point: i.e.

$$M_r > M_m \tag{4.1}$$

2) The shear resistance (V_r) at the notch section has to be less than the internal shear force (V_m) at the notch: i.e.

$$V_r < V_m \tag{4.2}$$

From (4.1), substituting the maximum bending moment into M_m and using classical linear elastic strength of material theory in M_r:

$$\sigma_{r\max} > \frac{3 \cdot P \cdot a}{t \cdot h^2} \tag{4.3}$$

$$\therefore \quad P < \frac{\sigma_{r\max} \cdot t \cdot h^2}{3 \cdot a} \tag{4.4}$$

From (4.2), substituting the external shear force (P) into V_m and assuming (τ_{ravg}) uniform shear stress distribution in the notch section, the average shear stress can be expressed as:

$$\tau_{ravg} < \frac{P}{t \cdot h_0} \tag{4.5}$$

$$\therefore \quad P > \tau_{ravg} \cdot t \cdot h_0 \tag{4.6}$$

Combining equation (4.4) and (4.6):

$$\frac{\sigma_{r\max} \cdot t \cdot h^2}{3 \cdot a} > \tau_{ravg} \cdot t \cdot h_0 \tag{4.7}$$

$$\therefore \quad \frac{\sigma_{r\max}}{\tau_{ravg}} > \frac{3 \cdot h_0 \cdot a}{h^2} \tag{4.8}$$

From equation (4.8), a cursory relationship is obtained between the depth (h_0), the total specimen height (h), the distance between two inner load points (a), and the parameters of material strength (σ_{rmax}, τ_{ravg}). Due to a limited knowledge of the properties of ECC at the present time, especially the shear property, the appearance of this parameter of material strength makes equation (4.8) more complex. The relationship between h_o and h is sensitivity to the ratio (shear strength/ tensile strength). A large ratio is conservative, as it produces a smaller required height in the notch relative to the total height. If the true ratio is higher, however, bending failure will dominate, instead of shear failure, which will render the test invalid. Therefore, an experiential ratio for τ_{ravg} : σ_{rmax} = 1.5 is assumed here. Therefore, equation (4.8) becomes:

$$h_0 < \frac{h^2}{4.5 \cdot a} \tag{4.9}$$

Equation (4.9) involves the global measurements of the specimen. To decide on these measurements, comprehensive factors should be considered, which include the production of the specimen, the testing of the specimen, and the cost of the specimen.

The production of the specimen will be by casting, which requires that the specimen should be removed by hand and is easy to strip. Therefore, the specimen should not be too large and heavy. The auxiliary surface bonded strain gage rosette with 21mm diameter will be used to measure the shear strain. Hence, h_0 should be more than 21mm. Of course, an economical specimen requires the volume of the specimen to be as small as possible. From this reasoning, the configuration of the specimen shown in figure 4.2 is considered suitable. Note that the thickness is 20mm over the total length.

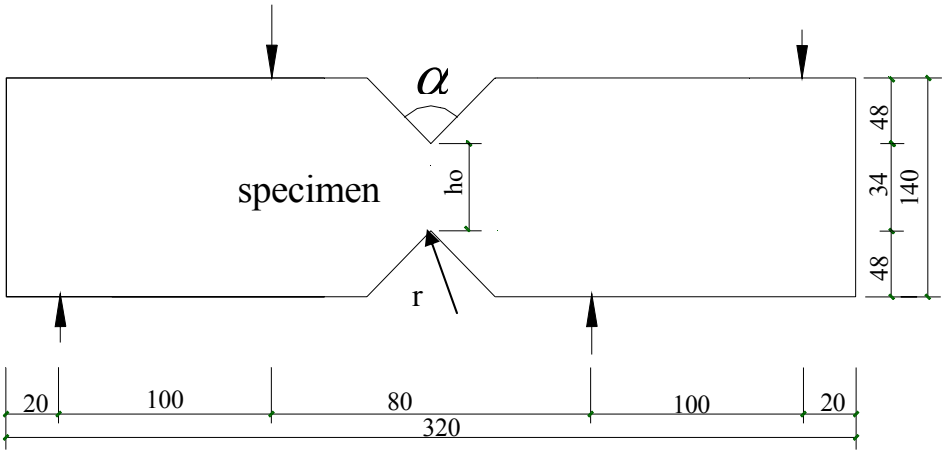

Figure 4.2 Configuration of specimen (all measurements in mm)

4.3 Pre-processing of finite element analysis

The parameters a, h and h_0 of the specimen have been addressed by simple analytical experimental design in the previous section. However, simplifying assumptions, including an estimated shear strength to tensile strength ratio have been made. In addition, the influence of the notch angle and notch tips radius was not considered.

As an accurate numerical analysis method, The Finite Element analysis (FE) method has been efficiently used in many fields. Without exception, the Iosipescu shear test method has also been subjected to FE analyses by several investigators. Many types of composite materials have been investigated, which include Plexiglas (Sullivan and Kao, 1984), carbon-carbon composites (Walrath and Adams, 1981), glass fibres-reinforced polyester sheet molding compounds (Adams and Walrath, 1982), unidirectional graphite-epoxy (Morton and Ho, 1992), etc. However, to the knowledge of the author cement-based composite materials have not been studied yet. In this section, the commercial finite element software Diana 8 is used to refine the specimen geometry.

As a normal procedure of finite element analysis, the model data should be prepared (known as pre-processing) before performing the analysis. This model data includes:

1) Definition of model geometry

2) Material and physical properties

3) Loads and constraints

4) Meshing of specimen and choice of element type

4.3.1 Definition of model geometry

The greatest advantage of the Iosipescu shear test method is the special specimen geometry, as mentioned in the previous chapter. The major region of interest in this analysis is the notch region. Consequently, the FE analyses focus on the notch geometry, specifically r and α. Based on the preliminary configuration of the specimen, different geometries of specimens are analysed in more detail in this section. In addition to the notch radius (r) and angle (α), the influence of the distance between the inner load point and the notch edge (d), the depth between two notch roots (h_0) is studied with regard to the objectivity of the test to characterise the shear behaviour of ECC.

4.3.2 Material and physical properties

As a relatively new composite material, the properties of ECC have not yet been determined fully. Therefore, the present study is performed assuming linear elastic behaviour as well as homogenious, isotropic material. ECC can be regarded as isotropic material due to the short fibres, which are distributed and orientated randomly in the matrix if the specimens are cast in moulds, unlike when they are extruded (De Koker, 2004). Note, however that, due to the relatively small thickness, the fibres are oriented primarily in the plane, i.e. two dimensionally. So plane stress is assumed. For evaluating the stress fields in the specimen, an elastic modulus E equal to 25 GPa and Poisson's ratio equal to 0.2 are used as material parameters, which are from normal concrete because ECC derived from it originally.

4.3.3 Loads and constrains

An antisymmetric four-point bending fixture will be used to provide the load and support which was developed by Sullivan and Kao (1984). The configuration of this fixture is shown in figure 4.3. It can be seen that a vertical load is translated to two loads on the specimen top by a load beam; two cylindrical rollers support the specimen. This simple fixture was mounted on the test machine (Zwick Z250). Through the loading configuration, 3/4 of the load passes through point A and 1/4 through point B.

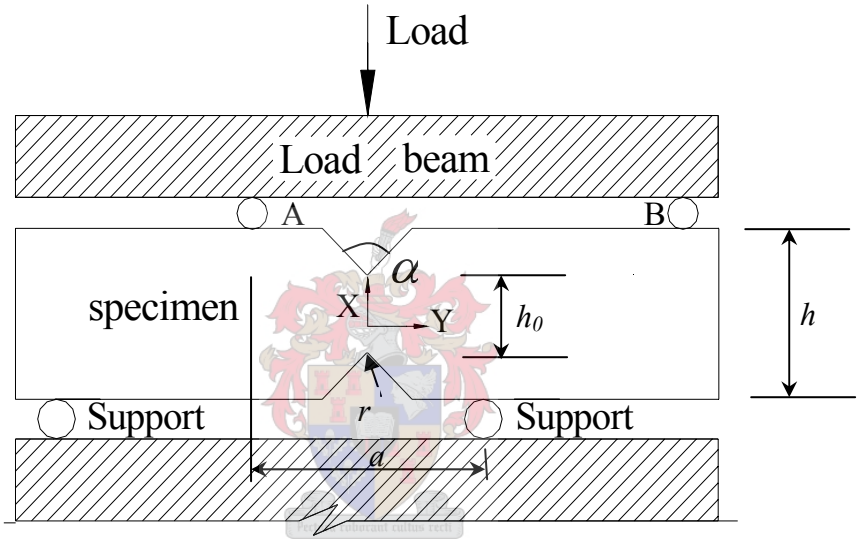

Figure 4.3 Configuration of the four-point bend fixture

4.3.4 Meshing of specimen and choice of element type

An eight-node quadrilateral isoparametric plane stress element, CQ16M, was selected for the analysis. It is based on quadratic displacement field interpolation and Gaussian integration. A refined mesh is made in the notch section, because an accurate stress field representation is required in this region. The element size along mid-length will be controlled within 1mm x 1mm per element approximately. Total elements and nodes will be presented in detail later according to different models.

A generalized finite element model for the loading, boundary condition, and general meshing is illustrated in figure 4.4. The fixed parameters of the model are given in table 4.1.

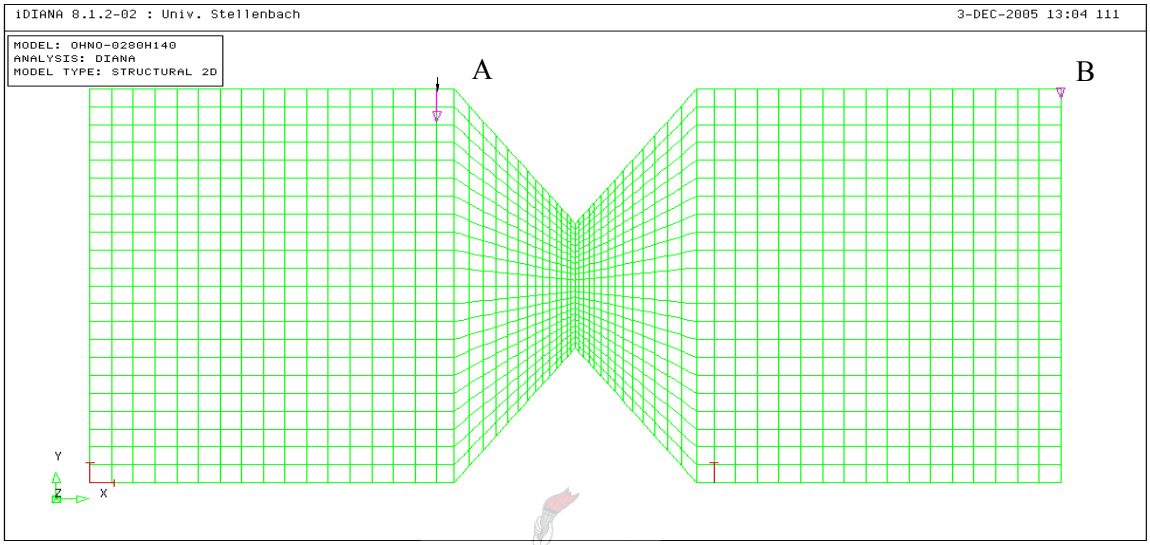

Figure 4.4 Loading, boundary conditions and meshing in modelling

Table 4.1 Fixed parameters of model

L (mm)	***a*** (mm)	***h*** (mm)	***E*** (GPa)	***v***	**Element type**	**Load at A point** (KN)	**Load at B point**(KN)
280	80	140	25	0.2	CQ16M	3000	857.14

4.4 Finite element analysis

Based on the above model data, different models are set up to study the influence of various notch configurations. The effect of different distances between the inner load point and the notch edge (*d*) is studied. Also, different notch angles and notch depths are examined. In addition, the effects of different notch tip radii are investigated. The purpose of the present study is to find a pure shear failure, viz., the failure of specimen occurs at the notch section, with a corresponding uniform shear stress along this notch section. As was mentioned before, there are three types of failure modes that can occur in the notch region. Therefore, the

location of the maximum principal stress will be regarded as the start of model failure, because it is well known that cement- based material fracture when the maximum principal stress exceeds the tensile resistance stress of the material.

Therefore, the tendency of shear stress distribution and principal stress distribution are expressed by contour graphs on the specimens. Also, graphs of normalised shear stress distribution (shear stress / average shear stress) along the central line are used to distinguish the uniformity. Graphs of normalised principal stress (principal stress /average principal stress) along the notch edge are used to find the failure initiation point in the different models. To compare these variations of different models, two critical lines that at the same position of different models are used as shown figure 4.5.

a) Line 1: the average stress per element drawn at element centre just to right of notch

b) Line 2: the average maximum principal stress per element along edge

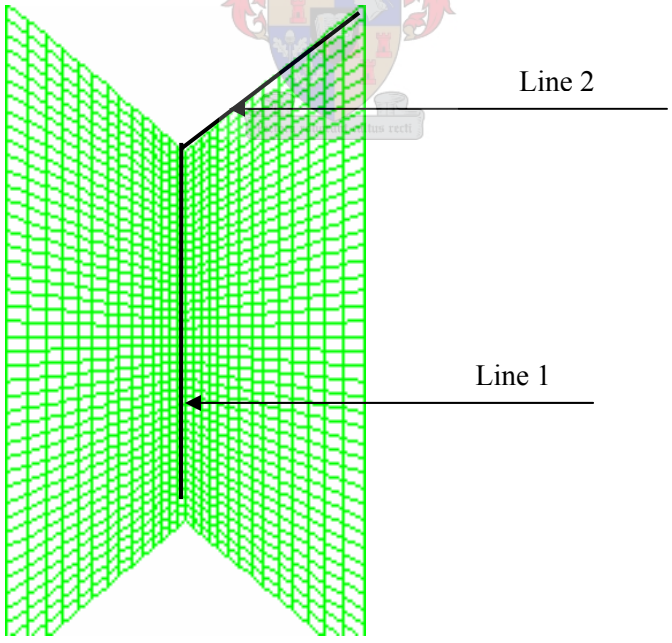

Figure 4.5 Configurations of line 1 and line 2 in the model

4.4.1 Effect of the distance between inner load points and notch edge (*d*)

The effect of the distance between the inner load point and the notch edge is first studied. The main reason is that this distance influences the position of inner load points with changing of notch angles and notch depths. For example, under a fixed inner load distance (a) and the depth between two notch roots (h_0), inner load points may go into the notch edge as the notch angle increases from 80^0 to 100^0 as shown in figure 4.6.

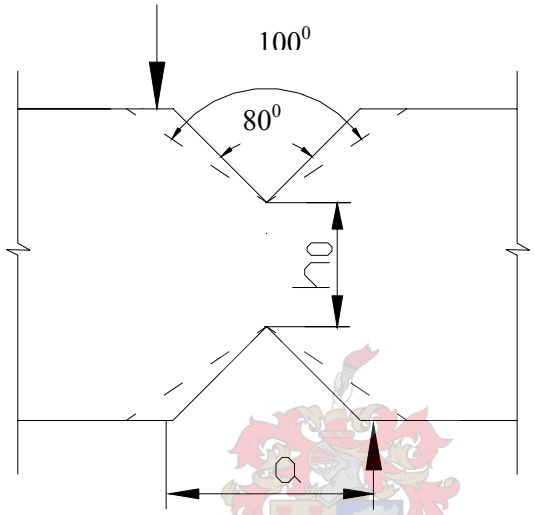

Figure 4.6 The situations of inner load point in 80^0 and 100^0 notch angle

So, the present study is to check if the result would be changed when the notch edges are moved close to the direction of notch roots. For this purpose, two finite element models were modelled, as shown in figure 4.7. The distances between inner load points are 5mm and 20mm respectively, the notch angle and notch depth are 80-degree and 34mm respectively. The 5mm and 20mm models consist of 17241 nodes and 5632 elements, and 19797 nodes and 6472 elements respectively.

The shear contours and the maximum principal stress contours are plotted in figures 4.8, 4.9. As can be seen, the tendencies of both the shear stress distribution and the principal stress are similar for the two models.

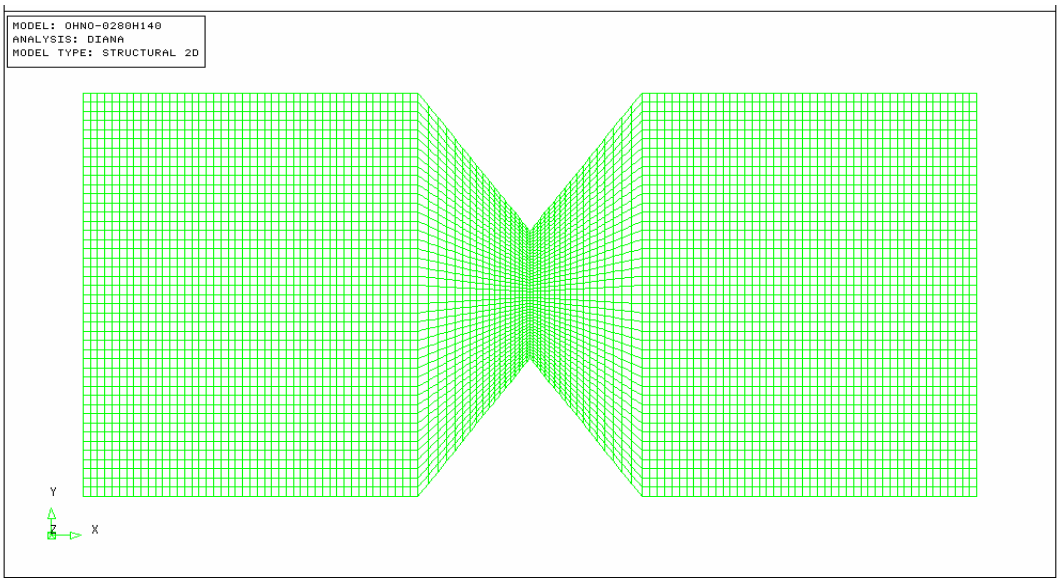

a) Distance = 5 mm

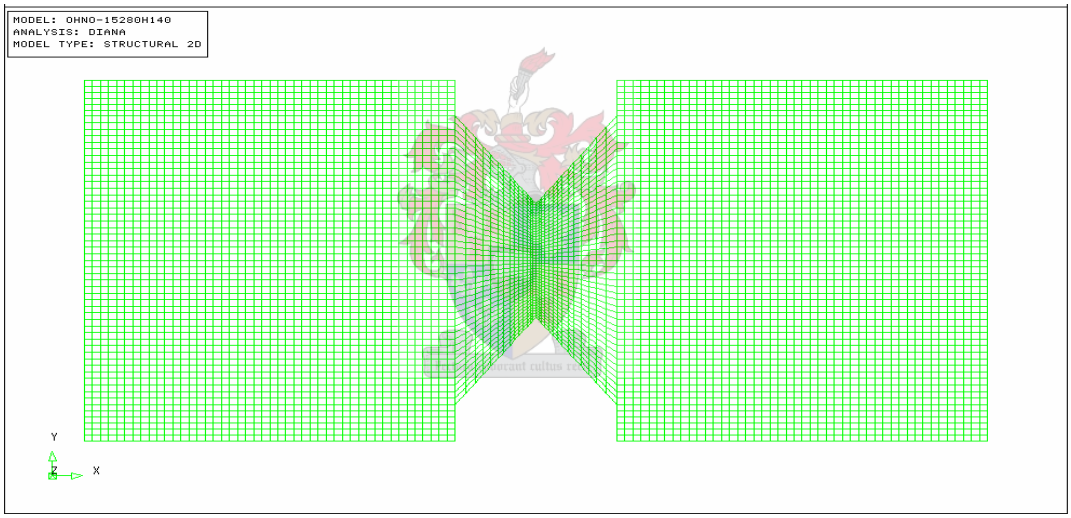

b) Distance = 20 mm

Figure 4.7 Finite element meshing for different distances between inner load points and notch edges

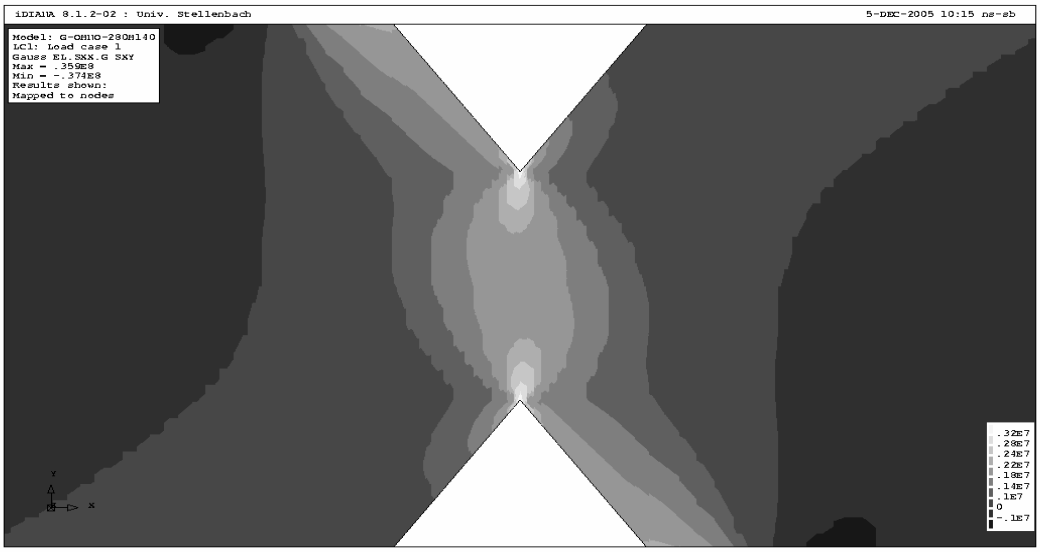

a) Distance = 5 mm

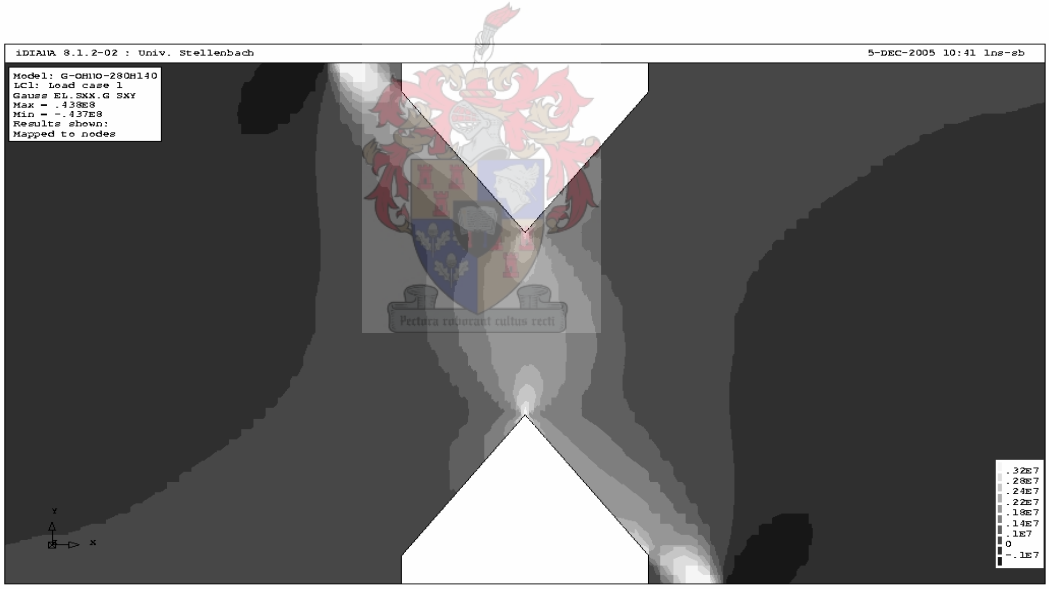

b) Distance = 20 mm

Figure 4.8 Shear stress contours for different distances between inner load point and notch edge (The stress unit is Pa)

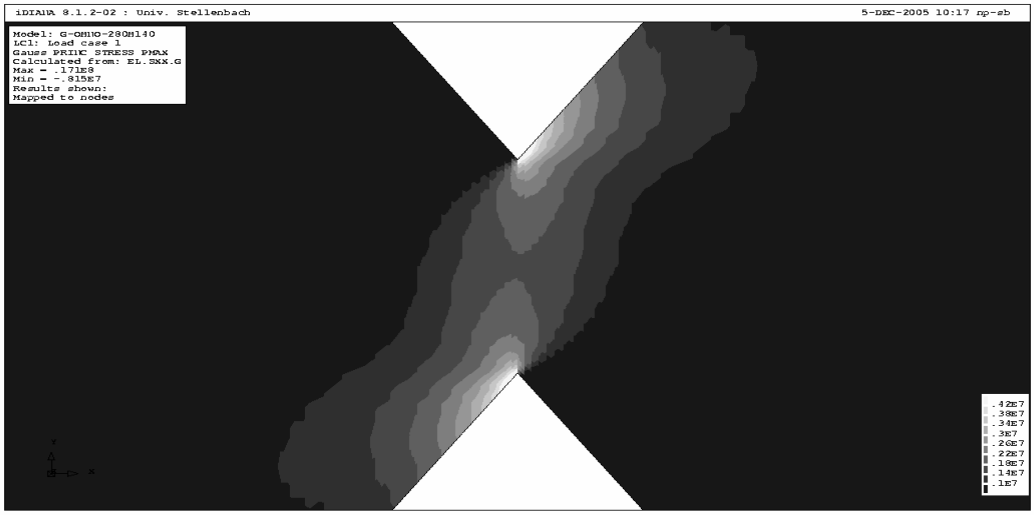

a) Distance = 5 mm

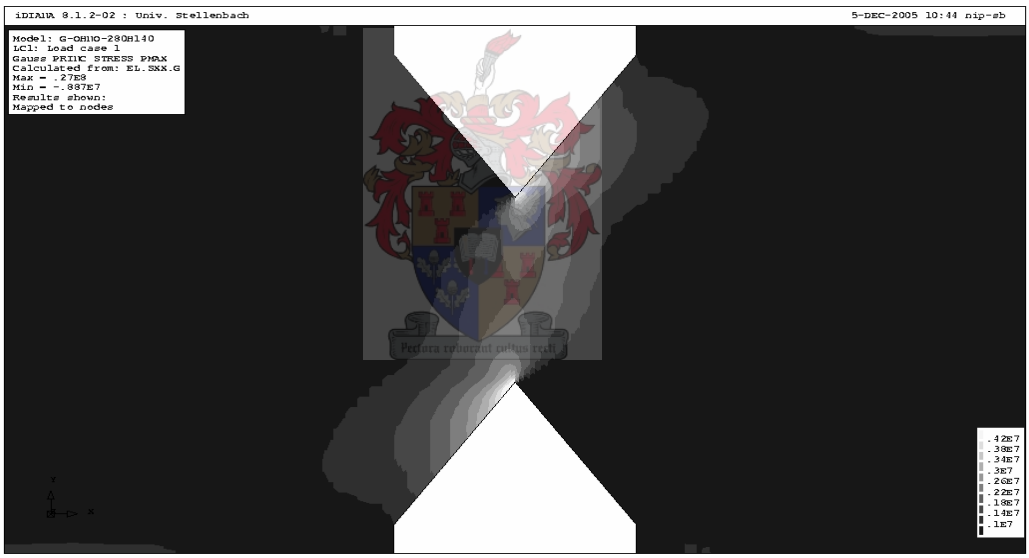

b) Distance = 20 mm

Figure 4.9 Maximum principal stress contours for different distances between inner load points and notch edges (The stress unit is Pa)

Normalised shear stress distributions along line 1 and the normalised principal stress along line 2 are plotted in detail in figures 4.10, 4.11. It can be noted the shear stress distribution and principal stress distribution are superpositioned along the notch depth and topside of

notch edge. Therefore, the distance between the inner load points and the notch edges does not have a significant effect on the shear and principal stress distribution.

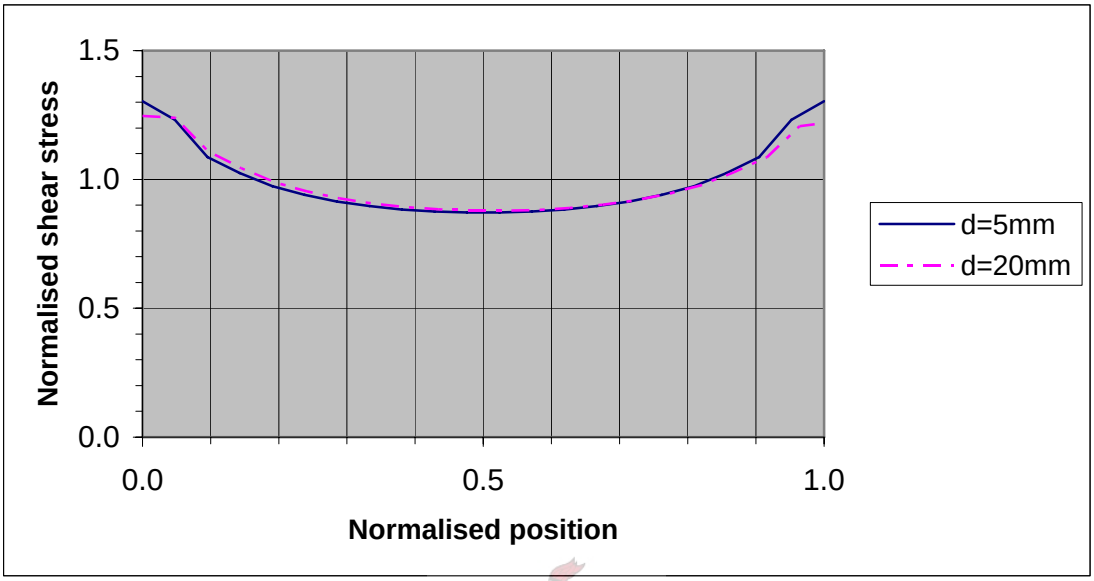

Figure 4.10 Normalised shear stress variations along line 1 for two different *d* values.

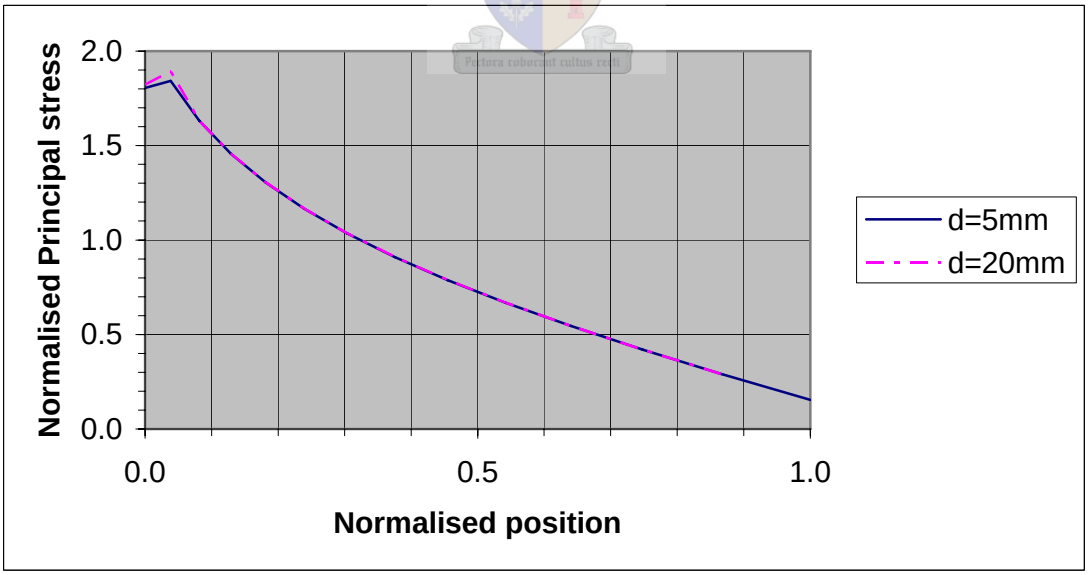

Figure 4.11 Normalised principal stress variations along line 2 for two different *d* values.

In addition, a bigger distance between inner load points and notch edges is provided. Hereby, the shortest distance from the load point through the material to the nearest free edge is increased, whereby the likelihood of spalling/splitting off of the edge is reduced. So, the 20mm distance model will be used to analysis the variance of notch angles, notch depth, and notch tip radius as a baseline model.

4.4.2 Effect of notch angle

Iosipescu's original argument for notch angle was 90^0, and this angle has been used in most Iosipescu shear tests. The purpose of the present study is to determine if this angle is a more favourable notch angle for the present configuration of model. Three notch angles were analysed, viz, the 80^0 configuration, as well as 90^0 and 100^0. Finite element mesh plots in the notch regions of the models are shown in figure 4.12. They represent the current baseline model with 0 mm notch tip radius, but with the three different angles.

Three models are modelled with the same amount of nodes and elements because the notch depth is the same. Each of the three models consists of 1618 nodes and 5272 eight-node isoparametric elements. The side lengths of the elements along the mid-length were restricted to within 1mm as mentioned before.

Numerical shear stress contours for the three models at the notch region are plotted in figure 4.13. It can be seen that there is a tendency for shear distribution to become more uniform in the notch section with increasing notch angles. The higher notch angles tend to slightly broaden the relatively constant shear stress region at the center of the test specimen. The contour shapes also tend to rotate with large notch angle. There is still some shear stress concentration at the notch tip. The maximum principal stress contours for the three models at the notch region is shown in figure 4.14. It can be noted that the maximum principal stress tends to move away from the notch roots with notch angles increasing. The area of relatively high principal stress increases with increasing notch angle.

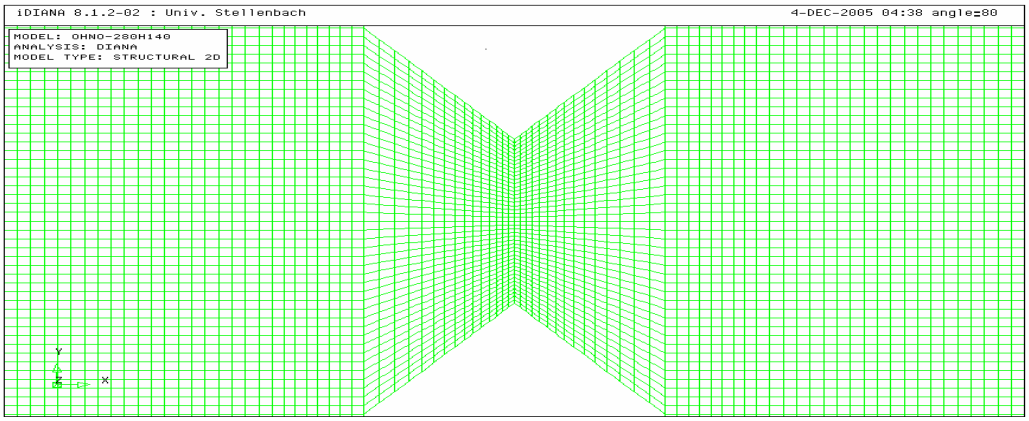

a) Notch angle =80^0

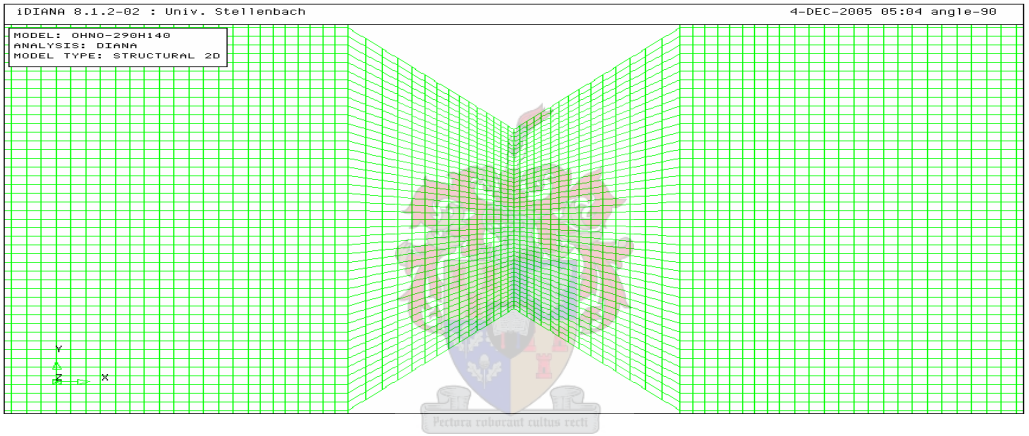

b) Notch angle =90^0

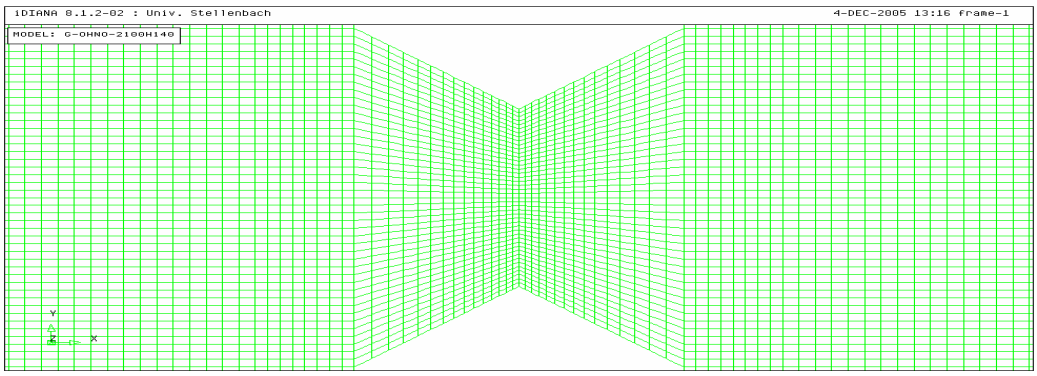

c) Notch angle =100^0

Figure 4.12 Finite element meshing for different notch angles

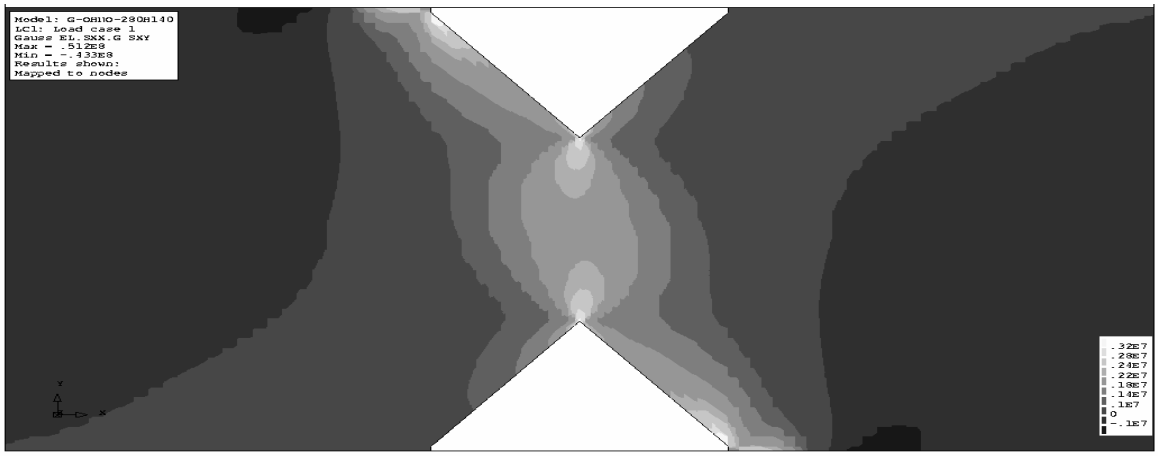

a) Notch angle =80^0

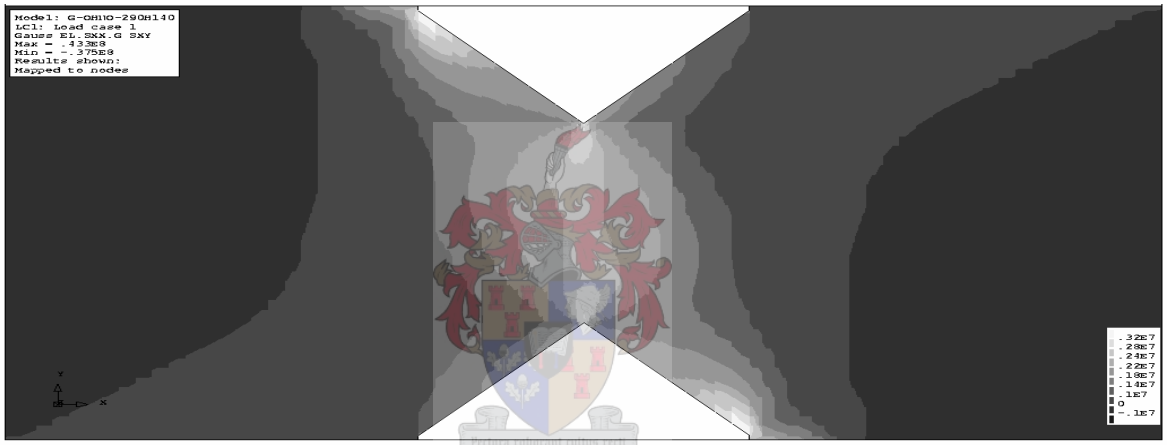

b) Notch angle =90^0

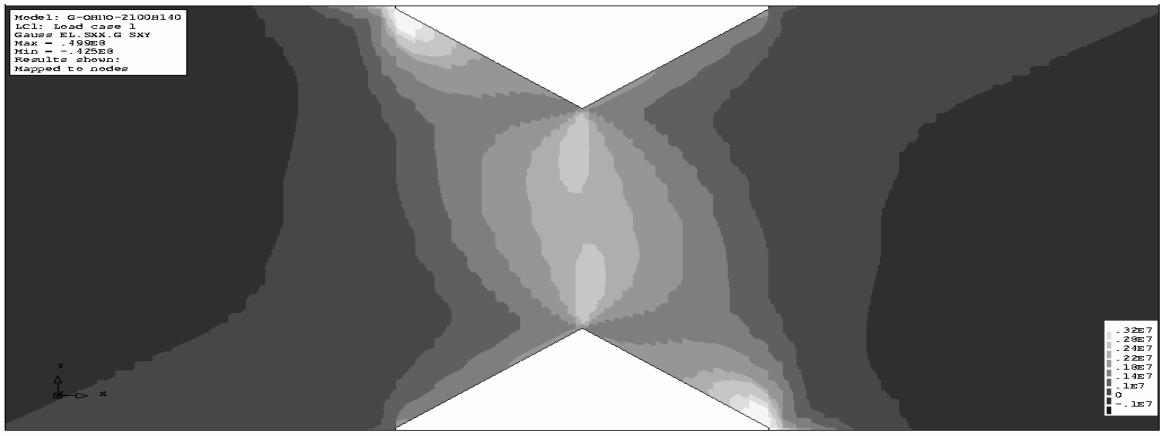

c) Notch angle =100^0

Figure 4.13 Shear stress distributions for different notch angles. (The stress unit is Pa)

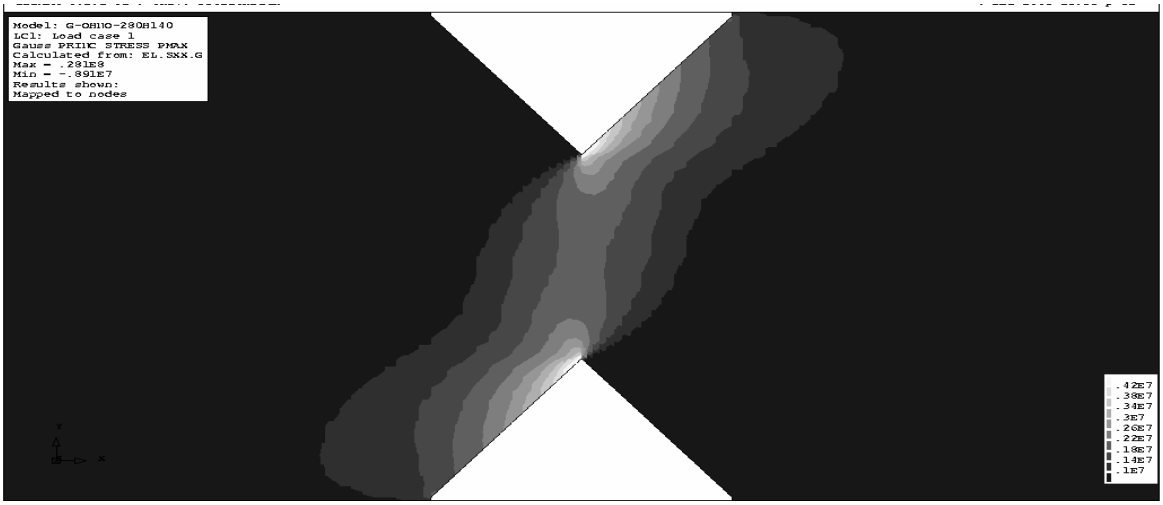

a) Notch angle =80^0

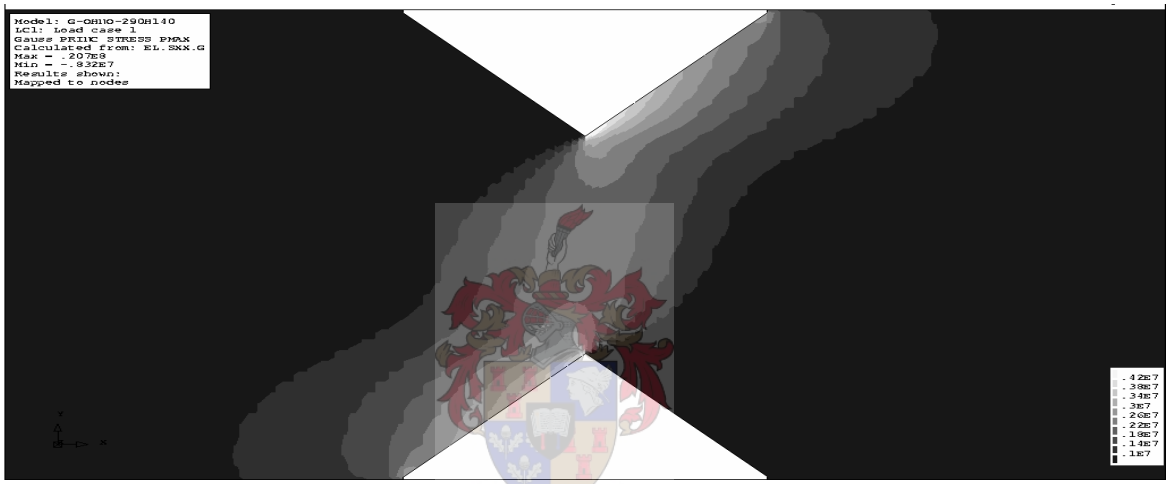

b) Notch angle =90^0

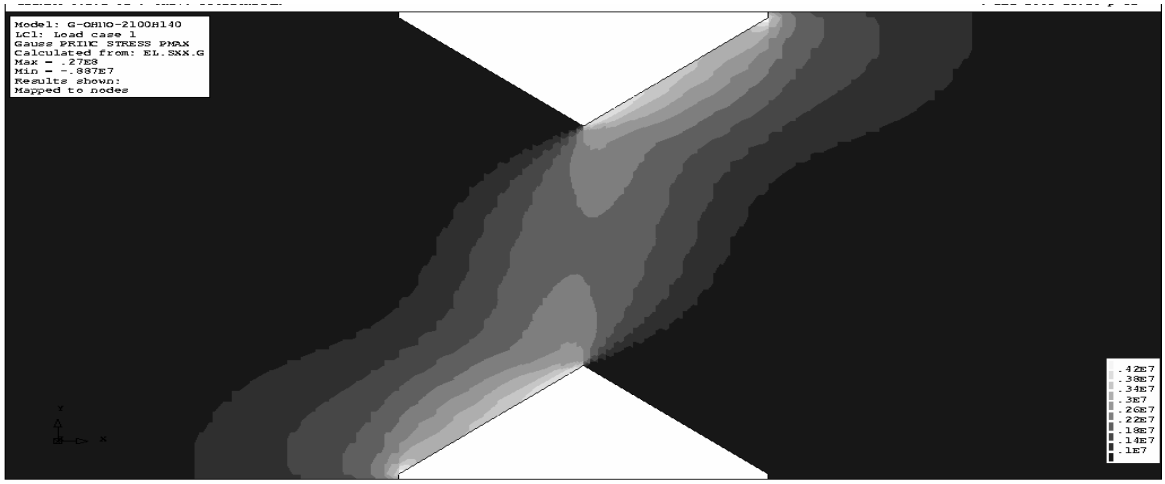

c) Notch angle =100^0

Figure 4.14 Principal stress distributions for different notch angles. (The stress unit is Pa).

To compare the variation of the shear stress distribution and principal stress in these models, two figures (figure 4.15, figure 4.16) are plotted. The normalised shear stresses along line 1 are used to indicate the shear stress distribution of three models in the figure 4.15. The normalised principal stresses along the line 2 are used to indicate the principal stress distribution of three models in the figure 4.16.

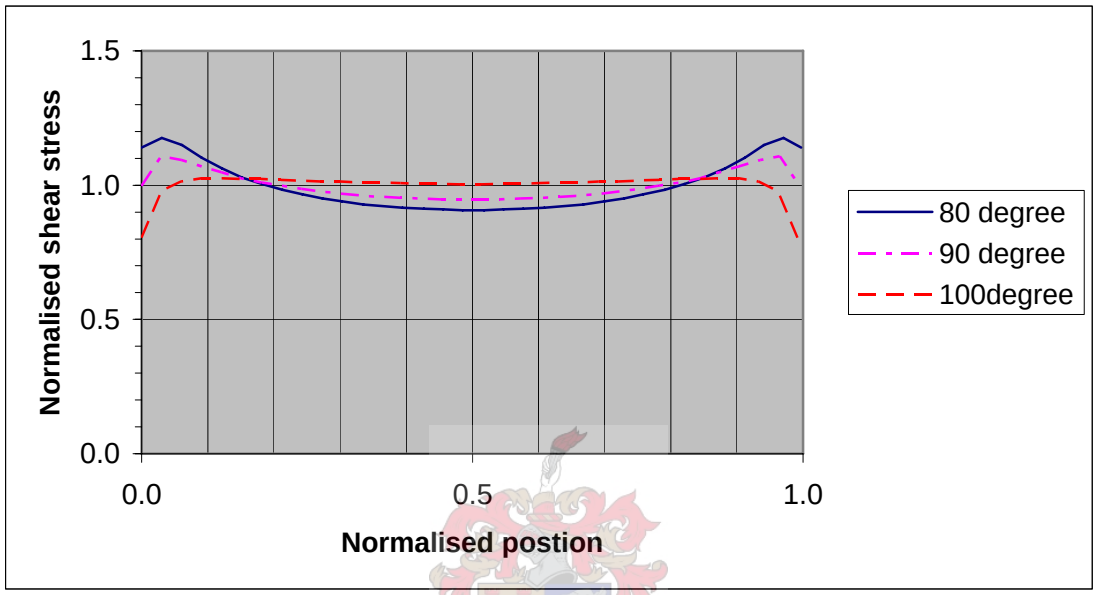

Figure 4.15 Normalised shear stress variations along line1 for three different notch angles

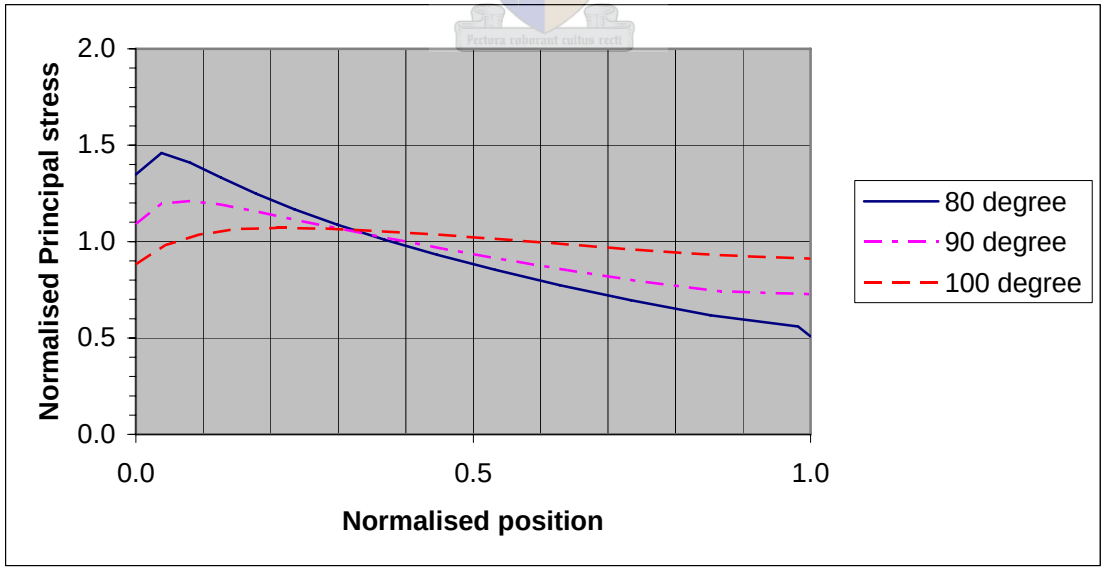

Figure 4.16 Normalised principal stress variation along line2 for three different notch angles

As can be seen from figure 4.15, the shear stress distribution of the 100-degree model is the closest to the average shear stress. However figure 4.16 shows that the maximum principal

stress of 100-degree model is the furthest away from the notch root in these three models. This means that cracking and failure will occur outside the pure shear notch, making the resulting shear data inaccurate. The 80-degree model has the worst shear stress distribution, but the maximum principal stress is the closest to the notch root. The 90-degree notch angle is a compromise between the favourable shear stress distribution and potential failure in the notch section.

4.4.3 Effect of the depth between two notch roots

The depth between two notch roots (h_0) was evaluated by simple mechanics theory in the last section. However, it can be noted that the calculation of this value was based on some simple assumptions and an experiential shear strength to tensile strength ratio. In this section, this value will be examined in more detail.

According to the baseline model and a 90-degree notch angle, three different notch depth models are set up, viz, the 24 mm configuration, as well as 34 mm and 44 mm. Finite element mesh plots in the notch regions of the models are shown in figure 4.17. As usual, the side lengths of the elements along two sides of central line are limited to within 1 mm. Due to different notch depths, the number of nodes and elements for each model differs.

The 24mm depth, the 34mm depth and 44mm depth models consist of 11313 nodes and 3664 elements, 16181 nodes and 5272 elements, and 16450 nodes and 5492 elements respectively.

Numerical shear stress contours and the maximum principal stress contours are plotted in figures 4.18, 4.19. The tendency of the shear distribution is to become more uniform with the depth increasing. However, the simple analytical model is confirmed by the increasing principal stress away from the notch with increasing notch depth. Thus, with increasing the depth between two notch roots (h_0) failure shift away from the notch root, relatively in flexural failure rather than shear failure.

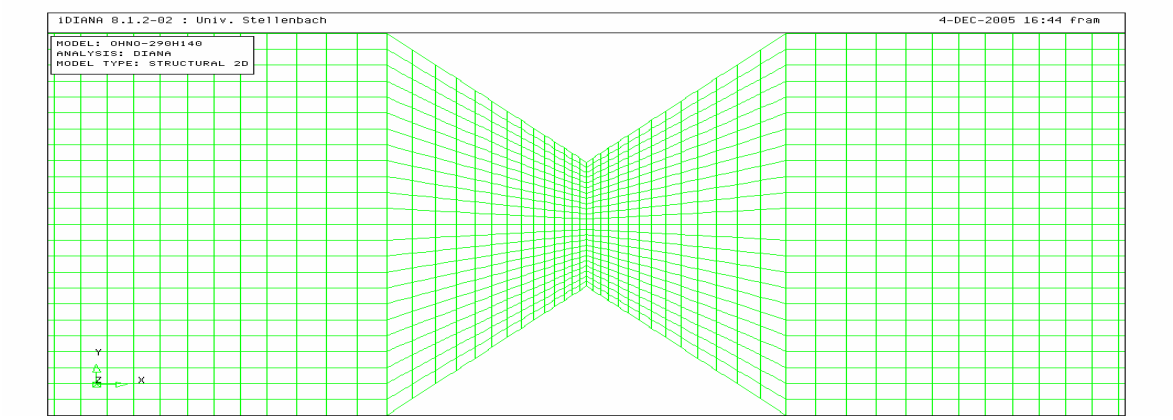

a) Notch depth = 24 mm

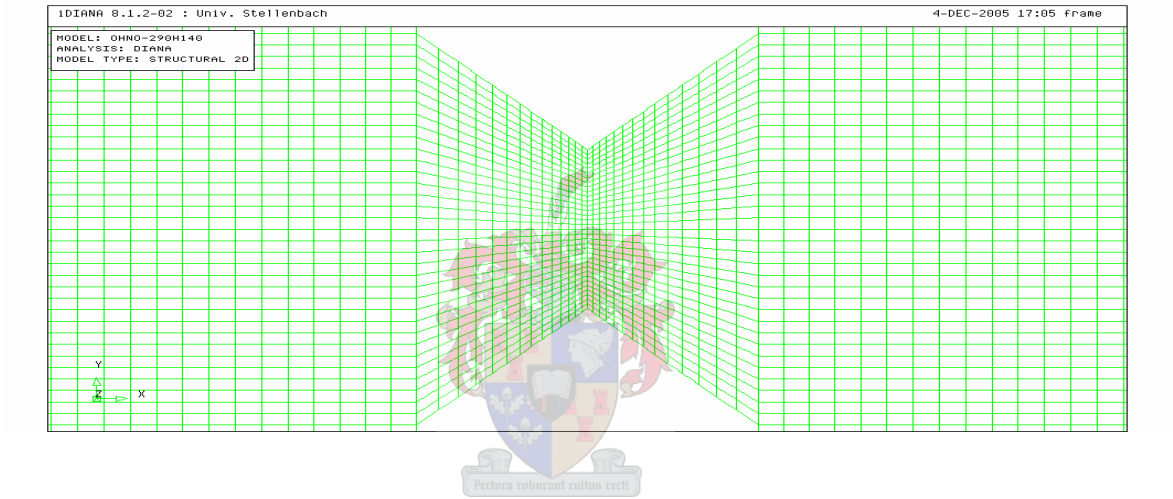

b) Notch depth = 34 mm

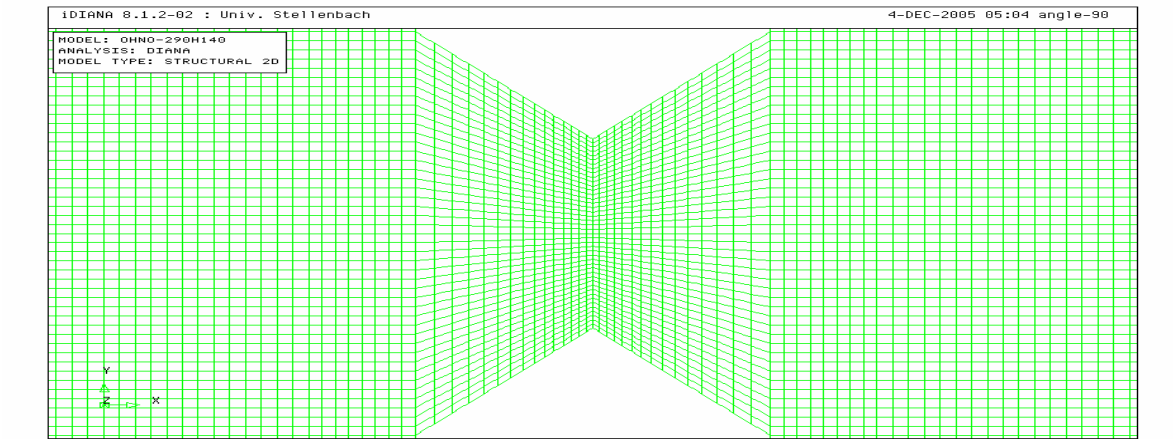

c) Notch depth = 44 mm

Figure 4.17 Finite element meshing for the different depth between two notch roots.

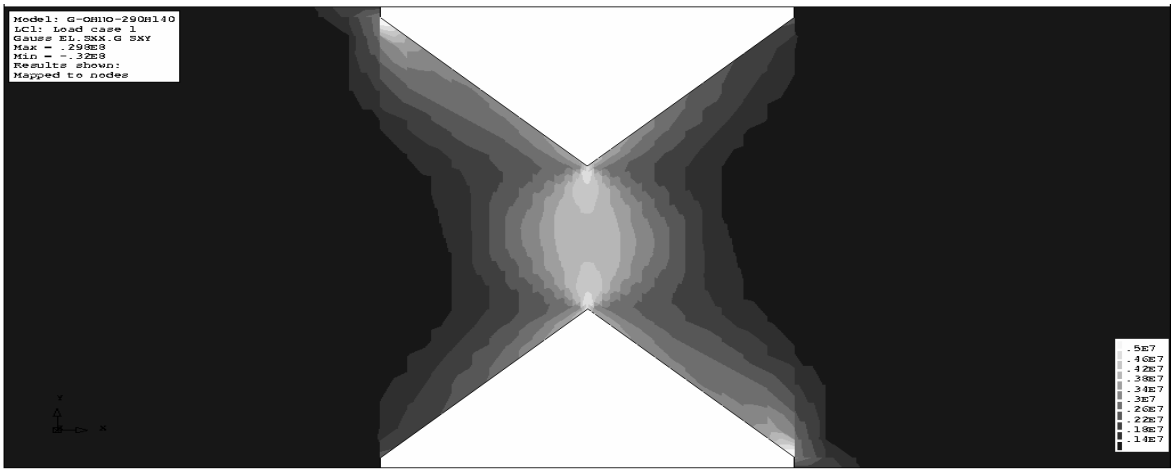

a) Notch depth = 24 mm

b) Notch depth = 34 mm

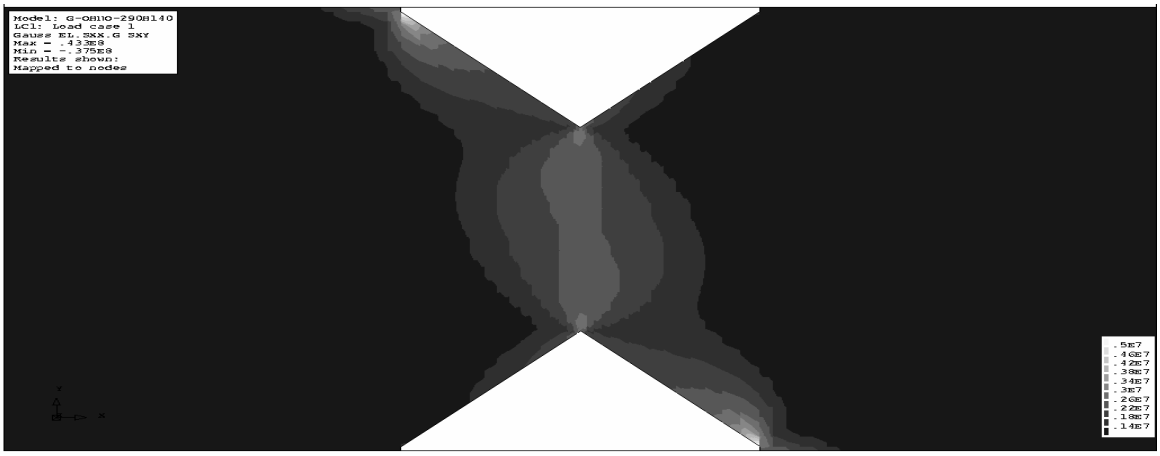

c) Notch depth = 44 mm

Figure 4.18 Shear stress distributions for the different depth between two notch roots. (The stress unit is Pa)

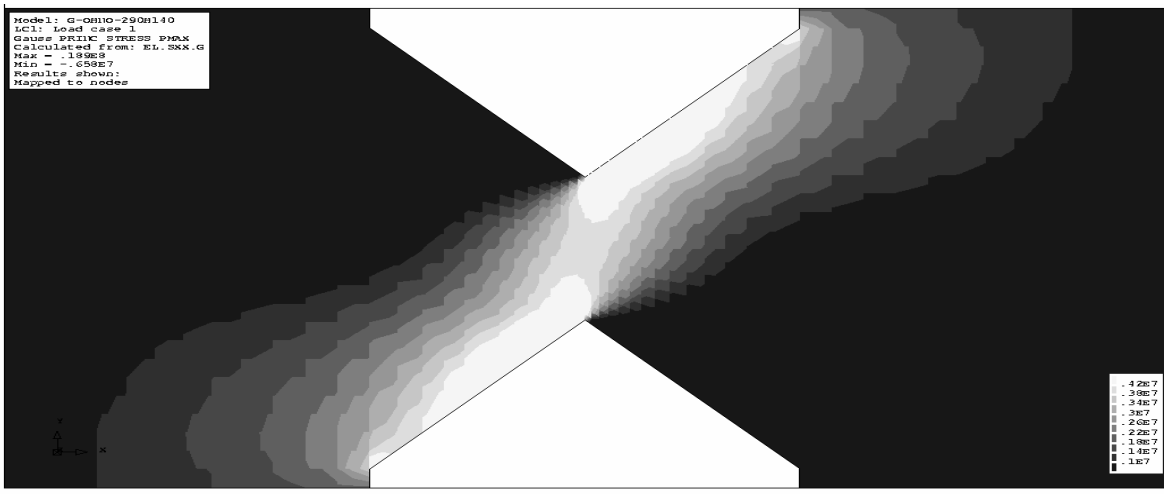

a) Notch depth = 24 mm

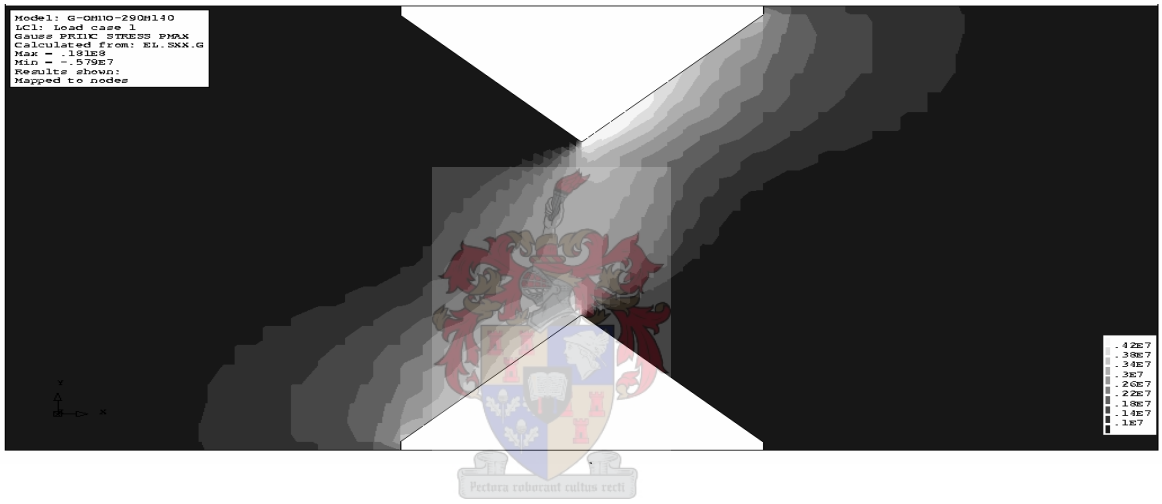

b) Notch depth = 34 mm

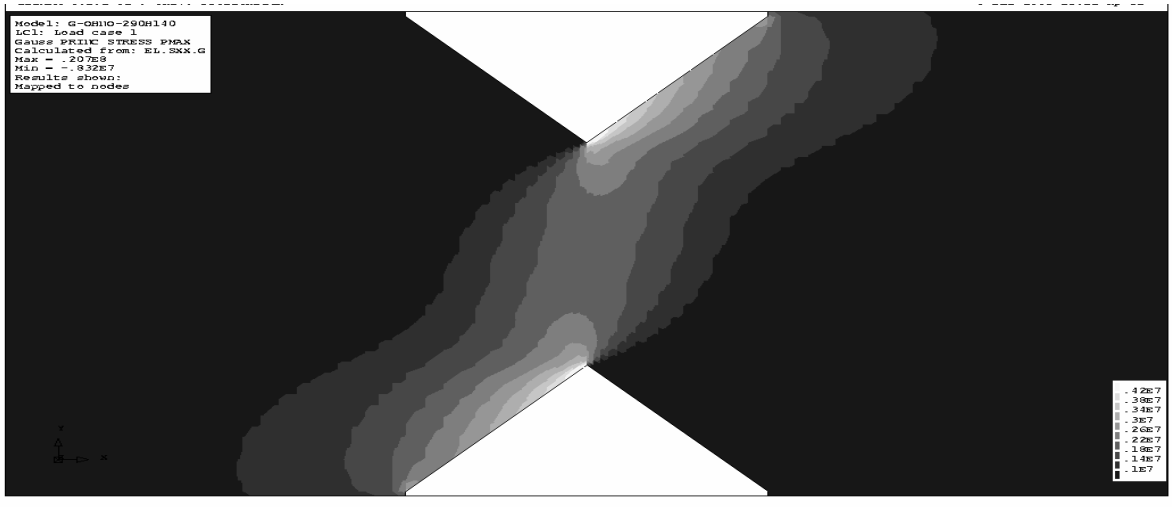

c) Notch depth = 44 mm

Figure 4.19 Maximum principal stress contours for the different depth between two notch roots. (The stress unit is Pa).

Again, two figures were plotted to compare the variation of the shear stress distribution and maximum principal stress in these models along lines2. The normalised shear stress along mid-length (line 1), shown in figure 4.20 are different due to the different notch depths.

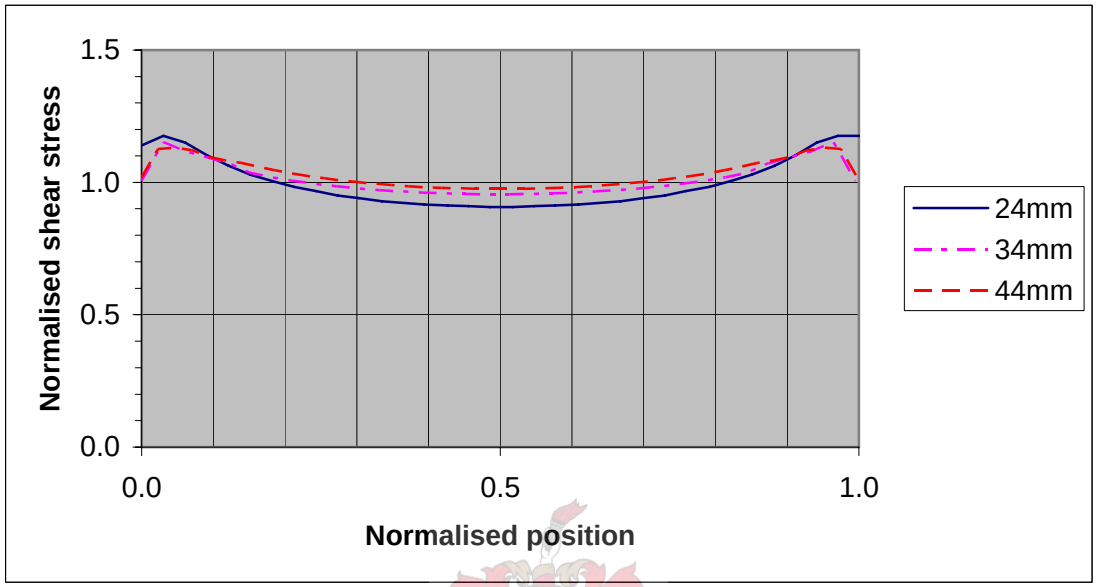

Figure 4.20 Normalised shear stress variations along line 1 for different notch depths

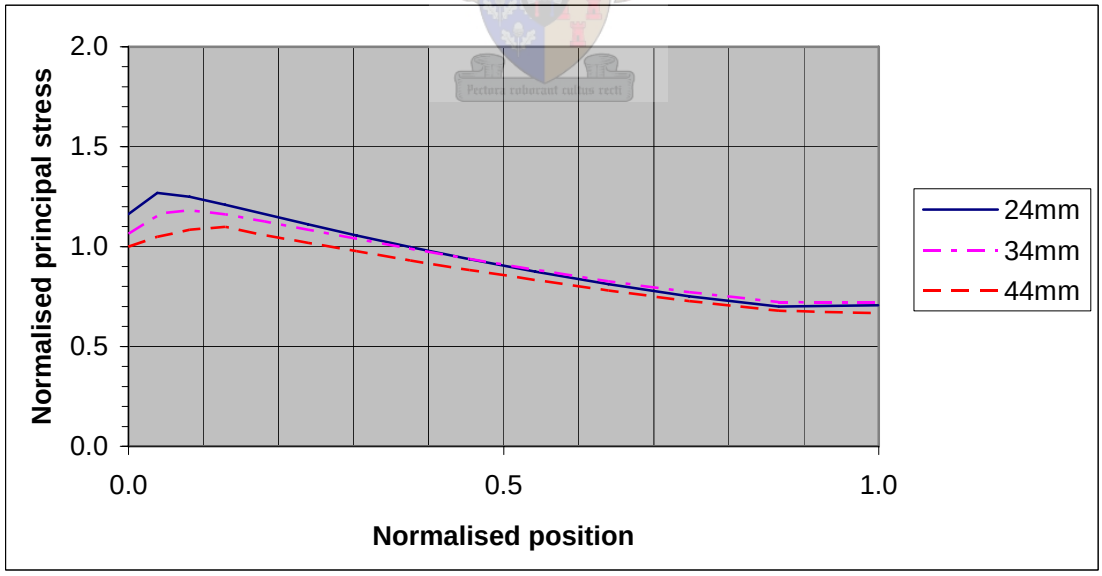

Figure 4.21 Normalised principal stress variation along line 2 for three different notch depths

As can be seen from figure 4.20, the shear distribution is more uniform with the depth

between two notch roots increasing. The shear distribution of 44 mm model is the closest to the average shear stress. However figure 4.21 shows that the maximum principal stress of 44mm model is the furthest away from the notch root in these three models. This means failure of specimen will occur outside the pure shear notch, making the resulting shear data inaccurate. The 24 mm model has a worst shear stress distribution, but the max principal stress is the closest to the notch root. The 34 mm depth is chosen as a compromise between the favourable shear stress distribution and failure in the notch section.

4.4.4 Effect of notch tip radius

As has been previously discussed, the notches are present in the Iosipescu shear specimen to ensure shear failure in the notch, as apposed to flexural failure away from the notch. And, it also alters the shear stress distribution from parabolic to a more uniform distribution. However, the sharp notch (tip radius =0 mm) does produce a shear stress concentration at the notch tip. The tip radii have been considered useful to reduce the stress concentration (Walrath and Adams, 1981). Therefore, in this section, three different notch tip radii are modelled, namely r = 0 mm, r = 2.7 mm and r = 3.5 mm respectively. The finite element meshing for these three configurations are shown in figure 4.22. The constitutions of three models are different due to the changing of notch tip radius. To keep the notch angle at 90-degree, the depth between two notch roots is slightly raised with notch tip radius increasing. The depths (h_0) are 34 mm for r = 0 mm, 36 mm for r = 2.7 mm and 38 mm for r = 3.5 mm. The models consist of 1618 nodes and 5272 elements for r = 0 mm, 22909 nodes and 7504 elements for r = 2.7 mm, and 22989 nodes and 7512 elements for r = 3.5 mm.

The shear stress contours and principal stress contours of the three models are presented in figure 4.23, 4.24. As would be expected, the shear stress gradients around the notch tips are also reduced with larger notch tip radius. The point of maximum shear stress tends to move away from the centreline of the models for increasing notch tip radius. It can be seen from the principal stress contour that the maximum principal stress also tends to move away from notch roots with the notch tip radius increasing.

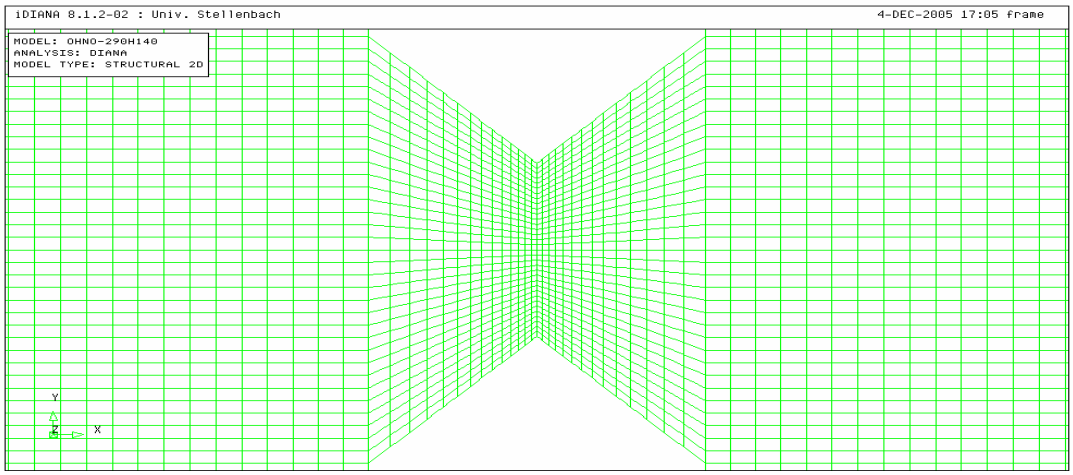

a) Notch radius = 0 mm

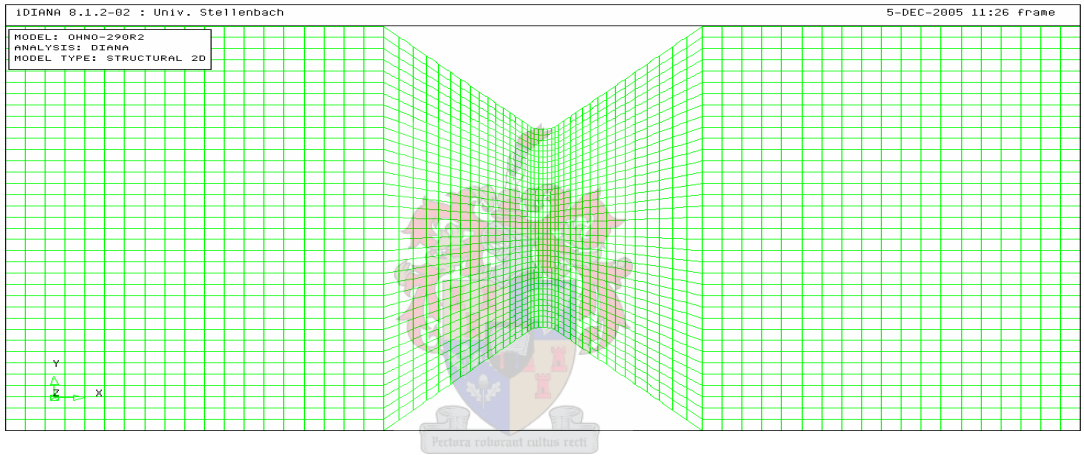

b) Notch radius = 2.7 mm

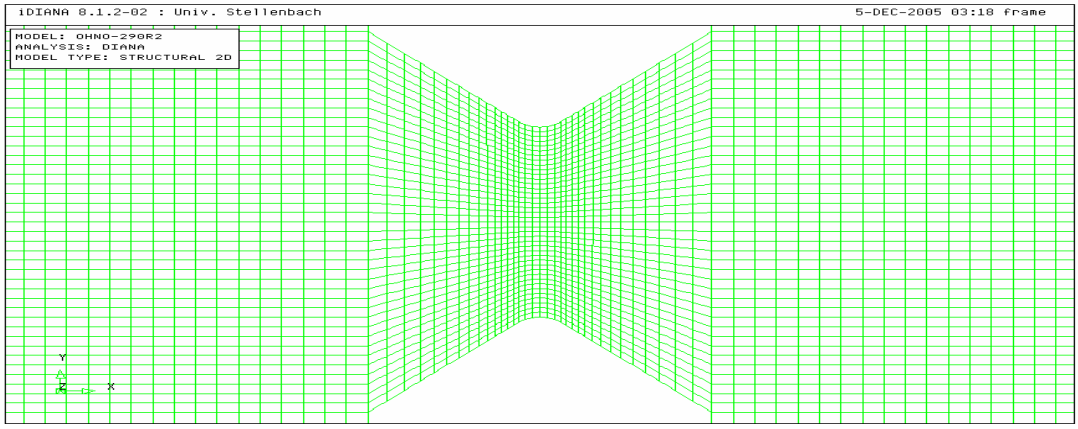

c) Notch radius = 3.5 mm

Figure 4.22 Finite element meshing for different notch tip radii.

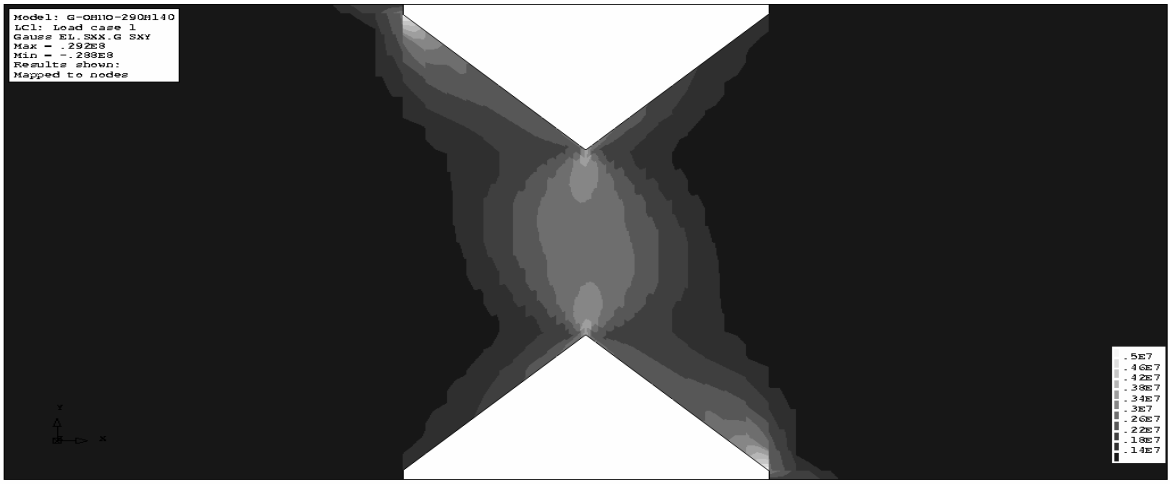

a) Notch radius = 0 mm

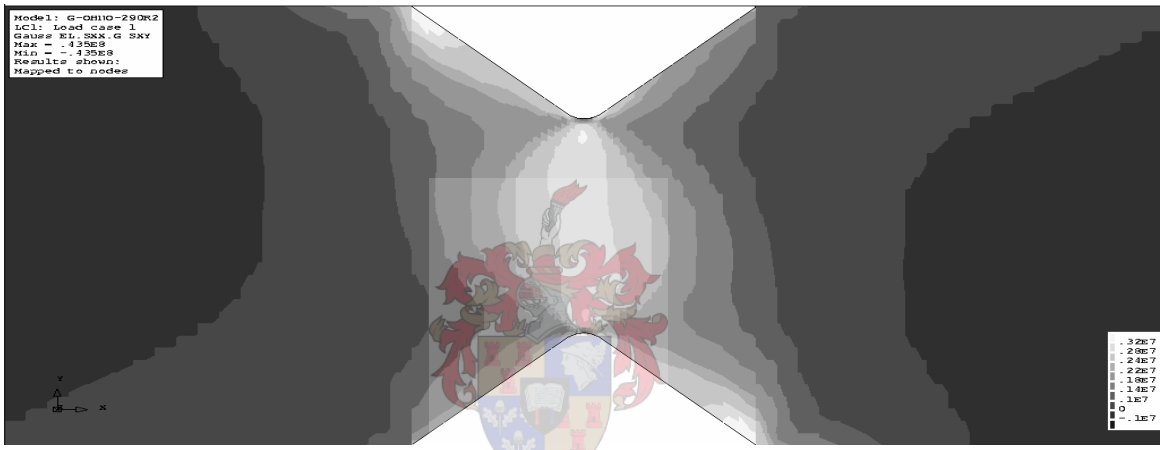

b) Notch radius = 2.7 mm

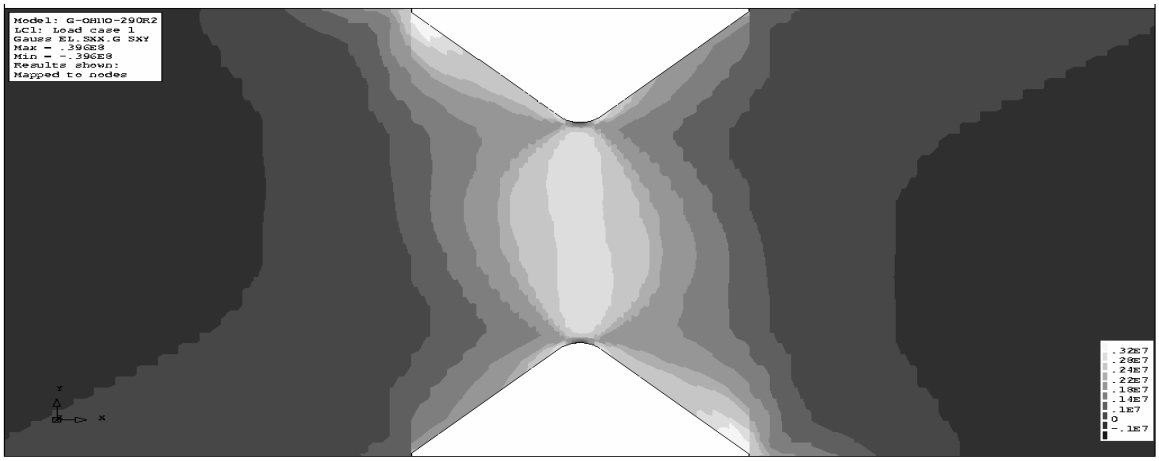

c) Notch radius = 3.5 mm

Figure 4.23 Shear stress contours for different notch tip radii. (The stress unit is Pa).

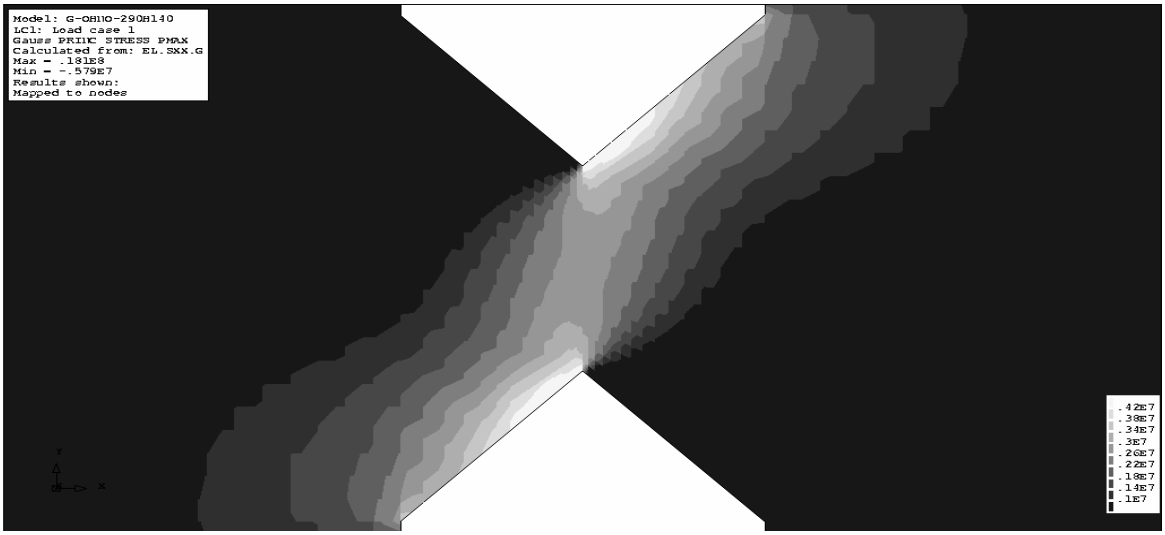

a) Notch radius = 0 mm

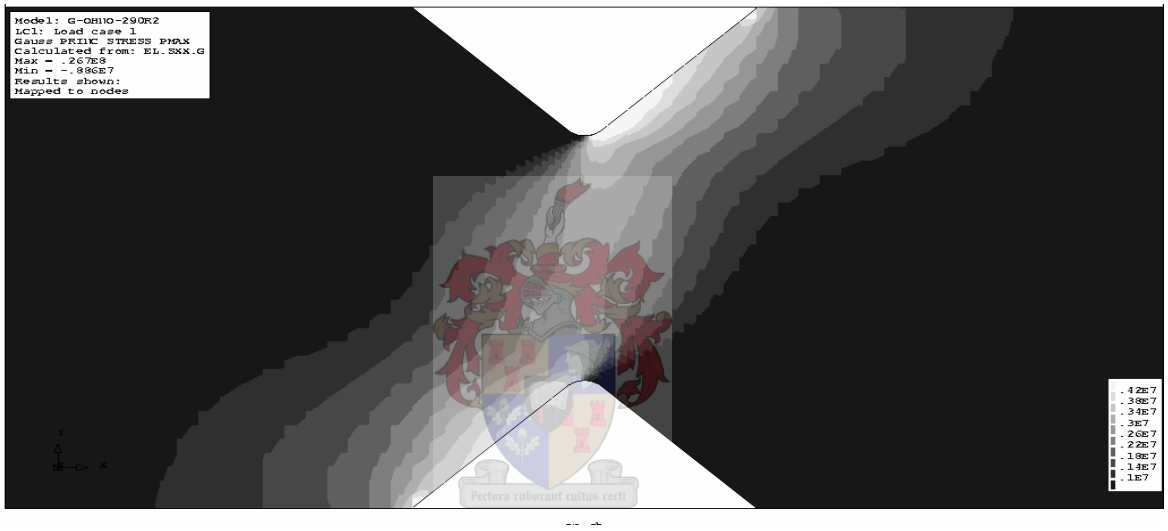

b) Notch radius = 2.7 mm

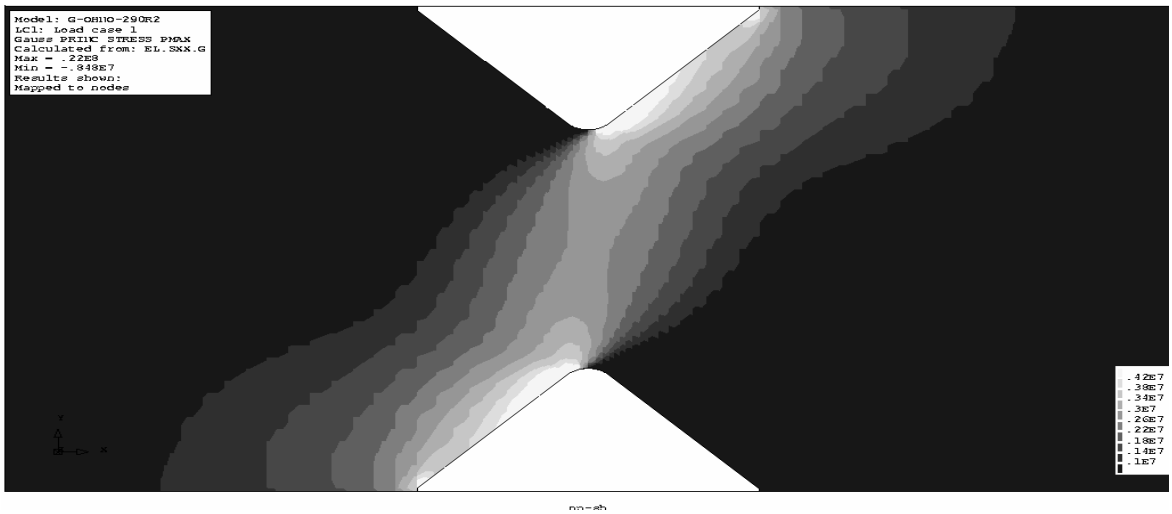

c) Notch radius = 3.5 mm

Figure 4.24 Principal stress contour for different notch tip radii. (The stress unit is Pa)

The normalised shear stress distribution along middle length (line 1) and the normalised principal stress along line 2 these three models are presented in figures 4.25, 4.26. It can be seen that with increasing tip radius, the shear stress distribution becomes more uniform and the shear stress concentration is reduced at the notch roots.

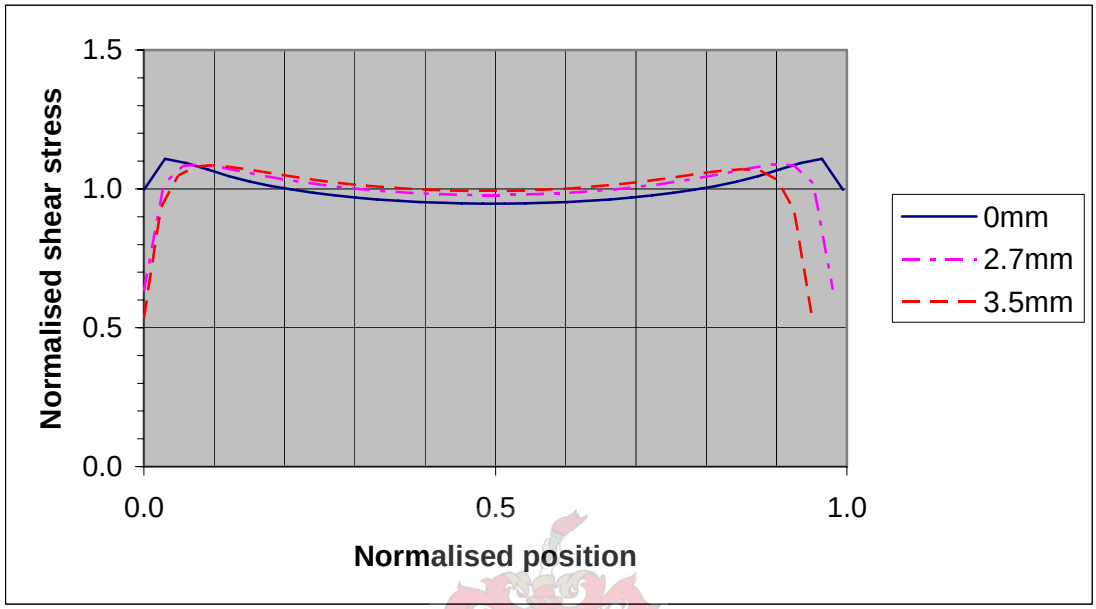

Figure 4.25 Normalised shear stress variations along line 1 for different notch radii

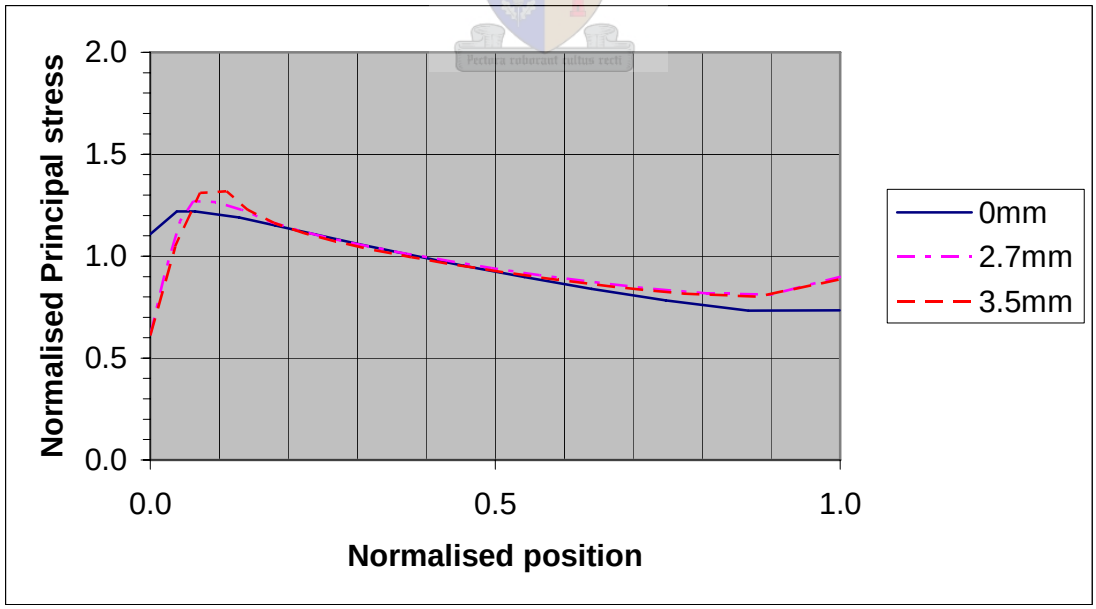

Figure 4.26 Normalised principal stress variation along line 2 for three different notch radii

However, the maximum principal stress moves away from the notch root with increasing tip radius as shown in the figure 4.24. The model with r = 2.7 mm is chosen as a compromise between a uniform shear stress along the centre line and the position of failure. However, this radius has been slightly adjusted to more or less the value 3mm, when the moulds were manufactured in the workshop.

4.5 Conclusion

A process of analytical and numerical design of an Iosipescu shear test specimen for ECC has been performed. This has led to the final geometry:

1) The length of total specimen: 280 mm
2) The total height of specimen: 140 mm
3) The distance between inner load points: 80 mm
4) The distance between inner load points and notch edge: 20 mm
5) The notch angle: 90-degree
6) The depth between two notch roots: 36 mm
7) The notch tip radius: 3.0 mm.

The criteria were uniform shear stress distribution along the notch section and ensure of failure in that section, indicated by the maximum principal stress as close as possible to the notch root. Also, a stress concentration always existed in the end of the notch edge. For reducing these stress concentrations, a smooth arc was made in that area. Eventually, the configuration of the specimen as shown in figure 4.27 is chosen.

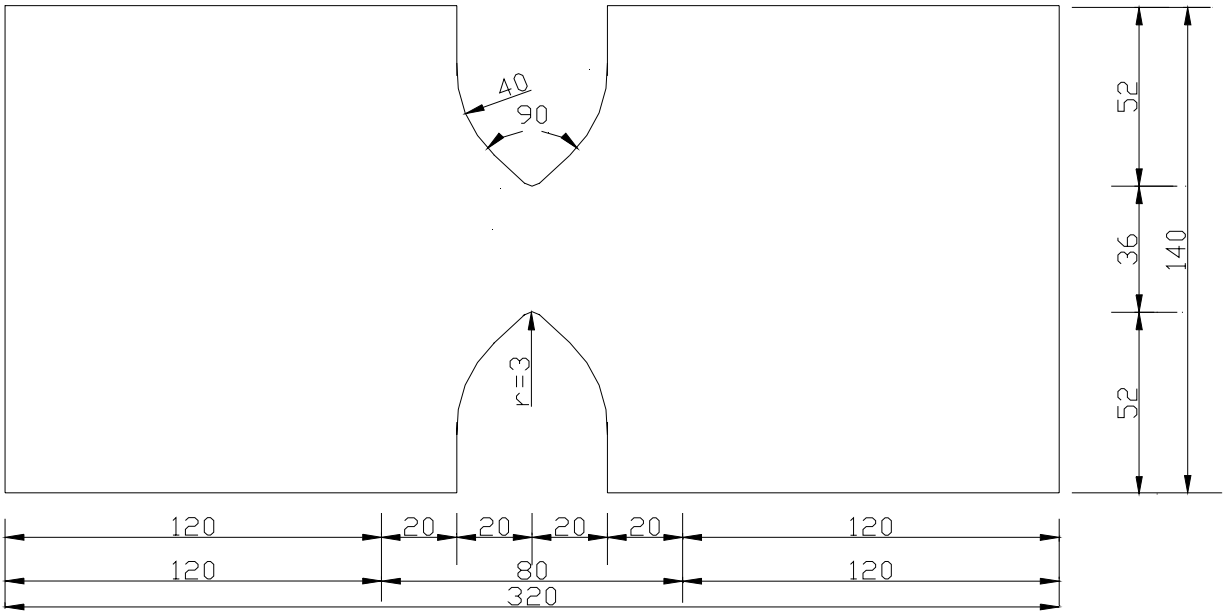

Figure 4.27 Configuration of ECC Iosipescu shear test specimen.

In addition to the parameters determined through the foregoing sensitivity study, a new shaped notch has been chosen. Note that this does not alter the parameter study, but reduces the danger of spalling/splitting of the corners of the notch close to the load point.

In the next chapter, this specimen will be used in shear experiments.

Chapter 5
Experimental programs

5.1 Introduction

In the previous chapters, the Iosipescu shear test method and specimen geometry for ECC were chosen and designed in theory. It must be implemented in practice to verify whether it effective expresses the shear behaviour of ECC.

In this chapter, an experimental program that includes the mix materials, proportion, casting and curing of specimens, test methods and testing procedure is introduced. The shear behaviour of FRC (fibre reinforced concrete) is influenced strongly by its tensile property after the first cracks, which has been described extensively in the literature (Li et al, 1992, Kabele et al 2003). The most important reason for this is that the behaviour of materials is dominated by the pull-out of fibre from the matrix after the material cracks. Therefore, the uniaxial tensile test is also included in this experimental program. The whole experimental program is conducted in the concrete laboratory of Structural Engineering Division, Stellenbosch University.

5.2 Mix proportion

As a new class of HPFRCC mentioned in chapter 2, there are many types of ECC that have been developed depending on the different application purposes. In this study, FA and Slag-ECC as mentioned in the chapter 2 are used as a base mix proportion for this study. The cement content, FA content, and slag content of total binder are fixed. Various fibre volume fractions as the most important factor influencing the property of ECC, are investigated. The detailed mix proportion is shown in table 5.1.

It should be noticed here that the admixtures such as Superplasticizer and Viscous agent are added by mass proportion of total binder. Fibre content is expressed as the volume of fibre as a percentage of the volume of the whole mix. The water to binder ratio is 0.4 in all the mixes.

Table 5.1 Mix proportion design

Nr	Binder							V_f	W/B
	CEMI 42.5	FA	Slag	SP Type	SP Content	Sand	VA	Fibre content (PVA)	
S1	0.50	0.45	0.05	A200	1.0%	Philippi sand	0.25%	0%	0.40
S2	0.50	0.45	0.05	A200	1.0%	Philippi sand	0.25%	1.0%	0.40
S3	0.50	0.45	0.05	A200	1.0%	Philippi sand	0.25%	2.0%	0.40
S4	0.50	0.45	0.05	A200	1.0%	Philippi sand	0.25%	2.5%	0.40

5.3 Materials

5.3.1 CEMI 42.5

Portland cement is a hydraulic cement consisting essentially of hydraulic calcium silicates. The cement is composed of a heterogeneous mixture of several compounds; the hydration process consists of reactions of the anhydrous compounds with water occurring at the same time. The hydrations of some components are faster, while others follow later, producing a family of calcium silicate hydrates. This is currently named CEM in accordance with international practice, specifically CEMI 42.5.

5.3.2 Slag

Slag is a potential hydraulic material with a low hydration speed. The reactivity of slag in a cementitious system depends not only on the chemical components, but also on its fineness. Slag can be divided into two types, Ground Granulated Corex Slag (GGCS) and Ground Granulated Blast furnace Slag (GGBS) according to the different production processes. Both types of slagment are by-products of steel manufacturing. GGBS is alternated from grinding Blast furnace slag, while GGCS is the ground product of slag from the Corex process of steel manufacturing. One particular source of GGCS is the Saldanha steel manufacturing company in the Western Cape, South Africa. GGBS is usually cheaper than GGCS because of the beneficial influence of the latter on concrete strength and ductility (Alexander et al., 2003). In

this research, only GGCS is used.

5.3.3 Fly ash (FA)

FA is extracted by electrostatic precipitators from the flue gases of furnaces fired with pulverized coal in coal burning electricity generation plants. It is one of the most important cost reducing materials used in concrete. The FA used in this research is Pozz-Fill supplied by Ash Resources (Ash Resoures, 2005). The particles size is about 74% below 100um with 52% less than 45um. Most are of perfect spherical shape. Usually, the main constituents or elements of fly ash are heterogeneous glassy and crystalline phases of aluminium, silicon, iron, calcium and magnesium, depending on the component ions in the parent coal (Gao, 2005). Oxides of elements of current FA are shown in Table 5.2 as obtained by XRF analysis. With the FA used in the current research, the chemical content of SiO_2 and Al_2O_3 amounted to 85%.

Table 5.2 Chemical component of FA used in current research (Gao Song, 2005)

LOI*	Sum	Al_2O_3	CaO	Cr_2O_3	Fe_2O_3	K_2O	MgO	MnO	Na_2O	NiO	P_2O_5	SiO_2	TiO_2
1.77	100.74	28.10	4.93	0.003	3.97	0.71	1.36	0.09	0.70	0.02	0.38	57.22	1.49

*Note, the LOI is the loss on ignition.

5.3.4 Sand

The Aggregate used in the research is Philippi sands originating from the Western Cape Province. It is dune sand, of which the poor grading is usually improved for concrete application by blending it with other sand, for instance crusher dust. In this study, Philippi sand was sieved in the grading according to American standard F95 for PVA-ECC mixes.

5.3.5 Superplasticizer (SP)

A200 types of superplasticizer (SP) supplied by ChrySo were used in this research. SP improves the mix workability significantly and, subsequently affects the matrix flaw number, flaw size and flaw spatial distribution, as well as fibre distribution. Matrix flaw and fibre distribution both control tensile strain and stress. Fibre distribution is considered as an

extremely important factor to determine ECC performance, because materials will always fail at fibre disconnections. Poor workability provides a weak matrix and affects fibre distribution.

5.3.6 Viscous agent (VA)

Another admixture in this experiment, namely the viscous agent methyl cellulose (MC), was added into the fresh mortar to provide good rheology and also even fibre distribution. The former is necessary for heavy fibres to be placed into the moulds and vibrated without the fibre settling on the bottom of the specimen. Also, for less heavy fibres, such as PVA fibre, MC enhances good fibre distribution in the matrix, an essential feature for good strain-hardening ECC.

5.3.7 Polyvinyl alcohol (PVA) fibre and steel fibre

In the present study, Polyvinyl alcohol fibre (PVA) is produced by Kuraray Co., Ltd., Japan. PVA fibre is hydrophilic, therefore, the strong bond between the matrix and fibre tends to break the fibre rather than pull it out of the matrix. This bounds the multiple cracking and leads to less or no strain hardening. To overcome this, PVA fibre is currently oil coated. Such treated fibres slip in the matrix, rather than break (Li et al. 1997). The physical properties of PVA fibre are listed in Table 5.3. Figure 5.1 shows the SEM photo image of the surface of PVA fibre.

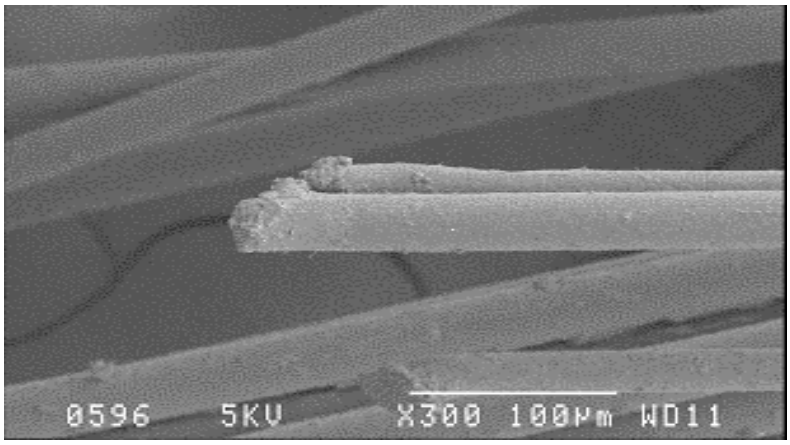

Figure 5.1 The surfaces of PVA fibre (Gao Song, 2005)

Table 5.3 Geometry and physical properties of PVA fibre

Fibre type	Length (mm)	Diameter (um)	Elasticity modulus (kN/mm)	Ultimate strain	Tensile strength
PVA	12	40	40	6%	1600N/mm^2

5.4 ECC mixing procedure and cast procedure

The tensile testing specimens (also called dog-bone specimen) and shear testing specimens were cast in the moulds with different configuration. The dog-bone specimen is shown in figure 5.2. The size was 230 mm (length) x 60 mm (width) x 15 mm (thickness). The neck section was 30mm wide. The configuration of the shear testing specimen has been discussed in the previous chapter. The configuration of figure 4.25 is used for the size of the testing specimen. All cast mixes were mixed by 'cake'–mixer.

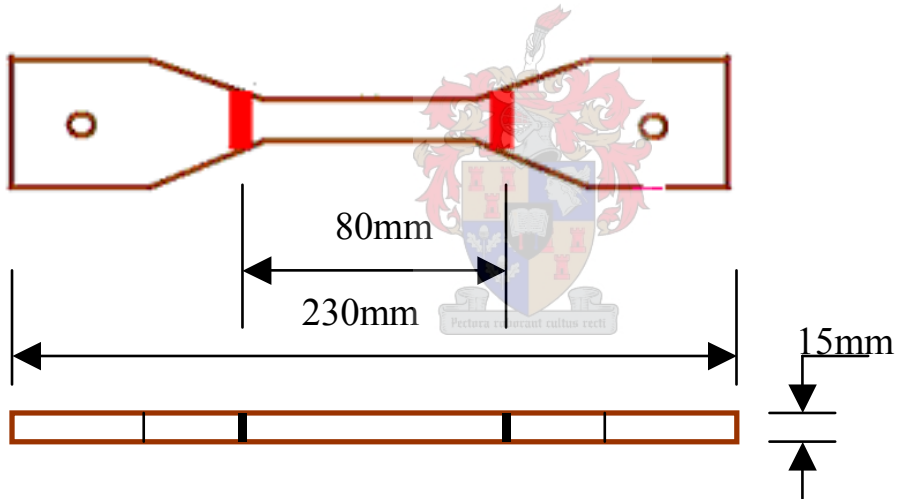

Figure 5.2 Configuration of Dog-bone specimen and LVDT frame clamp positions

Prior to mixing, all ingredient materials are weighed off separately. The PVA fibre is blown by 4 bar air pressure in a specially prepared bin to separate the fibre. Subsequently, the fibre is pre-wetted with 10 percent of the total water. All dry materials except PVA fibre are thrown into the 'mixer' for the dry mix with minimum speed. After 30 seconds of dry mixing, the remaining 90% water is added into the mixer. The mixer speed is increased gradually to maximum speed. SP is added into 1 minute after the water is added. The final step of the mixing procedure is to add the damp PVA fibre into the mixer. The mixture is mixed at a high speed for another minute. The whole mixing procedure is shown in figure 5.3.

After mixing is completed, the fresh mix is first poured into the middle region of each

dog-bone moulds and shear specimen moulds, which can cause a better quality specimen and avoid the fibre becoming blocked at the notch area in the shear testing specimen. The specimens are vibrated for approximately one minute in their moulds.

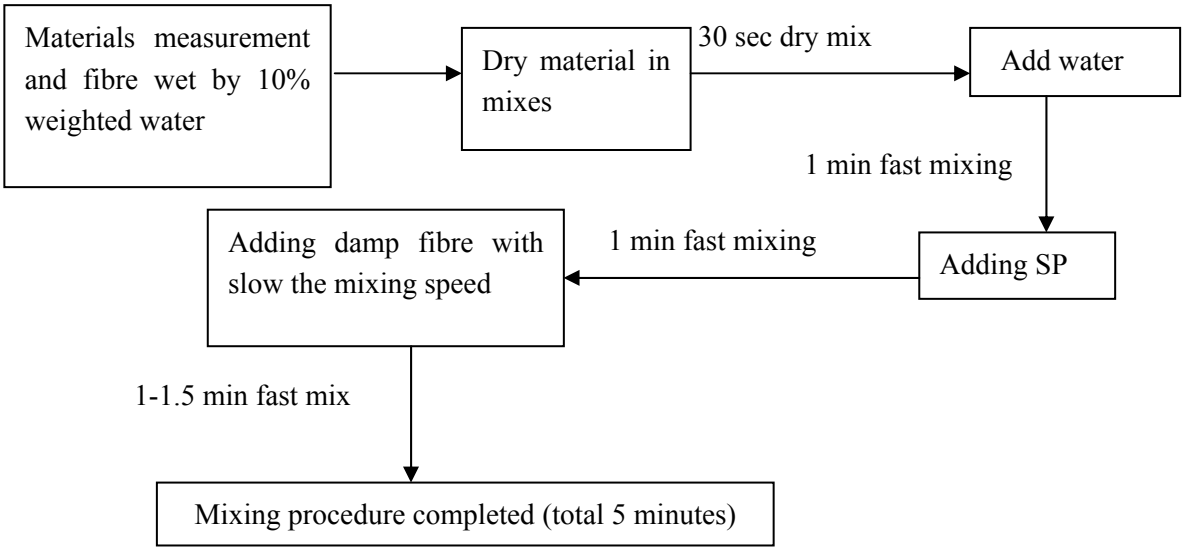

Figure 5.3 Flow chart of PVA fibre-ECC mixing

5.5 Curing procedure

The curing procedure of the specimen is shown in figure 5.4. All dog-bone specimens and shear testing specimens are stripped at the age of two days and then promptly taken into constant temperature (23℃) water to cure. The specimens are taken out and kept for 3days in a controlled climate of 23±2^{0}C temperature and RH 60±5% room before testing.

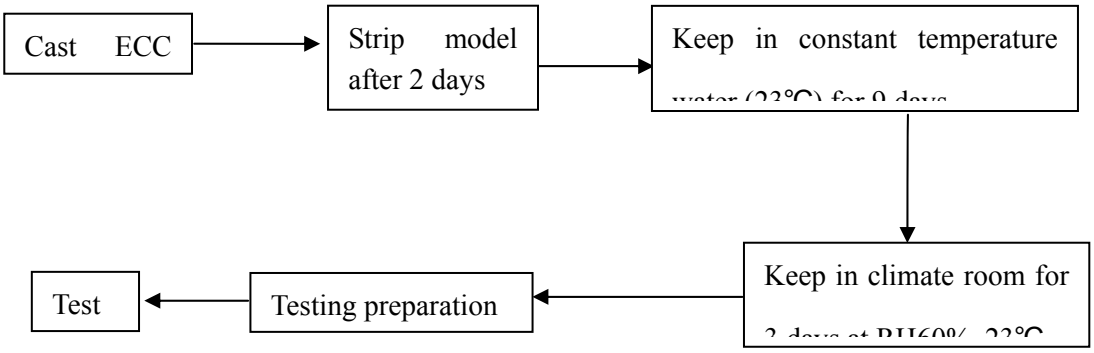

Figure 5.4 Curing procedures

5.6 Test method

Both the Uniaxial tensile tests and the shear tests are carried out for ECC in a mechanical testing apparatus (Zwick Z250). A Spiderman8 data collecter connected to a computer is used to record the test results. In each case, the test conditions and testing procedure are introduced as following.

5.6.1 Uniaxial tensile test

The uniaxial tensile test specimens were tested under a constant displacement rate of 1.5 mm per minute in the testing apparatus. The specimen was fixed on the Zwick apparatus by two clamps. Two linear variable differential transducers (LVDT's) with a gage length of approximately 80mm were used to measure tensile deformation on the specimen surface. An aluminium frame was used to fix the LVDT's on the specimen surface. A 500kg load cell was used to measure the force. The uniaxial tensile test set up is shown in figure 5.5.

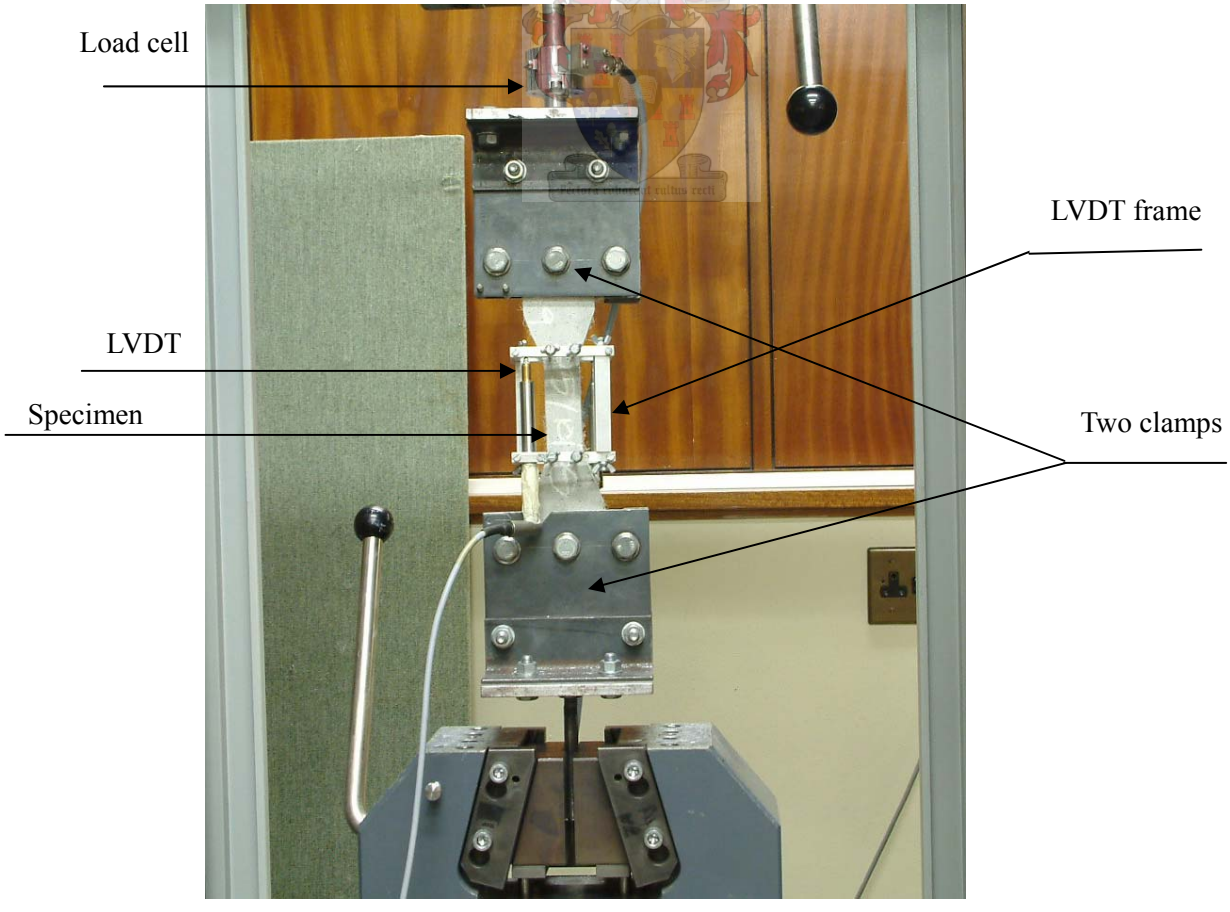

Figure 5.5 The direct tensile test set-up

The uniaxial tensile test process is summarized as follows:

Step 1: all the dust on the surface of a specimen is carefully cleared away; the accurate thickness and width of specimen neck are measured by vernier calliper.

Step 2: two LVDT's are fixed in a custom built frame on the specimen surface. The distance between the top and bottom of the LVDT frame is measured by vernier calliper.

Step 3: the specimen is encased in the upper clamping on the Zwick apparatus and is tightened in it. The bottom clamp is raised until the hole through the clamping was directly in line with the hole in the specimen. Then, the specimen and clamping are tightened with six twist drills.

Step 4: the LVDT's are connected to the Spiderman8, and the reading of loading and displacement is set to zero in the computer. Subsequently, the testing is started.

The test data are collected by a specialised computer program called Catman. The tensile stress is calculated as the force measured by the 500 kg load cell divided by the neck cross-section area. The tensile strain is calculated as the average variational distance registered by the LVDT divided by the distance between the top and bottom of the frame. Thus, the tensile stress-strain curves are obtained.

5.6.2 Iosipescu shear test

According to the Iosipescu shear test mechanism, the specimens are put on the support frame of the Zwick apparatus; a vertical load from the Zwick apparatus is translated to two loads applied on the specimen top by a load beam. The load beam consists of a connection, a beam, and two load points. A connection with four screws is used to connect the load beam with the Zwick apparatus. Four screws are used to set the distance between the load beam and the specimen more accurately. The load beam is made of steel that has adequate high stiffness relative to the specimen. The load points are two half steel cylinders with radius r=50mm that are connected to the beam. The Iosipescu shear test set up is shown in figure 5.6.

To improve this new shear test method gradually, the tests are carried out in three phases. The

aim of the first phase is to check if the failure of the specimen is a pure shear failure. The second phase is to obtain the shear stress and shear strain of the specimens with the pure shear failure mode, measured by the load cell and a strain gage. In the third phase, the strain-hardening property of ECC is measured by a LVDT. Each phase of the test is summarized here.

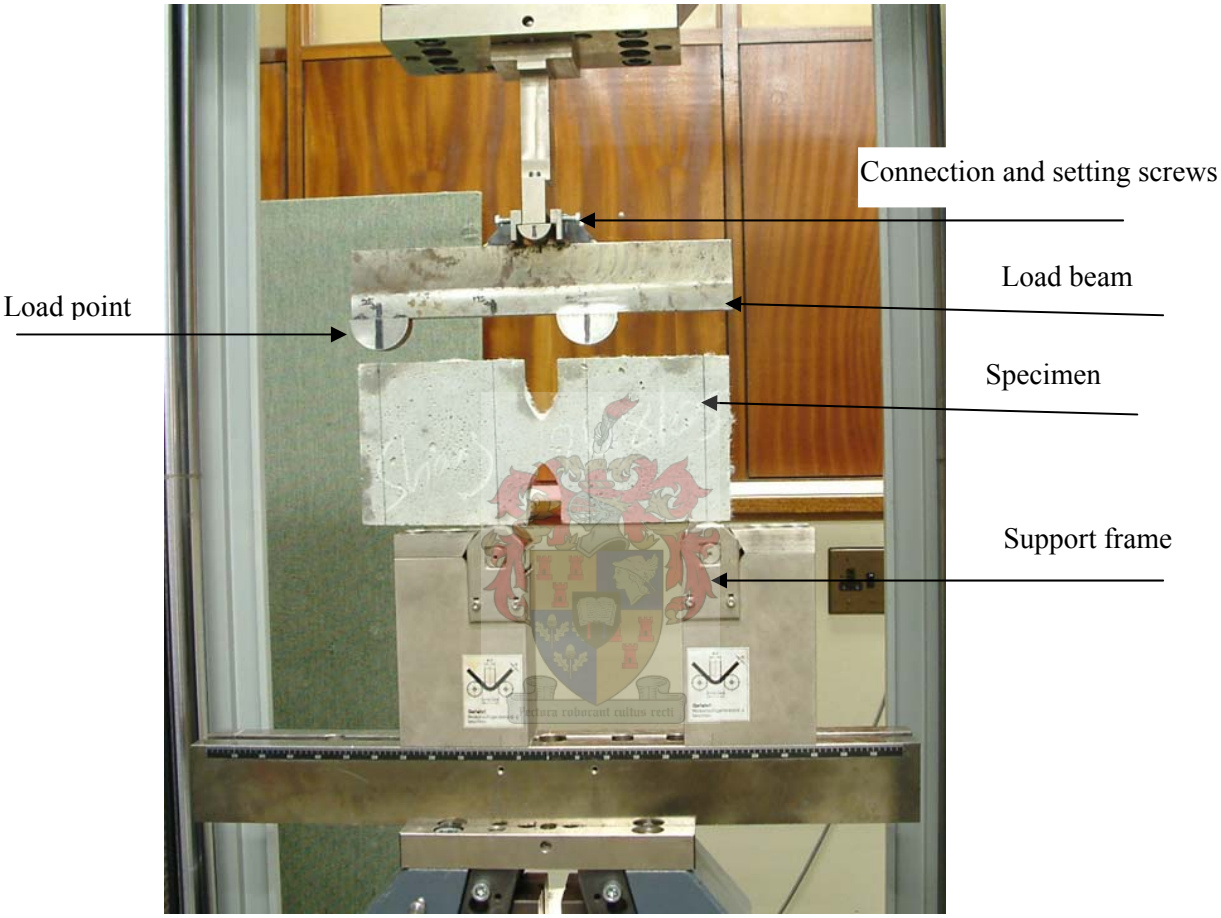

Figure 5.6 The Iosipescu test set-up

The first phase

In the first phase, the test is only conducted on the Zwick apparatus. A computer connected with the Zwick apparatus records the loading and the deflection of middle-line. The procedure of the test is as following:

Step 1: all the dust on the surface of a specimen is carefully cleared away; the top and bottom sides are smoothed with sand paper.

Step 2: the position sign of the load points and the support point are drawn on the surface of

specimen, and the notch depth and thickness of specimen are measured accurately by vernier calliper.

Step 3: the load beam is connected to the Zwick apparatus; the specimen is put on the support frame of Zwick apparatus.

Step 4: the specimen and the load beam are set in the one plane, to make the two load points on the top of the specimen load position sign.

Step 5: the specimen is raised carefully to touch the load beam, the position of the specimen in relation to load points is set precisely by the screws of the load beam.

Step 6: the reading of the computer is set to zero, and the test is started.

Whereas the first phase has the sole purpose of establishing whether the failure is indeed in pure shear, the second phase is intended for accurate measurement of the shear deformation.

The second phase

The second phase is more complex than the first phase. The stacked rosette strain gage is used to measure the strain of the specimen. Again, the Spiderman8 connected with a computer is used to record the test results. It is necessary to introduce the mechanism of the strain gage before describing the procedure of testing.

Consider an array of two strain gages oriented at arbitrarily different angles with respect to an X-Y coordinate system, which, in turn, is arbitrarily oriented with respect to the principal axes, as illustrated in the figure 5.7

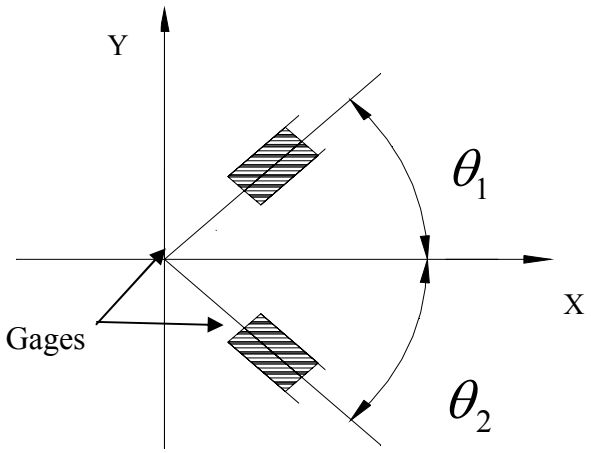

Figure 5.7 Arbitrarily oriented strain gages in x,y coordinates

From elementary mechanics of materials, the strains along the gage axes can be written as:

$$\varepsilon_1 = \frac{\varepsilon_x + \varepsilon_y}{2} + \frac{\varepsilon_x - \varepsilon_y}{2}\cos 2\theta_1 + \frac{\gamma_{xy}}{2}\sin 2\theta_1 \tag{5.1}$$

$$\varepsilon_2 = \frac{\varepsilon_x + \varepsilon_y}{2} + \frac{\varepsilon_x - \varepsilon_y}{2}\cos 2\theta_2 + \frac{\gamma_{xy}}{2}\sin 2\theta_2 \tag{5.2}$$

Subtracting (5.2) from (5.1) and solving for γ_{xy} :

$$\gamma_{xy} = \frac{2(\varepsilon_1 - \varepsilon_2) - (\varepsilon_x - \varepsilon_y)(\cos 2\theta_1 - \cos 2\theta_2)}{\sin 2\theta_1 - \sin 2\theta_2} \tag{5.3}$$

It is now noticeable that if $\theta_1 = -\theta_2 = 45°$, then, Equation (5.3) becomes:

$$\gamma_{xy} = \varepsilon_1 - \varepsilon_2 \tag{5.4}$$

In this experiment, the $0^0/90^0/45^0$ rosette strain gage with diameter = 21 mm is stuck on the centre surface of specimen symmetrically. Because of the pure shear state, only two gages are used to measure the principal tensile strain (ε_1) and principal compressive strain (ε_2), as shown in the figure 5.8.

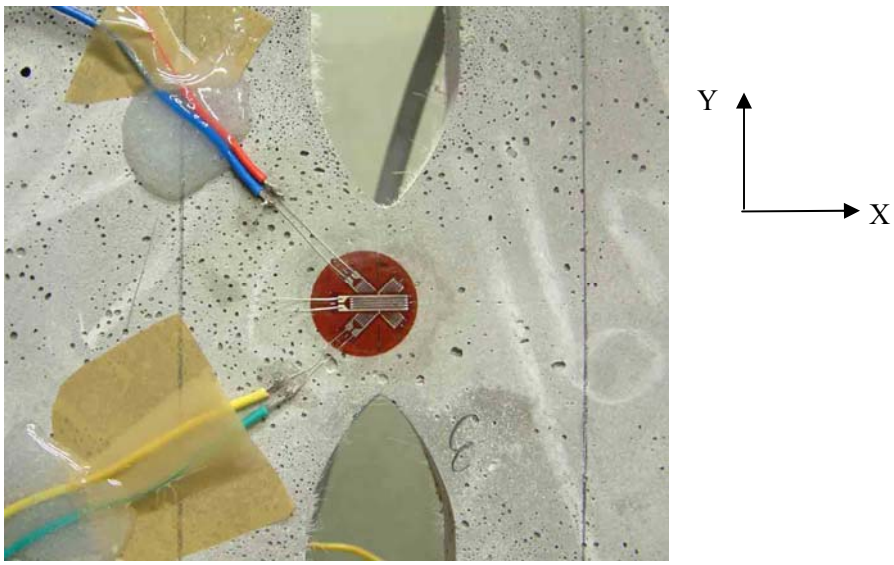

Figure 5.8 The strain gauges stuck onto the surface of specimen

Two full bridge connections are used to translate the varying resistances of strain gages to the Spiderman8.

The procedure of testing can be summarized as follows:

Step 1 and step 2 are same as the first phase

Step3: according to the specification of strain gages from the manufacturer, the stain gages are stuck on the surface of specimen carefully. The full bridge connections are made by resistances and cables.

Step 4 is the same as step 3 of the first phase

Step 5: connect the strain gage, the full bridge connection, and Spiderman8, and check that each circuitry is connected.

Step 6 and step 7 are the same as step 4 and step 5 in the first phase

Step 8: set the reading of computer program to zero. Start testing

The test data are collected by the catman computer program in the same way as the uniaxial tensile test. The average shear stress in the specimen is calculated as the shear force at the specimen centre line divided by the notch cross-section area. The two principal strains can be obtained from the testing data directly. Thus, the shear stress-strain curves are obtained.

The third phase

The data-reduction relationships used with the rosette strain gages are derived from the strain-transformation equations. Eqs. (5.1), (5.2), (5.3), (5.4)], which are based on “small-strain” theory. Therefore, it cannot reflect the strain-hardening behaviour of ECC. A new measurement method is desired. According to the experimental conditions at present, the principal tension strain measured by LVDT is regarded as a convenient and more accurate method to measure the trends of shear deformation of ECC.

To fix the LVDT, two square plastic plates are glued on the surface of the specimen. The LVDT goes through the centre of the specimen at 45-degree to the longitudinal (x) axis. The distance between the two plastic plates is approximately 25mm. The LVDT measurement detail is shown in the figure 5.9.

Figure 5.9 LVDT fixed on the surface of specimen

The procedure of testing in this phase is summarized as follows:

Step 1 and step 2 are the same as the first phase

Step 3: drawing of the measurement region, and glue two plastic plates on the surface of specimen.

Step 4: after the glue has dried (approximately 1– 2 hours), fix the LVDT between two plates.

Step 5 to Step 8 is the same as step 3 to step 6 in phase 1.

The collection of testing data is as same as for the uniaxial tensile test. The calculation of shear stress in this phase is the same as for the first and second phases. The principal tensile strain is calculated as the change in gauge length distance, measured by the LVDT, divided by the original distance between the two plates.

Chapter 6
Experimental result and analysis

6.1 Introduction

In the previous chapters, the experimental program has been introduced. The result and analysis of testing are presented in this chapter.

The analysis process of result of testing is according to the three phases of the experimental program as mentioned in the previous chapter. In the first section, the failure modes of four types of specimens are presented and analysed by photo of crack pattern and shear stress versus vertical displacement. Subsequently, the strain gauge rosettes are stuck on the surface of proper shear test specimens to investigate the relationship between shear stress and shear strain. The uniaxial tensile testing is also conducted in this section to compare the differences between shear and tensile behaviour of specimens. Due to the limitation of strain gauges, the LVDT's are used to predict the development of shear strain in the third section. The conclusions are presented in the last section.

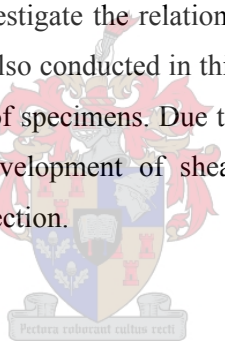

6.2 First phase

6.2.1 Failure mode

As discussed in the previous chapters, the failure modes of specimens influence the accuracy of shear test result markedly, i.e. the more pure shear failure model can indicate the more accurate shear behaviour of material. Crack development of cement-based material is the most important criterion to distinguish the failure type of specimens (Li, 1994). Therefore, the first phase of experimental program focuses on the study of failure type of specimens.

The typical model of failure for the case of S1 (called plain cementitious materials) can be seen in figure 6.1. The first cracks to appear are marked as point A (see figure 6.1) which seem to initiate on the symmetry point of the middle line at the same time. Two first crack points are 1-1.5 mm away from the notch tip. After first cracks occur, two cracks develop quickly on the surface of specimen with inclined direction and the width of two cracks also increases rapidly (see line 1 in the figure 6.1). The specimens indicate almost instantaneous

failure following the first cracks. The failure is always the 45^0 aligned crack which form perpendicular to the maximum principal stress direction.

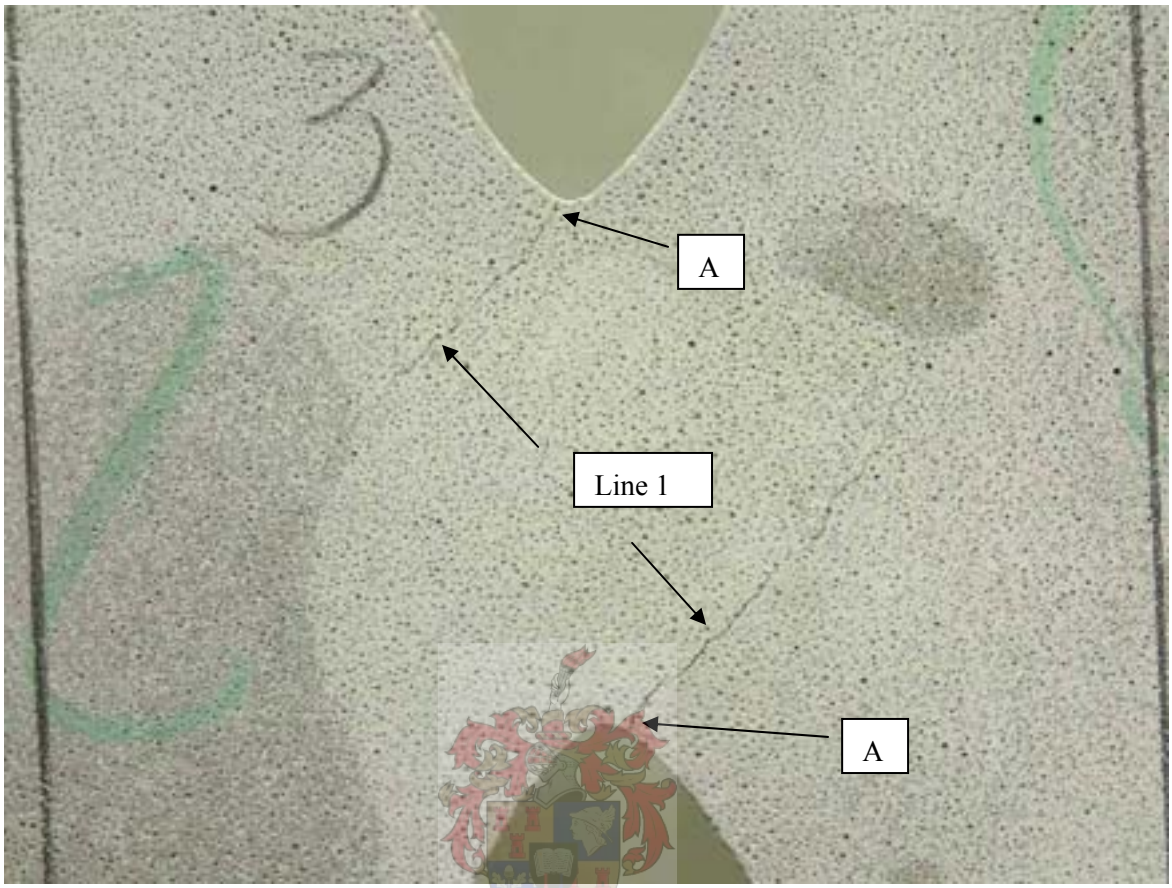

Figure 6.1 Typical failure mode for S1specimens

According to the development process of this crack pattern, it can be noticed that the failure mode of the specimens are more dominated by shear before the first cracks occur. With the development of inclined cracks, the failure model is dominated by the shear and flexure, as the cracks eventually align vertically. The flexural proportion increases gradually until the specimens break. So, this test method can be regarded as being inapplicable for obtaining the shear behaviour of plain cementitious materials.

The model of failure in S2 (V_f=1%) is different to that of plain cementitious materials as seen in the typical failure patterns of figure 6.2. Often, the first cracks start at the point A (see figure 6.2) which are also on the symmetry points of the centre line, at about 1-1.5 mm from notch tips. After first cracks occur, a few cracks appear on the specimens around the centre line. The first cracks are later arrested after development of a length of about 1 to 1.5 cm. With the development of first cracks, other cracks also propagate on the specimen with inclined direction. The developments of these cracks are slower than the cracks in the S1

specimens. With the adding of load, a main diagonal crack is formed (see line 2 in figure 6.2) and then the specimen fails.

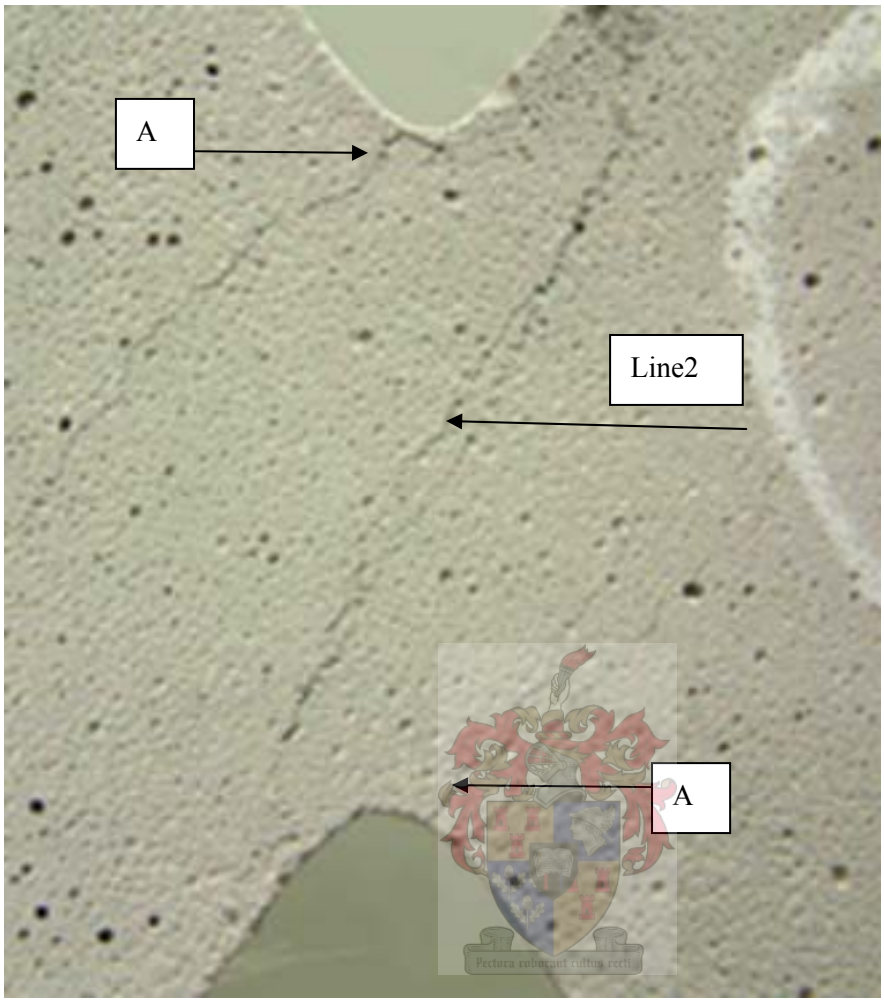

Figure 6.2 Typical failure mode for S2 specimens

As compared with plain cementitious materials, the first cracks of two materials start at the similar position which means the failure model of S2 specimens are also dominated by shear before first cracks. In the S2 specimens, the development of first cracks is slow and arrested later. Several cracks appear. The final failure cracks in the S2 specimen are much closer to the middle line than plain cementitious materials and pass through the middle line. As the final failure crack extends into the flexural region, the failure mode cannot be regarded as a pure shear failure mode. So, this test method also is regarded as being inapplicable for obtaining the shear behaviour of S2 materials.

The mode of failure in S3 specimens (V_f = 2%) is similar to that in the S4 specimens (V_f = 2.5%). However, these failure modes in the S3 and S4 are significantly different from those in the S1and S2 specimens. Figure 6.3 shows the typical failure patterns of S3 and S4. The appearance of first cracks in these specimens are similar to the S1 and S2 specimens, with the

first cracks starting at the point A (see figure 6.3) that is about 1-1.5 mm from notch tips. With the load increased, more micro-cracks appear on the surface of the specimens along the middle line. The cracks are also inclined more than the S1and S2 specimens. The development of cracking is more gradual than in the S1 and S2 specimens. The majority of cracks develop to a length of about 5 mm. Finally, the micro-cracks are connected with a vertical crack, which is situated almost in the middle line (see line 1 in figure 6.3), causing the specimen to fail.

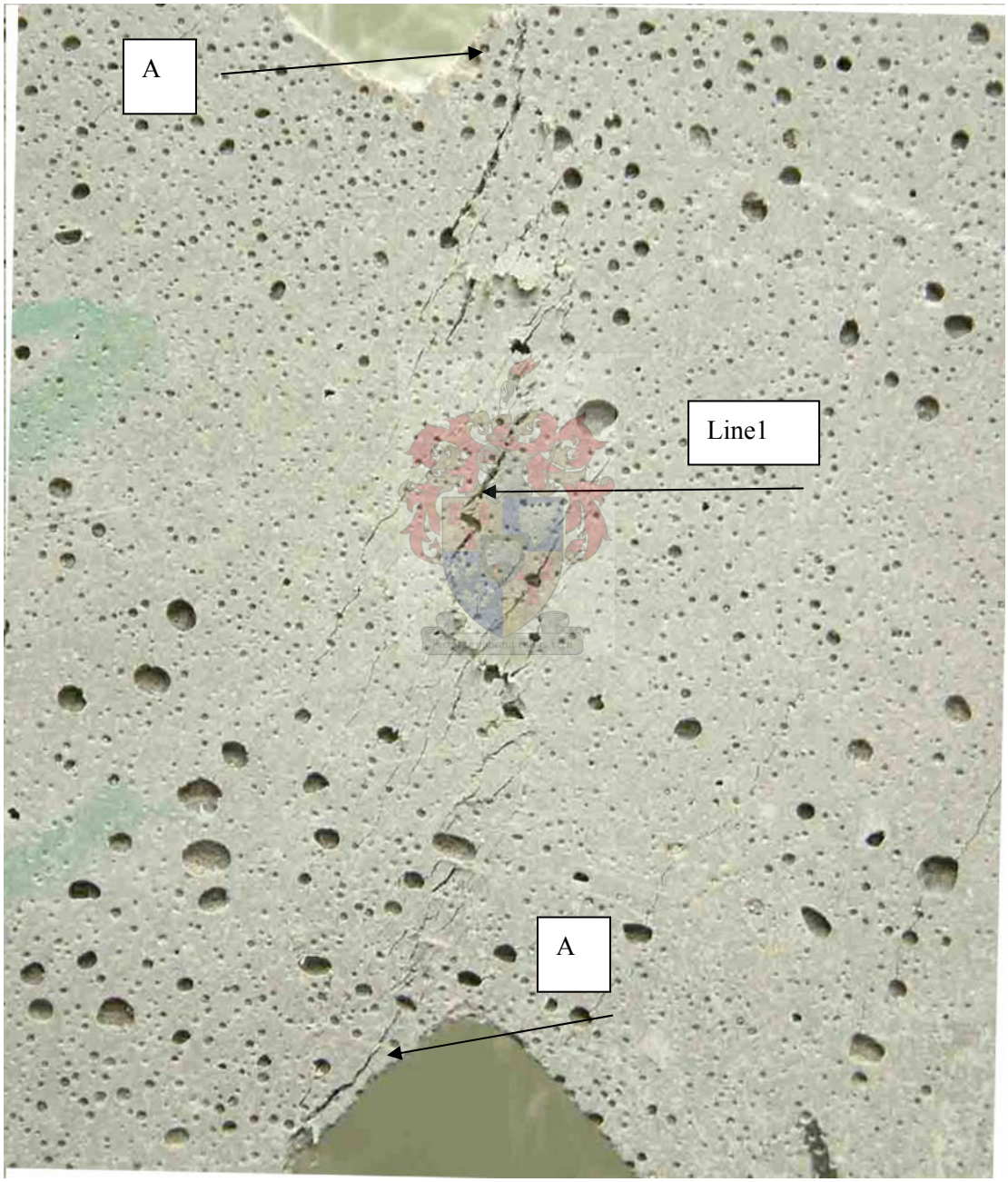

Figure 6.3 Typical failure mode for S3 and S4 specimens

To review the failure process of S3 and S4 specimens, it can be found that the development of cracks from beginning to end are around middle line of specimen that has been considered as

a pure shear region. Therefore, this failure model can be regarded as shear dominated failure mode. This test method is applicable for obtaining the shear behaviour of S3 and S4 specimens.

6.2.2 Shear stress and vertical displacement

In addition to observing the crack pattern of specimens, the relationship between the shear stress and vertical displacement of middle point of the load beam also can be obtained in the first phase. As mentioned in the previous chapter, the average shear strength in the specimen is the shear force at the centerline divided by the cross-sectional area resisting the shear force. The vertical displacement reflects the development of the displacement at the centreline of specimens, which can be obtained from the testing apparatus (Zwick Z250) directly. The relationship between the shear stress and the vertical displacement can indicate the variation of the failure of different fibre content specimens more evident.

Results from the testing of the four groups of specimens are plotted in the form of average shear stress versus average vertical displacement in figure 6.4.

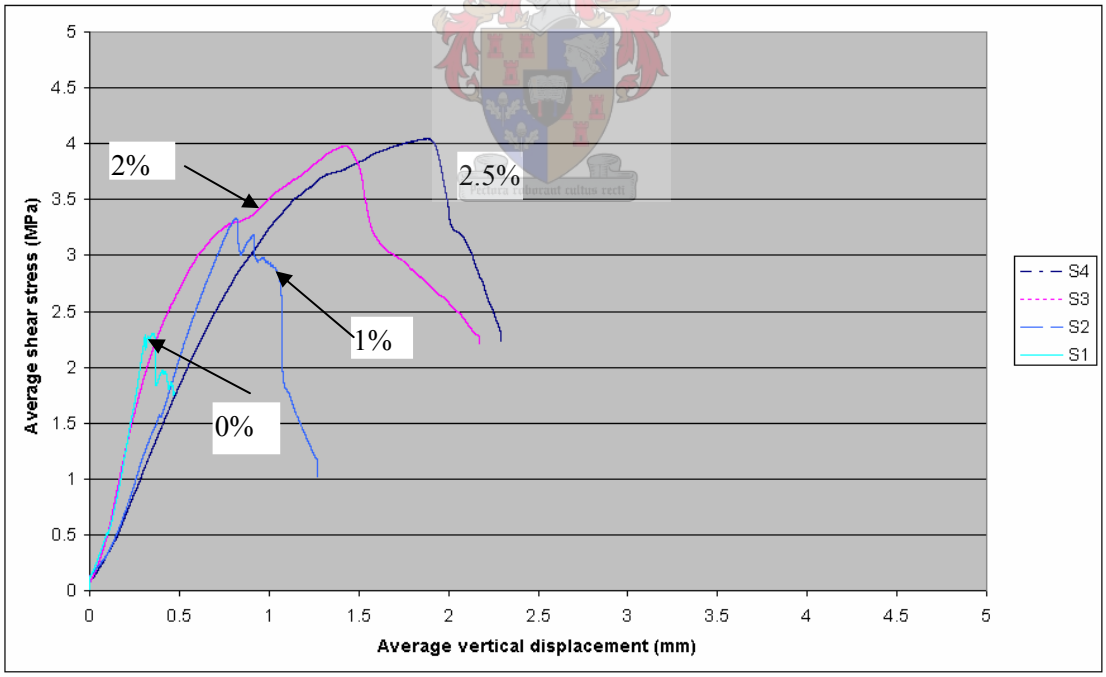

Figure 6.4 Average shear stress versus vertical displacement

It can be observed that the ultimate shear stress of four group materials increase with the fibre content. The stress at which the first cracks occur in the S3 and S4 (V_f=2%, 2.5%) specimens can be easily found (see point A and B in the figure 6.4). Subsequently, the shear stress still increases. The failure process of S3 and S4 can be considered as ductile failure. However, it can be seen that is difficult to distinguish the points of first cracking in S1and S2 (V_f=0%, 1%) specimens in figure 6.4. After first cracks, the shear stress of S1 specimens decreases rapidly. The first crack shear stress is also the ultimate shear stress (see point C in figure 6.4). The vertical displacement evolution in S2 specimens has a few jumps following the first crack. After the ultimate shear stress occurs, the decreasing of shear stress and the increasing of vertical displacement become slower than S1 specimens and faster than S3 and S4 specimens. The first crack shear stress is also close to the ultimate shear stress (see point D in the figure 6.4). The failure process of S1 and S2 specimens can be regarded as brittle failure.

By observing the crack pattern and analysing the relationship between the shear stress and vertical displacement, it can be seen that the specimens with fibre content more than 2% can indicate pure shear failure in linear and non-linear field, and the failure mode can change to ductile. Therefore, S3 and S4 specimens can be regarded as suitable specimens for the ECC Iosipescu test. For these specimens the accurate determination of the shear stress and strain properties are determined through testing, in the next phase.

6.3 Second phase

6.3.1 Strain gauge

From the analysis of last section, the strain gauges are used to analyse the relationship between the shear stress and strain of S3 and S4 specimens. According to the procedure of the experimental program as mentioned in the previous chapter, the three rosette strain gauges are stuck on the surface of specimens of each group materials.

Result from the testing of two groups of specimens is plotted in the form of average shear stress versus gauge normal strains in figure 6.5, 6.6. The calculation of average shear stress has been mentioned in the previous chapter. Gauge normal strains consist of compression strain and tension strain, which come from 45^0 strain gauges. The minus one indicates the compression strain, and the plus one indicates the tension strain. It can be observed that the development of compression strain and tension strain in the two group specimens are similar in elastic range. After ultimate shear stress is reached, the tension strain continues to increase. However, the compressive strain is small. The reason is that the principal tension strain is

dominated by fibre pullout mechanism, but the principal compression strain is dominated by the aggregate interlocking. The interlocking function of specimen weakens rapidly as the cracks of specimen increase after first crack. The principal tension strain can still increase due to the fibres that are slowly pulled out from the matrix.

According to the elastic theory, the strains of the symmetrically placed off- axis gauges ($\pm 45^0$) are equal in magnitude and opposite in sign in elastic range (Sullivan, et al. 1988). However, it can be see in the figure 6.5, 6.6 that the compression strain and the tension strain are not symmetric before the first crack. The testing error can be regarded as the major reason to cause this difference.

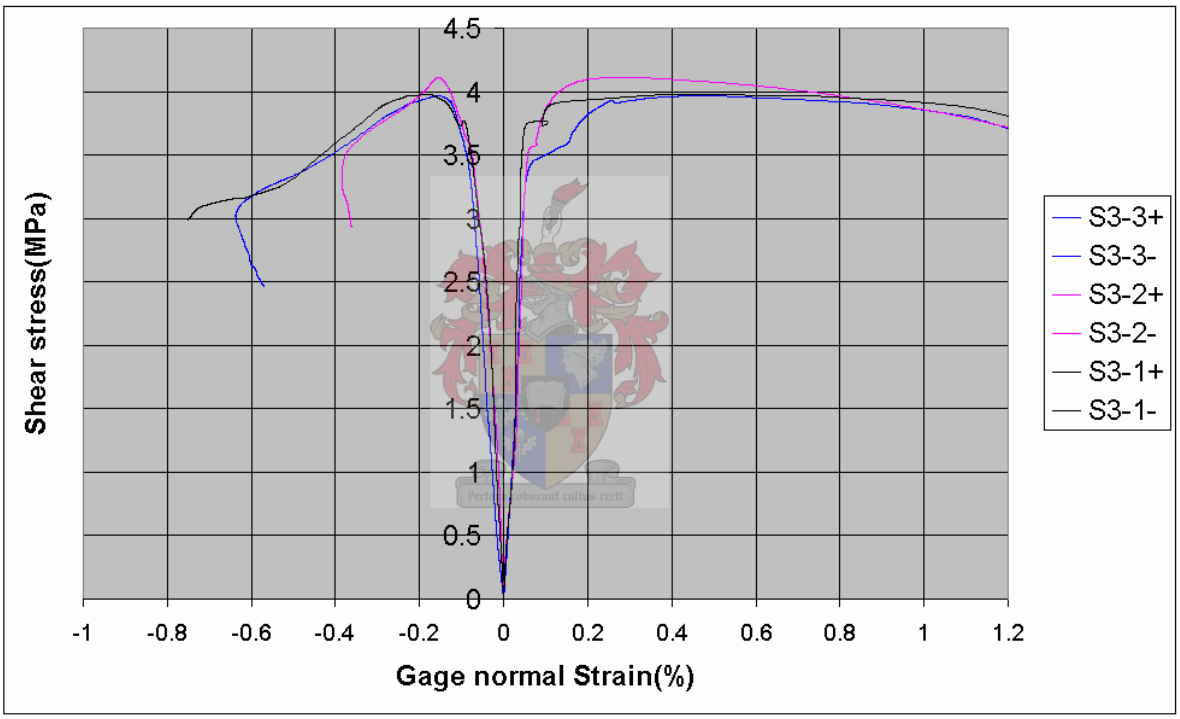

Figure 6.5 Shear stress versus strain gauge normal strain in S3

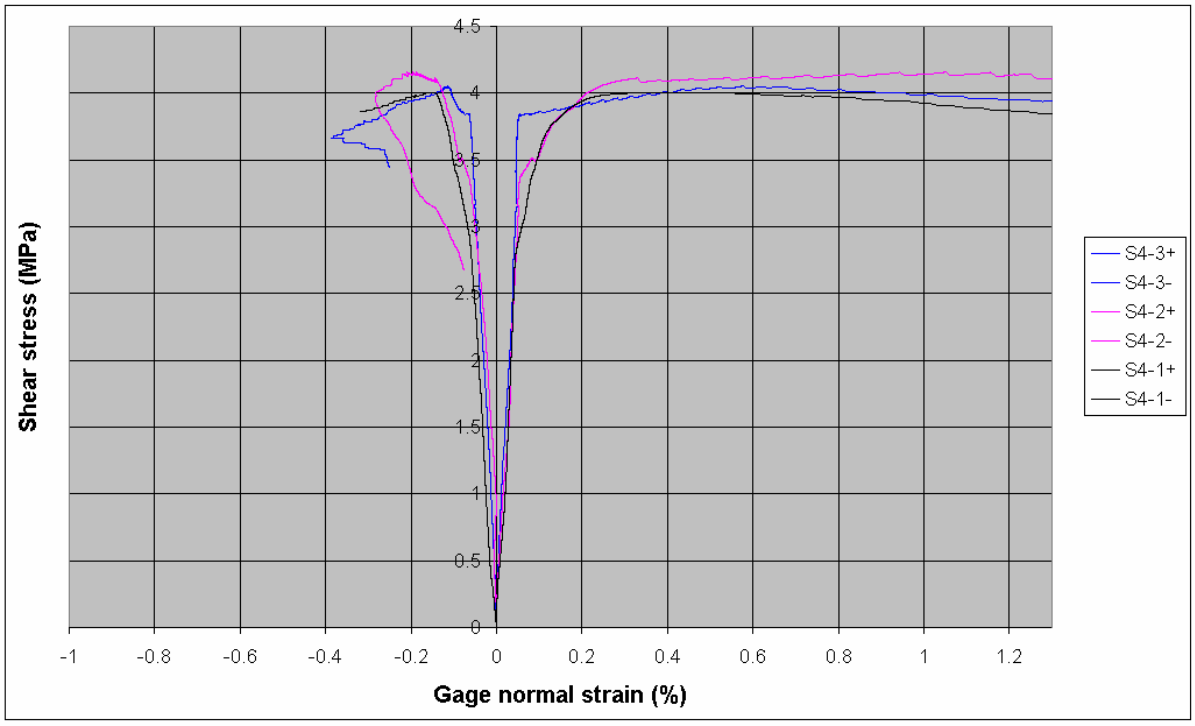

Figure 6.6 Shear stress versus strain gauge normal strain in S4

6.3.2 Shear strain

According to the mechanism of rosette strain gauges as mentioned in the previous chapter, the shear strain can be obtained by subtracting the tension strain from the compression strain. In figure 6.7 and 6.8, average shear stresses are plotted as a function of shear strain as determined from the strain gauges for S3 and S4 specimens. The study of shear strain in here is only limited in the 1.0% due to the mechanism of rosette strain gauge based on "small-strain" theory. All shear parameters as determined from the resulting stress - strain data, are listed in Table 6.1. The graph to illustrate these shear parameters are similar to tension parameters as shown in chapter 2:

$\gamma_{M:}$ first crack shear stress

$\tau_{M:}$ first crack shear strain

$\gamma_{U:}$ ultimate crack shear stress

$\tau_{U:}$ ultimate crack shear strain

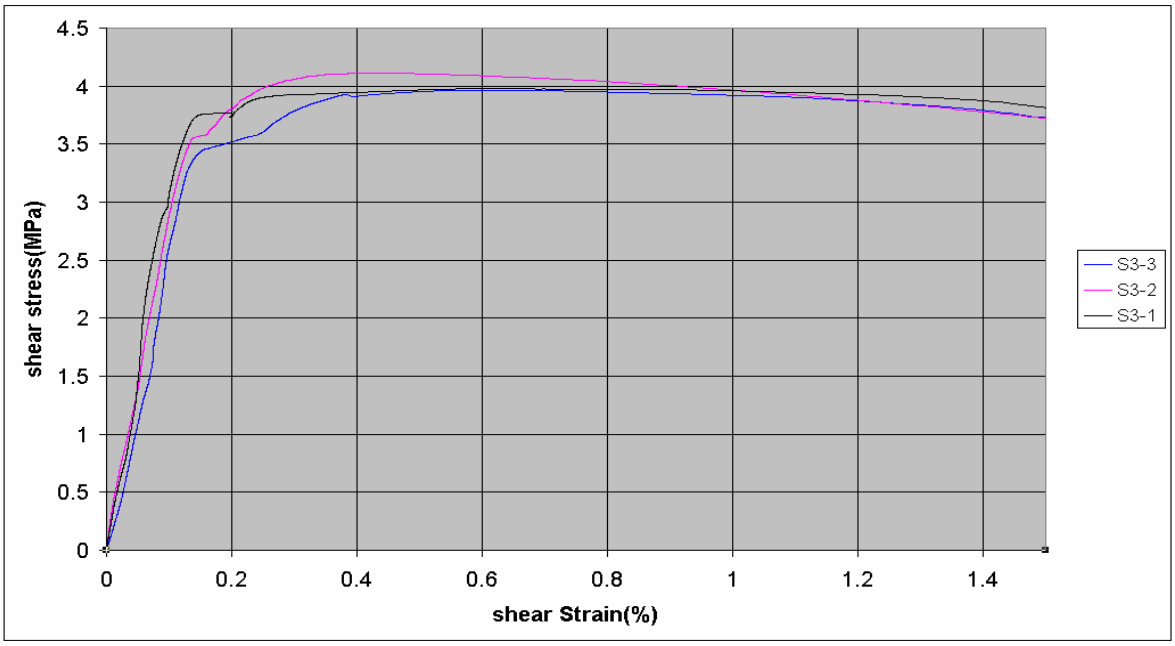

Figure 6.7 Shear stress versus shear strain in S3

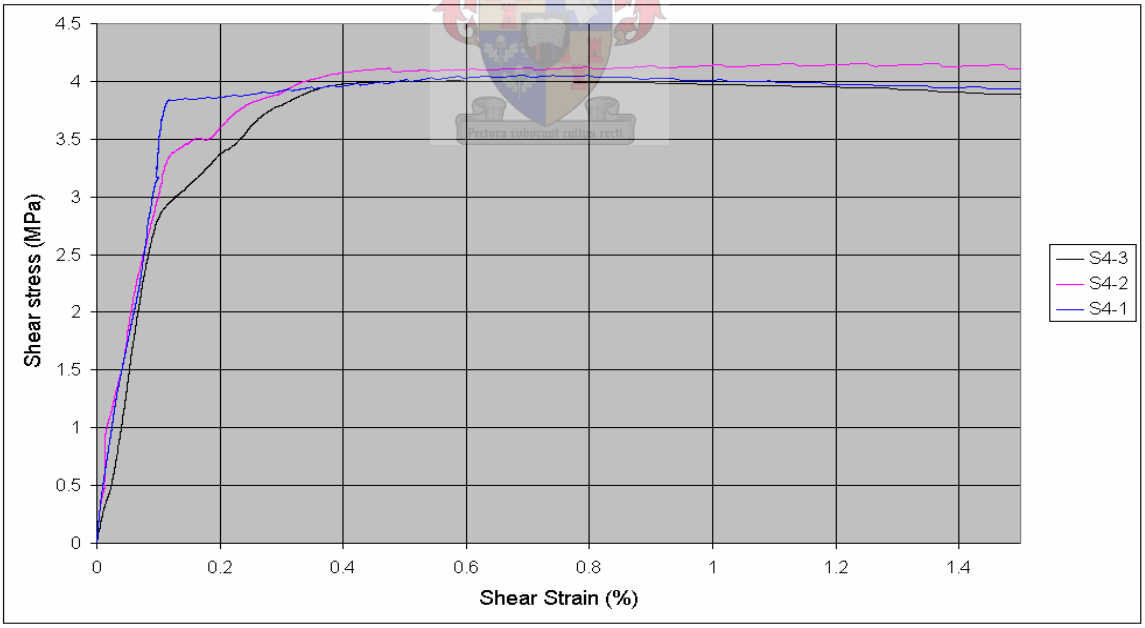

Figure 6.8 Shear stress versus shear strain in S4

Table 6.1 Ioscipescu shear results for S3 and S4 specimens

	γ_M [%]	τ_M [N/mm^2]	γ_U [%]	τ_U [N/mm^2]
S3	0.13	3.64	0.62	3.98
	0.12	3.38	0.60	3.97
	0.14	3.55	0.71	4.02
MIN	0.12	3.38	0.60	3.50
Average	0.13	3.52	0.64	3.99
MAX	0.14	3.64	0.71	4.07
STEDV	0.01	0.13	0.06	0.03
C.O.V	7%	4%	9%	1%
S4	0.11	3.69	0.71	4.09
	0.12	3.68	0.83	4.15
	0.14	3.72	0.73	4.10
MIN	0.11	3.68	0.71	4.09
Average	0.12	3.70	0.76	4.12
MAX	0.14	3.72	0.83	4.15
STEDV	0.02	0.02	0.06	0.07
C.O.V	12%	1%	8%	2%

The shear strain capacity (γ_F) are omitted in here due to it is over 1%. As to compare shear and tensile properties and calculate the elastic tension modulus (E), the uniaxial tensile tests were also done. The results of S3and S4 from uniaxial tensile test are presented in figure 6.9 and 6.10. Further uniaxial tensile test results are tabulated in Table 6.2. The graph to illustrate these parameters was shown in chapter 2.

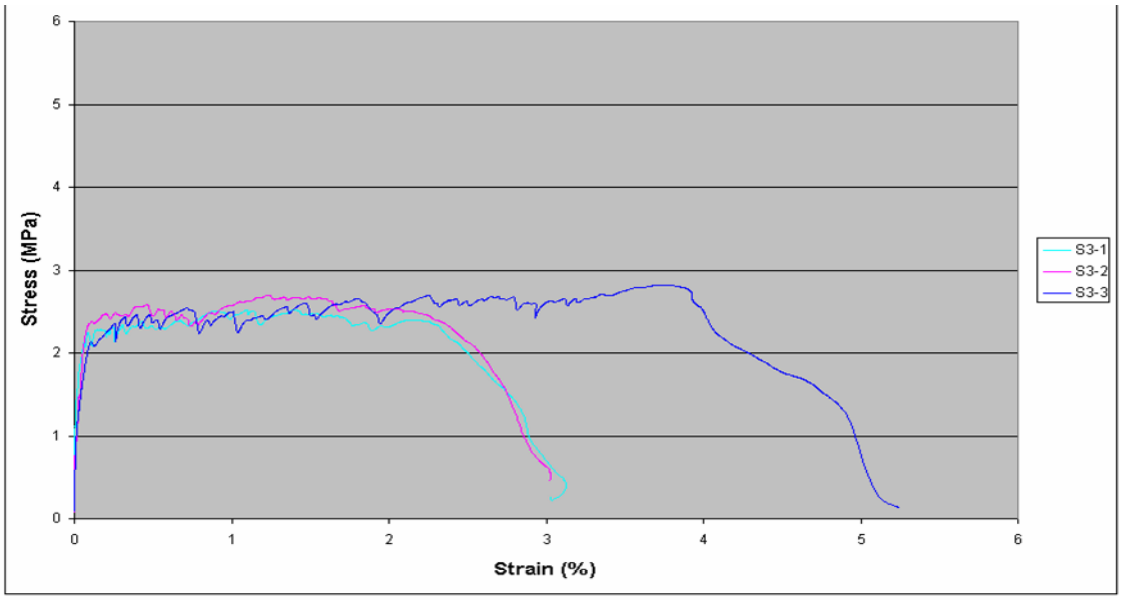

Figure 6.9 Tension stress versus tension strain in S3

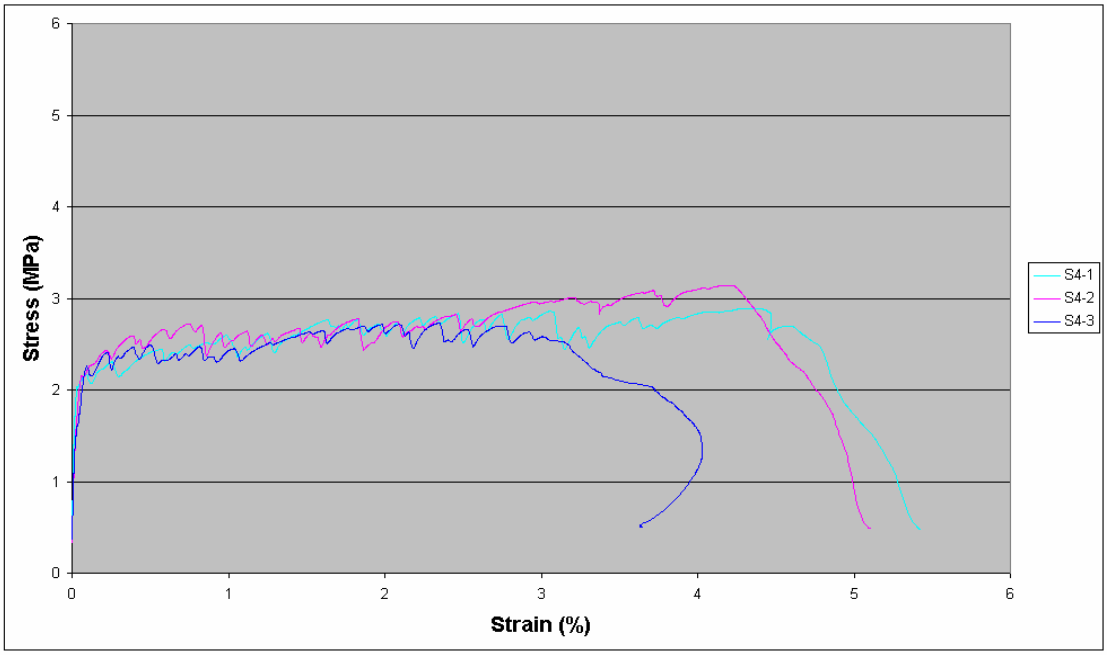

Figure 6.10 Tension stress versus tension strain in S4

Table 6.2 Uniaxial tensile results for S3 and S4 specimens

S3	ε_M [%]	σ_M [N/mm^2]	ε_U [%]	σ_U [N/mm^2]	ε_F [%]
	0.04	1.94	1.63	2.52	2.53
	0.05	1.84	2.23	2.7	2.64
	0.04	1.52	3.77	2.82	4.76
MIN	0.04	1.52	1.63	2.52	2.53
Average	0.04	1.77	2.54	2.68	3.31
MAX	0.05	1.65	3.77	2.82	3.03
STEDV	0.005	0.22	1.10	0.15	1.26
C.O.V	10%	13%	38%	6%	28%
S4	0.04	1.96	4.17	2.89	4.89
	0.05	1.87	4.12	3.14	4.82
	0.05	1.72	2.31	2.73	3.95
MIN	0.04	1.52	2.31	2.52	2.53
Average	0.05	1.85	3.51	2.92	4.55
MAX	0.05	1.65	4.17	2.82	3.03
STEDV	0.005	0.17	1.06	0.21	0.52
C.O.V	10%	9%	31%	7%	11%

From the experimental results shown in Table 6.1 and 6.2, some trends can be observed.

1. The variation of the shear stress and shear strain between two groups of material is

not significant. The average first cracking shear strain of S3 and S4 is 0.13% and 0.12% respectively, and the average shear stress of S3 and S4 is 3.52 MPa and 3.70 Mpa.

2. With increase of the fibre content, the ultimate shear stress and shear strain both increase. The increment of ultimate shear strain from S3 to S4 is 17.1%, and the increment of average ultimate shear stress is 5%.

3. All the unxial tensile parameters of S3 and S4 indicate the tendency of increasing with increasing of fibre content.

4. For the same material, the tensile strain indicates a more ductile behaviour than shear strain from first crack to ultimate strength.

5. The coefficient of variance (COV) of all the shear parameters are smaller than those for the tensile parameters, which means the shear behaviour of materials is more stable than tensile behaviour.

6.3.3 Elastic modulus (*E*) and shear modulus (*G*)

The elastic modulus is a very important engineering parameter of any building material. It represents the stiffness of the material to describe the linear elastic behaviour. Two parameters are required, for instance the elastic modulus (E) and the shear modulus (G). The original aim of Iosipescu shear testing is to define the shear modulus (G) of composites materials. Here, both the tensile elastic modulus (E) and shear modulus (G) are calculated from the test results.

The determination calculation of the elastic modulus is not easy because the stress-strain relationship for cement-based material is not perfectly linear. The non-linearity of the stress-strain relationship for cement-based material is mainly due to the microcracking in the matrix (Addis and Owens, 2001). Usually, the initial portion of the curve is regarded as effectively linear, and at stresses within this portion the elastic modulus is taken as the slope of this linear portion; it is referred to as the initial tangent modulus as show in figure 6.11. Two other forms of elastic modulus (also see figure 6.11) are considered, namely the tangent

modulus, represented by the slope of the tangent to the curve at a particular stress, and the secant modulus represented by the slope of the line connecting the origin to the point on the curve corresponding to the stress selected.

However, the method of determining the E-modulus is different according to the different country standards and there is no unanimous method to calculate the E- modulus of cement-based composite materials.

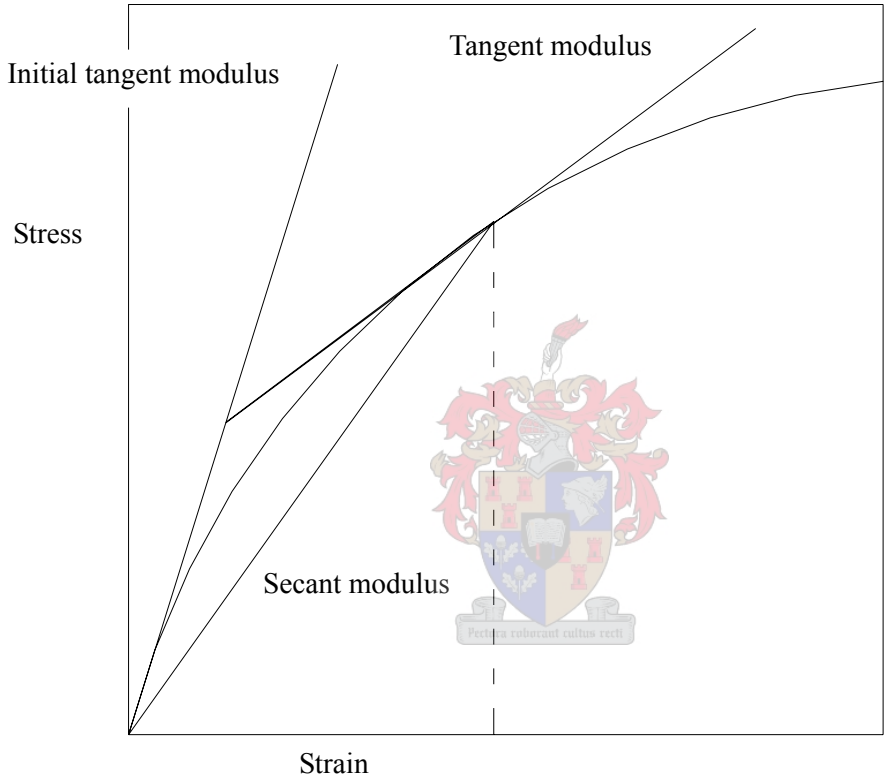

Figure 6.11 Three forms of elastic modulus

Here, the calculation method from RILEM (The International Union of Testing and Research Laboratories for Materials and Structures) is used to calculate the elastic modulus of S3 and S4 material as follows:

$$E = \frac{\Delta P}{\Delta \varepsilon} = \frac{P_a - P_b}{\varepsilon_a - \varepsilon_b} \quad G = \frac{\Delta P}{\Delta \gamma} = \frac{P_a - P_b}{\gamma_a - \gamma_b} \tag{6.1}$$

Where:

E : Modulus of elasticity, G : Shear modulus

P_a: is the Stress of 1/3 ultimate stress (N/mm^2)

P_b: Initial stress = 0.1 N/mm^2

ε_a or γ_a: Mean strain under stress P_a

ε_b or γ_b: Mean strain under stress P_b

The calculated values for tensile elastic and shear moduli are shown in table 6.3. Poisson's ratio (ν) is then calculated from equation (6.2). The results are also presented in table 6.3.

$$\nu = \frac{E}{2 \cdot G} - 1 \tag{6.2}$$

Table 6.3 *E* - modulus and *G* - modulus for S3 and S4 specimens

S3	E (GPa)	G (GPa)	ν	S4	E (GPa)	G (GPa)	ν
	8.5	3.01			8.95	3.26	
	6.5	2.55			9.6	3.31	
	7.2	2.84			7.02	2.85	
MIN	6.5	2.55		MIN	7.02	2.92	
Average	7.4	2.8	0.32	Average	8.52	3.16	0.35
MAX	8.5	3.01		MAX	9.6	3.26	
STEDV	1.01	0.23		STEDV	1.34	0.22	
COV	14%	8%		C.O.V	16%	7%	

It can be noticed that the elastic tensile modulus and shear modulus both increase with the fibre content increasing. The COV indicates that the variation of elastic shear modulus in the specimens is smaller than the elastic tensile modulus.

6.4 Third phase

Due to the limitation of strain gauge measurements, the shear stress and strain behaviour cannot be indicated after ultimate strength. It has been noticed in the second phase that the

principal tension strain dominates the shear strain beyond ultimate shear strength. Therefore, it makes sense to study the principal tensile strain. In the third phase, three specimens of each group material (S3, S4) are tested and the tensile diagonal deformation measured by LVDT. However, the LVDT measurement also includes deformations within regions of combined shear and flexure due to the LVDT gauge size, dominated by the finite size of this equipment. A small gauge size of 25 mm was achieved, and the deformation measurements serve as an indicator of the shear inelastic behaviour, for instance for validation with FE analysis.

The results of each group are presented in the form of average shear stress versus average principal tensile strains in figure 6.12. It can be seen that the development of principal tensile strain after ultimate shear stress accompanies the slow decrease of shear stress in both groups of specimens. With increasing fibre content, both the shear strength and ductility increases.

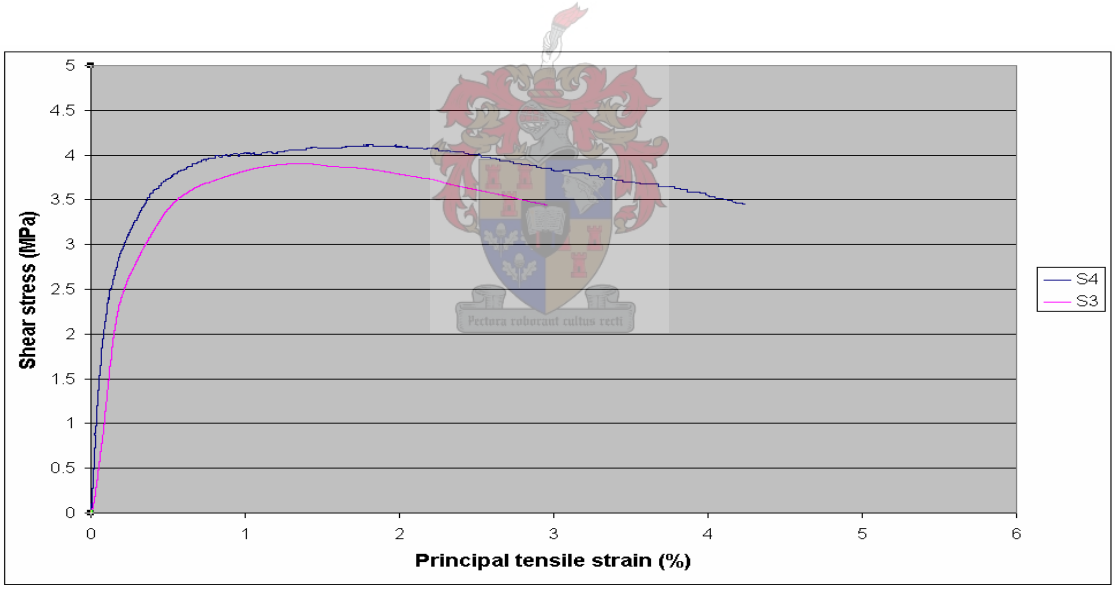

Figure 6.12 Shear stress versus diagonal tensile strain

6.5 Conclusion

A preliminary experimental investigation of the shear behaviour of FA and Slag-ECC with various fibre contents was presented in this chapter. The results indicate that the Iospescu shear test method is applicable for ECC material in the elastic range. This confirms the FE results in chapter 4. In the inelastic range, only fibre contents more than 2% are suitable for

Iospescu shear testing method, or vice versa, this method is only suitable for ductile material.

The crack patterns can distinguish the failure modes of specimens from brittle to ductile with increasing fibre contents. In the same material groups, the strain-hardening phenomenon in tension is more pronounced than in shear. The shear strain is dominated by principal tension after ultimate shear stress, which is believed to the consequence of the fibre pull-out function.

However, some disadvantages have been found in the shear testing. The limitation of strain gauges to small deformations causes that the total nonlinear deformational response in the experiment can not be recorded accurately. Therefore, the Ioscispescu shear test should be improved to enable accurate deformational measurement in the pure shear zone in the future.

Chapter 7
The study of shear capacity of R/ECC

7.1 Introduction

As mentioned in chapter 2, two experiments involved using ECC to reduce the shear reinforcement in normal concrete beams and columns have been done in the concrete laboratory of structural Engineering Division, Stellenbosch University (Van Dyk, 2004; Avenant, 2005). In this chapter, the detail introductions of these two experiments are presented firstly. Then, the program RESPONSE based on the MCFT and the TA are used to predict the shear capacity of reinforced concrete (R/C) beam. Subsequently, the shear capacity of R/ECC (R/C beam with ECC crust) is predicted.

7.2 The introduction of experiments

7.2.1 The application of ECC as permanent channel formwork

This purpose of this experiment is to investigate the possibility of applying ECC as permanent channel formwork for reinforced concrete(R/C) beams, is addressed by performing a series of tests on small R/C beams and R/ECC beams (R/C beams with ECC channels). Wood was used to build a mould for casting the ECC channels, as shown in figure 7.1. The channels were manufactured with ECC material of the same mix as S3 in chapter 5. The R/C beams and the R/ECC beams were tested in three-point bending to determine the influence of the ECC. See figure 7.2 for the test setup and beam sections of the R/C and R/ECC beams.

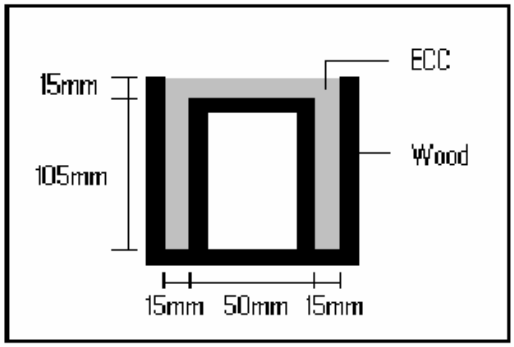

Figure 7.1 Illustration of wood mould for casting ECC channel

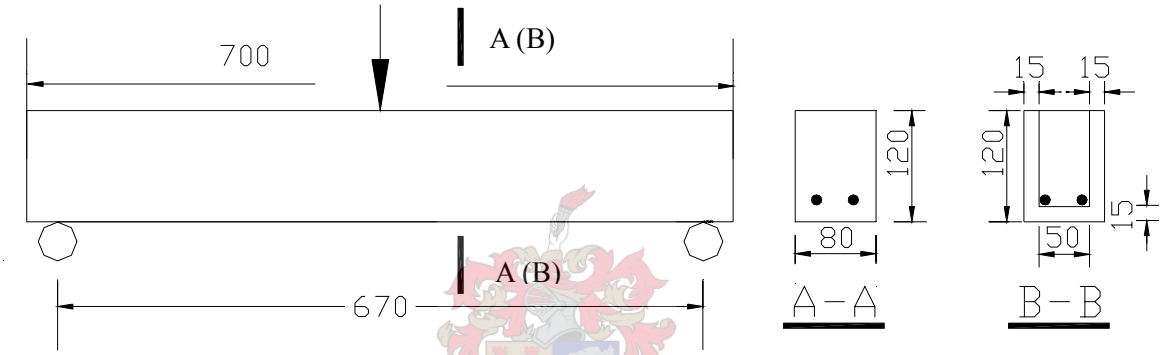

Figure 7.2 Setup of test and R/C beam section (A-A) and R/ECC beam section (B-B)

The procedure was that three ECC channels were cast and moist cured in a curing room with constant water spray for 7 days and then filled with 25MPa concrete and two Y10 longitudinal steel reinforcement bars. Three beams consisting entirely of normal concrete (25MPa) and two Y10 longitudinal steel reinforcement bars were also cast. Note that the exact same mix was used for the R/C beams as for the concrete filling the ECC pre-cast permanent formwork channels. All the beams were then cured in water until the (concrete) age of 14 days, when they were tested.

The R/C beams and the R/ECC channel beams failed in completely different failure patterns. R/C beams showed brittle load-deflection responses and typical shear failure - see figures 7.3 and 7.4. However, R/ECC channel beams showed ductile load-deflection responses and apparent bending failure - see figures 7.5 and 7.6. In summary, from figures 7.3 and 7.5 the average maximum forces for R/C and R/ECC channel beams are 21.0 kN and 23.8 kN respectively, and the average deflection at maximum load for R/C and R/ECC beams are 4.6 mm and 8.4 mm respectively.

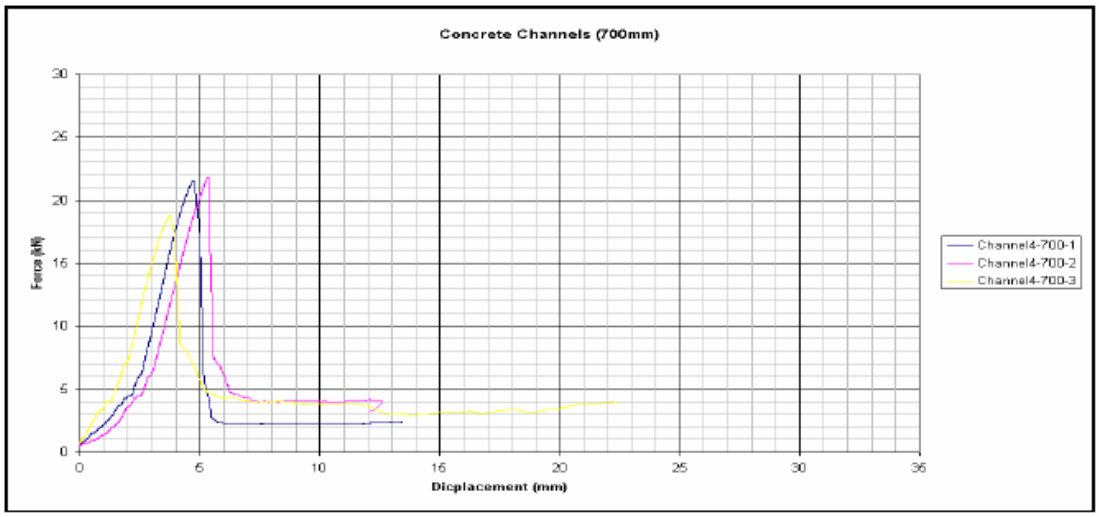

Figure 7.3 Central deflection versus external load of R/C beam (van Dyk 2004)

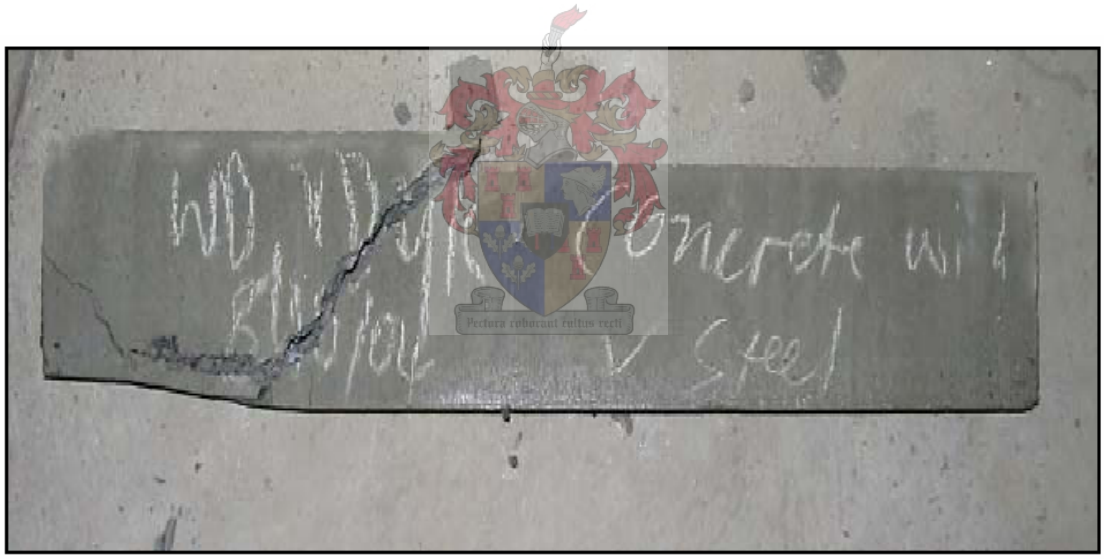

Figure 7.4 Shear failure pattern of R/C beam

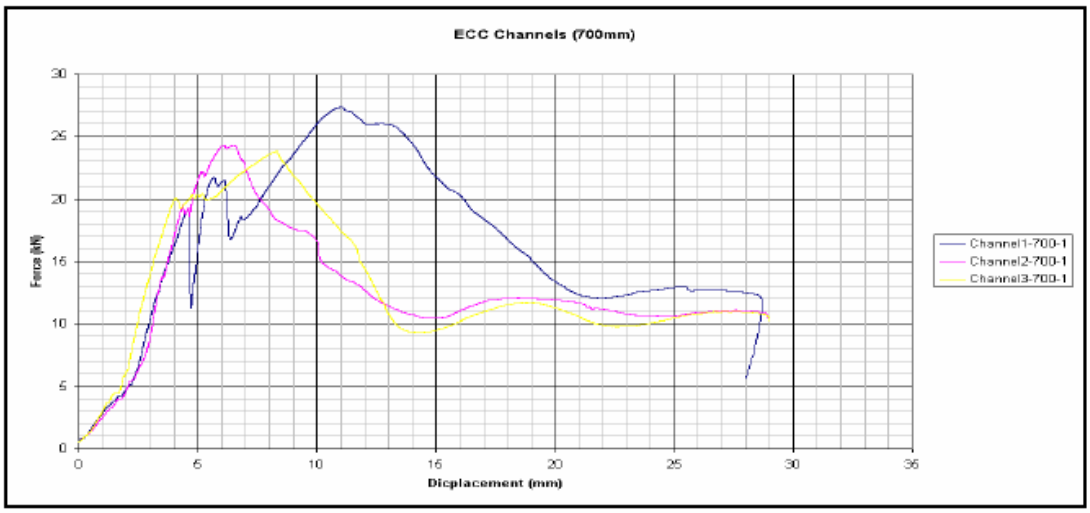

Figure 7.5 Central deflection versus external load of R/ECC beam

Figure 7.6 Bending failure pattern of R/ECC beam

From these results, it appears that the R/ECC channel beams resisted higher load and were more ductile than R/C. ECC can increase the shear capacity of a beam and therefore less or no shear reinforcement may be required.

7.2.2 The application of ECC as permanent column formwork

The experimental study of ECC as permanent formwork for R/C columns was conducted by Avenant (2005). This experiment intended to study the axial-flexural behaviour and shear capacity of R/C columns cast in ECC permanent formwork. Two normal R/C columns and two columns consisting of an ECC tube with a reinforced concrete core, termed R/ECC

column- beams, were tested.

All four columns were 2.5 m long and of section dimensions as shown in figure 7.7. Columns A1 and A2 were normal R/C columns with 3% axial reinforcement (6Y20 bars) and nominal (SABS 0100-1) steel shear reinforcement (R8 stirrups at 250 mm spacing) throughout their length. Columns B1 and B2, known as the R/ECC column- beams, consisted of ECC tubes of dimensions as shown in figure 7.7, filled with R/C and 3% axial reinforcement (6Y20 bars). The R/ECC column-beams were reinforced with 50% less steel shear reinforcement (R8@500) than columns A1 and A2.

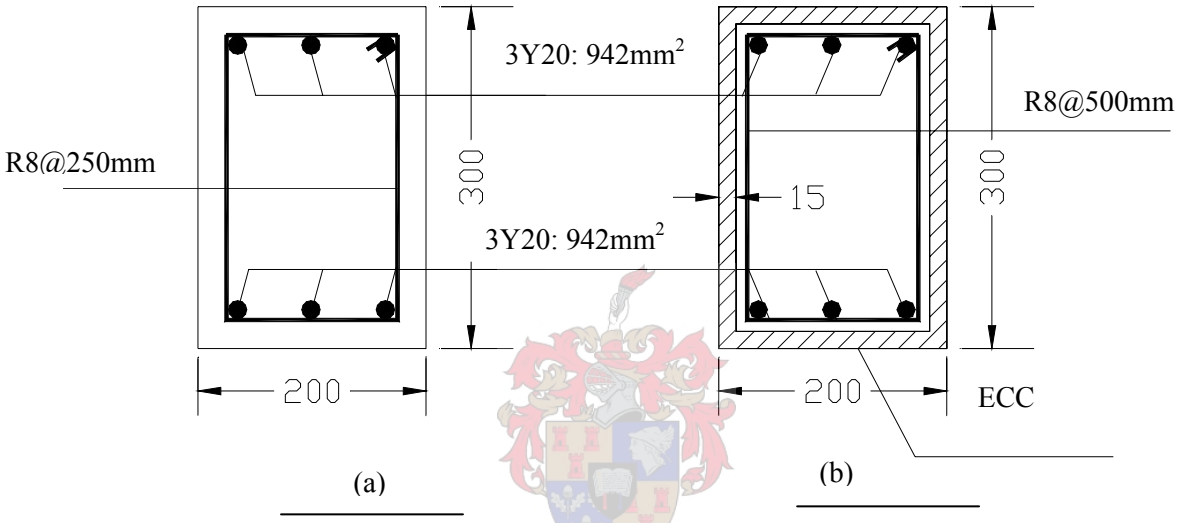

Figure 7.7 The sections of the (a) R/C and (b)R/ECC columns

The R/ECC columns were cast in specially made wooden moulds that consisted of an outer and inner mould, and a 15mm gap between them to form the walls of the tube. The entire mould was secured vertically on a vibrating table and ECC was cast from the top. The ECC mix design and mix procedure were also the same as S3 in chapter 5. The inner and outer moulds were removed after 12 days. Figure 7.8 shows a complete ECC tube. The bottom end of the tubes were covered with a wooden board and connected by steel tension rods to a steel frame fitted around the top ends as shown in figure 7.9. The ECC tubes were then secured vertically with the open top end facing upwards. Steel reinforcement was prefixed and lowered into the tube from top. Concrete was then cast from the top and the tubes themselves provided the formwork. The steel tension rods connecting the frame fitted around the top and the wooden board at the bottom was fastened until sufficient pressure between the board and

the bottom of the tube developed for concrete not to leak out. A 30 MPa concrete mix was design for both R/C beams and R/ECC beams. The both R/C and R/ECC columns were left to cure for 14 days under moist conditions after the concrete was cast.

Columns were tested horizontally and subjected to concentric axial compression and a transverse load applied in the middle of the column for uniaxial strong-axis bending as in figure 7.10.

Figure 7.8 ECC tube

Figure 7.9 Tension rods and board to contain fresh concrete

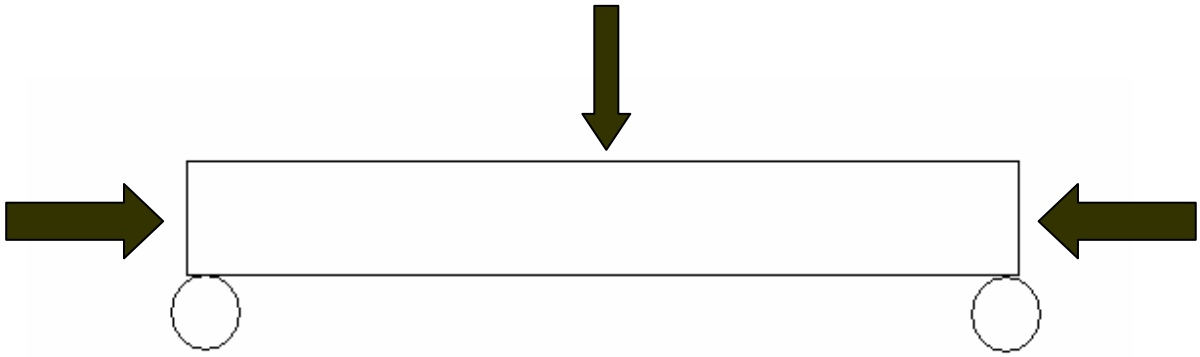

Figure 7.10 Beam-column load application during testing

Axial loads were applied using Enerpac Hollow Cylinder jacks with a capacity of 60 tons. An HBM 200 ton capacity load cell measuring the axial force was fitted to a fabricated steel plate and welded onto a second steel base. The columns were lowered from the top in between the bases onto concrete cubes, which provided vertical support at the ends. Bearings allowing rotation as well as lateral movement were provided at both these supports. For the transverse load a setup configuration comprising of a base, connected to the floor, vertical columns, and a horizontal beam were constructed. A jack and 50 ton capacity load cell, measuring the transverse force were connected to the horizontal beam. The total test layout is show in figure 7.11. During each test the axial load was increased to 300 kN. The transverse force was then increased to 30kN to ensure uniaxial strong-axis bending and to prevent weak axis bending due to possible eccentricities. The axial force was then further increased up to approximately 560 kN and then kept constant, while the transverse force was increased until failure occurred.

Figure 7.11 Beam-column test layout and connection (Avenant 2005)

The R/C columns A1 andA2 showed signs of small bending cracks during the gradual increase of the transverse load, but eventually failed in shear as shown in figure 7.12. The R/ECC columns B1 and B2 also failed predominantly in shear – see figure 7-13. Note that some finer cracks opened in the ECC tube/crust, as marked in figure 7-13. However, these cracks already formed during casting of the concrete, due to the hydrostatic pressure caused by the highly flowable mix concrete used for the concrete inner core. Table 7.1 gives a summary of the maximum transverse force resisted by each column and the accompanying deflection at maximum load during the tests.

Figure 7.12 Shear failure pattern of R/C column

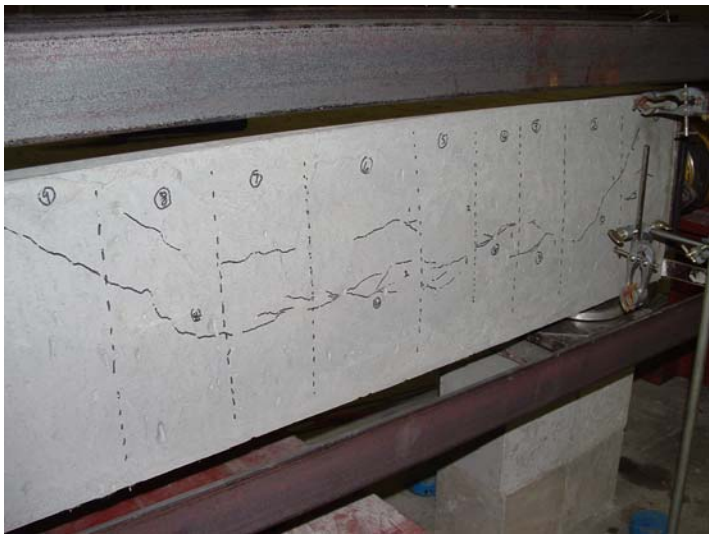

Figure 7.13 Shear failure pattern of R/ECC column

Table 7.1: Summery of deflections and forces (Avenant 2005)

	Axial load (kN)	Transverse load (kN)	Bending moment (kNm)	Mid span deflection (mm)
Column A1	570.0	249.2	161.6	10.4
Column A2	573.0	246.2	159.2	9.4
Column B1	564.8	250.5	163.8	12.7
Column B2	578.4	222.1	148.0	15.8

From these test results, it can be seen that the transverse load capacity of the beams A1, A2, B1 and B2 are comparable, despite the different levels of steel shear reinforcement in columns A1, A2 and B1, B2. The shear mode of failure resulting in diagonal tension was effectively resisted by the ECC which contained multi-directional orientated fibres.

7.3 The study of shear capacity of R/ECC beams

From the introduction of these two cases, there are indications that the shear capacity of normal concrete beams can be increased by partial concrete replacement with ECC. To use such R/ECC beams in practice, it is necessary to find a simple formula to predict the shear strength of R/ECC beams. As mentioned in chapter 2, the shear capacity of R/C beams is computed as a sum of shear carried by the concrete V_c and shear reinforcement V_s . Therefore, the shear capacity of R/ECC beams may be computed by the addition of a third term to account for contribution of the ECC crust to the shear strength. This can be expressed as:

$$V_{R/ECC} = V_C + V_S + V_E \tag{7.1}$$

where V_c and V_s are referred to as the shear carried by concrete and shear reinforcement, V_E is referred to as the contribution of the ECC crust to the shear strength.

To compute the shear strength as given in equitation (7.1), it is necessary to quantify the contribution of ECC to the shear capacity. A simple way to obtain the shear capacity of the ECC crust is to subtract the shear strength of reinforced concrete core in equation (7.1) from the measured total response in the experiments. For this method, it is important to predict the shear strength of reinforced concrete accurately.

From the detailed consideration of stress fields and variable principal stress directions in chapter 2, it is believed that the modified compression field theory is more accurate than the truss analogy (TA) model. In this section, the MCFT and the TA, as incorporated in BS8110, are both used to predict the shear capacity of concrete in R/C and R/ECC beams. Note that the SABS0100 is based on the BS8110, but the latter was strictly followed in these computations. The parameters of the considered R/C and R/ECC beams are summarized in table 7.2. The results of the computations are presented in tables 7.3 and 7.4 for channels (Van Dyk, 2004) and beam-column (Avenant, 2005) experiments respectively.

Table 7.2 The parameters for R/C and R/ECC channels (van Dyk, 2004) and beam-columns (Avenant, 2005).

	bXd(mmXmm)	fcu(MPa)	longutidual steel (mm^2)	Transverse steel(mm^2)	type of failure	Transverse load (kN)	axial load(kN)
R/C-channel1	80X120	25	157		shear	21.2	
R/C-channel2	80X120	25	157		shear	22.4	
R/C-channel3	80X120	25	157		shear	18.6	
R/ECC-channel1	50X105	25	157		bending	25.8	
R/ECC-channel2	50X105	25	157		bending	24.2	
R/ECC-channel3	50X105	25	157		bending	21.0	
R/C-column (A1)	200X300	34.1	942	R8@250	shear	249	570.0
R/C-column (A2)	200X300	32.5	942	R8@250	shear	246.2	572.9
R/ECC-column (B1)	170X270	29.6	942	R8@500	shear	250.5	564.8
R/ECC-column (B2)	170X270	30.8	942	R8@500	shear	222	578.4

In both tables, V is the shear force from the experimental result, V_p is the predicted shear resistance calculated with the MCFT with aid of the program RESPONSE. The latter was performed at the position of observed failure in the elements, i.e. at the support for channel beams and a distance of 1/3 of span from support for the beam-columns. Vt is the shear capacity prediction with the TA, as implemented in the BS8110. The values k_1 and k_2 express the deviation from the measured values by respectively the MCFT ($k_1 = (V-Vp)/V$) and the TA ($k_2 = (V-Vt)/V$).

Table 7.3 R/C and R/ECC channel experimental (Van Dyk, 2004) and computed results

R/C beam	V (kN)	Vp (kN)	Vt (kN)	V-Vp (kN)	k_1 (%)	k_2 (%)
1	10.6	9.7	7.8	0.9	8.5	26.6
2	11.2	9.7	7.8	1.2	13.8	28.6
3	9.3	9.7	7.8	-0.4	-4.3	16.4
R/ECC beam	V (kN)	Vp (kN)	Vt (kN)	(V-Vp) (kN)	k_1 (%)	k_2 (%)
1	12.9	6.8	5.8	6.8	47.2	57.3
2	12.1	6.8	5.8	5.3	43.8	51.8
3	10.5	6.8	5.8	3.7	35.2	44.5

Table 7.4 Beam-Column experimental results (Avenant, 2005) and computed results

	V (kN)	Vp (kN)	Vt (kN)	V-Vp (kN)	k_1 (%)	k_2 (%)
R/C Column A1	124.6	110.9	89.5	13.7	11.7	28.2
R/C Column A2	123.9	111.2	89.5	11.9	10.9	27.3
R/ECC Column B1	125.3	78.5	68.2	32.5	38.5	45.6
R/ECC Column B2	111.1	75.2	68.2	18.7	35.4	38.6

Note that, in R/ECC beams, Vp and Vt are the shear capacity of the reinforced concrete core only, i.e. without the ECC crust.

From these two tables, it can be seen that the results by MCFT and TA are different, with the TA consistently more conservative. Furthermore, for the channel experiments in Table 7.3, the predicted results are equal for the three R/C beams and R/ECC beams due to the same experimental conditions. However, in the beam-column experiments (table 7.4), the predicted results are slightly different due to the different axial loads and as well as slightly different concrete strengths of the different specimens.

It is considered that the MCFT is reasonably accurate, because the maximum error in these two experiments is below 14%, while the minimum error is 16% by the TA in these two experiments.

By calculating the shear strength of only the R/C core in R/ECC specimens using MCFT, the percentage of shear contribution by the ECC crust to the total shear strength of R/ECC can be presented by k_1. The section area of ECC is 45.3% of section area of the total R/ECC channel beam, and the average shear strength of ECC accounts for the shear strength of total R/ECC is 43%, but it should be remembered the failure type in R/ECC channel is bending failure. This means that there may be remaining shear capacity in the R/ECC channel beams, when failure by bending occurs. So, the full capacity of ECC shear is not utilised. In the R/ECC beam-column, the average shear strength of ECC accounts 35% of the shear strength of the R/ECC specimens, but the section area of ECC is 23% of section area of the total R/ECC beam-columns.

As an explanation, if bending and simultaneous axial compression are ignored, the shear strength of ECC in these two experiments may be found from:

$$V_{ECC} = \tau_{ECC} \cdot A_{ECC} \tag{7.2}$$

where V_{ECC} is the shear strength contribution of ECC in R/ECC specimens. From chapter 6, the value τ_{ECC} is 4.0 MPa for mix S3. A_{ECC} is the section area of ECC in the R/ECC specimens. By calculation with equation (7.2) V_{ECC} = 17.4 kN and 56 kN for R/ECC channels and

beam-columns respectively. To compare these values with the calculation results in table 7.3 and 7.4, it can be found these values are much higher than the values from table 7.3 and 7.4. It therefore seems that this shear potential is not exploited fully in the R/ECC composite structural elements. In the case of the channels the potential may still be in reserve, when the beam fails in bending. However, in the beam-columns shear failure occurs also in the case of R/ECC.

Several reasons can be given for ECC not realising its shear potential in these composite applications. However, equation (7.2) over simplifies the shear resistance computation by ignoring the total stress field acting in the elements. The shear capacity may be enhanced by axial compression, but reduced by flexural tension. The accurate formulation of a model for shear resistance in structural applications falls outside the scope of this study, but will be addressed in future research.

A reason for not realising the full shear resistance capacity by ECC may be the differences in the shear behaviour of concrete and ECC. The concrete is brittle and stiffer than ECC. This means that it reaches its capacity at low deformation, after which its resistance quickly reduces upon further deformation. ECC reaches its capacity at significantly higher deformation, when the concrete has lost its capacity. This means that the use of ECC to substitute steel shear reinforcing bars, which introduce crack distribution and some ductility to the R/C core in shear, should be considered carefully. The contribution of the steel itself, as well as the tension-stiffening effect of the steel with respect to the concrete contribution to shear resistance, must be substituted. In this respect an ECC crust may not be completely effective. This remains to be studied further. Issues of ECC – concrete bond are crucial in this regard and must be studied.

The shear capacity prediction by the MCFT deserves further clarification. In particular, the shear failure location predicted by MCFT with respect to the experimental result in R/C-columns is studied. The failure pattern from the experiment (see figure 7.12) indicates a diagonal crack through the beam, which clearly indicates that shear failure dominated. However, the shear capacity of the R/C beams computed by the MCFT decreases with increasing bending moment, i.e. in three point-bending, the shear capacity is highest at the

support and lowest at mid span. The shear–moment interaction diagram for beam-column A1 computed with RESPONSE based on the MCFT is shown in figure 7.14.

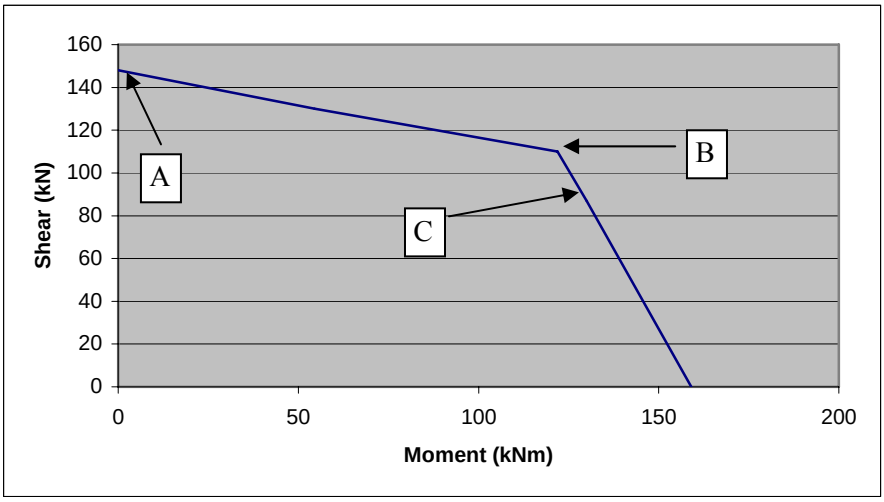

Figure 7.14 MCFT predicted Shear- moment interaction diagram for beam-column A1

It can be noted that the lowest shear capacity from the MCFT calculation is 81.5 kN (see figure 7.14 point C), which is lower than point B (110.9 kN) where the experimental beams failed. Point A in figure 7.14 indicates the shear capacity is 148.9 kN at the support. In the MCFT model, it is due to the high moment at mid-span, whereby the shear capacity is reduced there. This may be due to inaccuracy of the MCFT model, but other causes may be (i) variation in material properties of the experimental beams whereby the weakest point caused the onset of cracking in the observed position, (ii) other physical mechanisms of crack initiation like irregular stirrup spacing, or low concrete cover at the point of cracking.

In addition to the above, a postulation is given now that shear dominated failure in three point bending test will produce the observed failure crack, as opposed to a vertical crack at mid span in bending dominated failure. Consider that shear failure is associated with diagonal cracking at angles varying roughly between 20 and 50 degrees. For shear failure at mid span, inclined cracks should form at some point along the section height and then propagate at the mentioned angle. However, such cracking that transgresses under the central point load must be a mirror image about the centre-line, i.e. the line of loading, to be orientated in the

maximum principal stress direction. Eventually, these cracks must rotate vertically, to propagate along the centre line in what is in fact a flexural crack. For this, the material between inclined cracks should be cracked, in the fashion seen in the small ECC Iosipesco shear specimens in Chapter 5. In the three point bending situation, this is considered a higher mode of failure and unlikely to occur. Instead, failure should be initiated in tension at the farthest material fibre at mid-span and subsequently propagate upwards, vertically. However, in the R/C beam-columns, shear dominated, whereby shear diagonal cracks initiated first around the middle height of the beam. This would have occurred at the position of maximum shear stress, i.e. away from the mid span due to the self weight increase of the shear towards the support. Subsequently, the crack propagated diagonally as observed. This implies an inaccuracy in the MCFT, which does not carefully consider material point maximum principal stress, but considers the section as a whole. It is thus argued that the position of first occurrence of maximum principal stress, is most likely in the region of the observed crack, but in combination with the variation in material properties like strength, may dominate in determining the final failure pattern and position.

7.4 Conclusions

Two experiments to investigate the possibility of applying ECC as permanent formwork are presented and studied in this chapter. Here, the realisation of the ECC shear resistance, as studied in earlier chapters, in these applications, has been the focus. From the presentation of two experiments, it can be found that ECC can increase the shear capacity of concrete beam by replacing concrete partially. In studying a method to quantify the ECC shear contribution, the Modified Compression Field Theory (MCFT) as well as the Truss Analogy (TA) has been applied to the structural elements. The prediction of shear capacity by MCFT is more accurate than TA, and therefore these values have been used for finding the ECC total shear contribution. It was determined indirectly, by subtracting the shear resistance of the MCFT predicted shear resistance of the R/C inner core from the total shear resistance measured experimentally. From the results, it has been found that the ECC crust/outer layer formed by the permanent formwork, does not achieve its full potential. The full potential is indicated by

the ECC shear strengths in chapter 6.

Further work is required to quantify the ECC shear behaviour in such composite use with R/C. Also, ways of achieving its full shear potential in such applications should be studied. Here issues such as bond between concrete and ECC, to transfer shear effectively across the interfaces must be studied. By effective bond the composite beam section operates as a unit, significantly increasing stiffness and strength. Also, the ductility of the ECC may then be exploited to distribute concrete cracking, whereby the peak resistance of also the concrete core may be maintained until all material phases achieve their maximum resistance at greater total deformation.

Chapter 8
Conclusions and recommendations

The research described in this thesis was aimed at the investigation of shear properties of ECC. Towards this aim the existing shear test methods were investigated and a modified Iosipescu shear test was designed by simple analytical design and finite element analysis for further refinement. According to the modified Iosipescu shear test method, the locally developed new ECC type containing a high level of fly ash, as well as ground granulated Corex slagment was tested in the laboratory. In these specimens the fibre content was varied, with sets of specimens containing fibre quantities of V_f=0%, 1%, 2%, 2.5%. Three phases of shear measurements were used to check the shear test appropriateness and the shear properties of ECC specimens. Subsequently, the test results were analysed and presented according to these three phases of shear measurement. Some conclusions were made pertaining to the corresponding work as follows:

1) By review of the shear test methods of composite materials in the literature, three important criteria for accurate determine the shear property of composite material are:

   I) For quantitative shear measurements, the shear test method should provide a region of pure and uniform shear stress in the test section of the specimen throughout the linear and non-linear response regimes.

   II) A unique relationship should exist between the applied load and the magnitude of the shear in the test section.

   III) Failure should be in the plane of pure and uniform shear.

The Iosipescu shear test method is the closest in achieving these criteria, compared with others shear test methods.

2) Finite element analysis indicated that some geometry parameters of an Iosipescu shear test specimen can influence the pure and uniform shear stress in the specimen which are the notch angle, the notch depth between two notch roots and the notch radius. By optimizating these parameters, an appropriate specimen is obtained.

3) The shear property of modified Iosipescu shear specimens were measured in three phases,

which may be regarded as an appropriate procedure. In the first phase, the failures of specimens were identified to ascertain adherence to criterion nr III above, namely pure shear failure. In the second phase, the accurate shear property of pure shear failure specimens were measured by rosette strain gauge arrangements. In the third phase, the shear deformation in strain-hardening region was measured by simple LVDT measurements, from which the shear strain in the post-elastic regime can be approximated.

4) By analysing the result from laboratory tests, some conclusions pertaining to the shear properties of ECC were drawn:

I) The crack patterns indicated the change of failure modes of specimens from brittle to ductile with fibre contents increasing. The specimens exhibit pure shear failure when the fibre contents equal and exceed 2%. Nevertheless, the multiple diagonal cracks extend into the flexural zone, influencing the load-deformational measurement due to additional fracture energy dissipation in these cracks.

II) The results from the laboratory tests are in agreement with the results from finite element analyses, which indicated that shear failure would dominate, but with the danger of cracks outside the shear zone due to high principal stresses in those regions. In the mortar specimens, and even those with low fibre contents (< 2%), two, or a single diagonal crack led to failure. As this was not along the middle plane, where the state of pure shear exists, objective shear resistance characterisation cannot be done from the results for those specimens.

III) The shear strain is dominated by principal tension in the inelastic region, which is believed to the consequence of the fibre pull-out function.

IV) With the fibre content increased from 2% to 2.5%, the ultimate shear stress and shear strain capacity both increase.

V) For the same ECC, the tensile strain indicates a more ductile behaviour than shear strain from first crack to ultimate strength, but the shear strength is higher than the tensile stress.

VI) The coefficient of variance (COV) of all the shear parameters are smaller than those for the tensile parameters, which seem to indicate that the shear behaviour of materials is more stable than tensile behaviour. This may be attributed to the stabilising role of the diagonal compression.

VII) Poisson's ratio (ν) for two group ECC (V_f = 2%, 2.5%) can be calculated from the elastic tensile modulus and shear modulus which are 0.32 and 0.35 for V_f= 2%, 2.5 respectively. Ideally, these values should be obtained from strain gauge measurements of axial and orthogonal deformations of uniaxial tensile specimens, and not from separate shear and tensile tests. This will be done in future work.

5) By studying two experiments involving the use of ECC to reduce the shear reinforcement in reinforced concrete beams and columns in chapter 7, some conclusions can be drawn:

I) ECC can increase the shear capacity of reinforced concrete beams by replacing concrete and steel stirrups partially.

II) The predication of shear capacity of reinforced concrete by MCFT is more accurate than TA. This holds potential for adoption for a model for predicting R/ECC shear resistance.

III) However, the calculations and comparison with experimental measurements indicate that the full potential of ECC shear resistance is not achieved in the particular composite R/ECC applications studied. The reasons may be ineffective interaction between ECC and the concrete cores, due to poor bond, but also the inability of the ECC crust to control diagonal cracking in the concrete core. Thereby, the ECC and concrete do not act as a unit, and the concrete contribution to shear resistance may be lost or reduced significantly. These matters remain to be studied further.

Some shortcomings and problems also can be noticed by review of the whole study. These shortcomings as well as some recommendations are presented next:

1) The geometry of modified Iosipescu shear specimen can be refined more by finite element analysis so that more accurate shear property can be measured in the laboratory.

2) The shear test setup should be improved in terms of rotating bearing cylinders to prevent friction and improve robustness and ease of alignment so that the experimental error can be reduced.

3) Shear deformation measurement devices that can accurately measure the deformation in the "zero-length" pure shear region should be used so that the proper shear strain property after ultimate shear stress can be measured. Here, non-contact methods may offer a possibility due to its fine resolution and the removal of the need for miniscule

measurement devices to accurately measure deformation across diagonal cracks.

4) The finite size of the strain gauges prevent that the veracity of finite element analysis result can be checked in terms of the stress distribution along the middle plane. Larger specimens could be considered to enable a number of strain gauges to be installed along the height. However, contact less methods of deformation measurement will overcome this limitation.

5) As outlined above, several aspects need clarification in the composite use of ECC with reinforced concrete, to substitute or reduce shear steel reinforcement. On the one hand the interaction between ECC and RC must be improved through improved bond at the interfaces of these materials in the composite structural elements. On the other hand, improved prediction models must be formulated to incorporate the various composite parts and more realistic stress fields in the prediction of structural shear resistance.

References:

Addis, B., and Owens, G., 2001, Fulton's Concrete Technology, Cement and Concrete Institute, Midrand, South Africa.

Adams, D.F. and Walrath, D.E., 1982, Iosipescu Shear properties of SMC Composite Materials", Composite Materials: Testing and Design (Sixth Conference), ASTM STP 787.

Alexander. M.G., Jaufeerally. H and Mackechnie. J.R., 2003, Structural and durability properties of concrete made by Corex slag. Research monograph No. 6, Department of Civil Engineering, University of Cape Town, South Africa.

Arakawa, T. and Ohno, K., 1957, Shear Tests of Reinforced Concrete Beams by Special Type of Loading (In Japanese), Transactions of the Architectural Institute of Japan, 57, pp 581-584.

ASCE-ACI Task Committee 426, 1973, The shear strength of reinforced concrete members, American Concrete Institute.

Ash resouses. www.ashresouses.co.za , Web site referenced in February 2006.

Avenant, P., 2005, Engineered Cement-based Composites (ECC) for the application of permanent formwork, Final year BEng thesis, University of Stellenbosch, South Africa.

Batson, G, Jenkins, E. and Spatney, R., 1972, Steel Fibre as Shear Reinforcement in Beams, ACI-JOURNAL, 69(10), pp 640-644.

Bentz.E, http://www.ecf.utoronto.ca/~bentz/r2k.htm., 2001, Web site referenced in February 2006.

Collins, M. P., and Mitchell, D., 1991, Prestressed Concrete Structures, Canadian Prestressed Concrete Institute.

Fischer, G., and Li, V. C., 2002, Effect of Matrix Ductility on Deformation Behavior of Steel Reinforced ECC Flexural Members Under Reversed Cyclic Loading Conditions, ACI Journal of Structures.

Fukuyama, H., Matsuzaki, Y., Nakano, K. and Sato, Y., 1999, Structural performance of beam elements with PVA-ECC, in Proc. of HPFRCC3, Mainz, Germany, (RILEM Publications S.A.R.L., 1999), pp 531-541.

Gao, S., 2005, Matrix Manipulation to Study ECC Behaviour, M. Sc. Thesis, University of Stellenbosch, South Africa.

Gao, S and Zijl, G. van, 2004, Tailoring ECC for commercial application, Department of Civil Engineering, University of Stellenbosch, South Africa, proceedings of BEFIB Como, Italy, pp. 1391-1400.

Gopalaratnam, V. S., and Shah, S, 1987, Failure Mechanisms and Fracture of Fibre Reinforced Concrete, Fibre Reinforced Concrete-Properties and Applications, SP-105, American Concrete Institute, Detroit, pp. 1-25.

Hodgkinson, J. M., 2000, Mechanical Testing of Advanced fibre Composites, Woodhead Publishing Ltd, Abington Hall, Abington Cambridge CB1 6ah, England.

Hognestad, E., 1952, What do we Known about Diagonal Tension and Web reinforcement in Concrete, University of Illinois Engineering Experiment Station, Circular Series, No. 64.

Iosipescu, N., 1967, Journal of Materials, 3, 537.

JCI-DFRCC Committee, 2002, JCI-DFRCC summary report on DFRCC terminologies and application concepts, Proceedings of the JCI International Workshop on Ductile Fiber Reinforced Cementitious Composites (DFRCC) - Application and Evaluation (DRFCC-2002), Takayama, Japan, Oct. 2002, pp. 59-66.

Kabele, P., 2003, New Developments in Analytical Modeling of Mechanical Behavior of ECC, Journal of Advanced Concrete Technology, 1(3), pp. 253-264.

Kabele, P., 2005, Fracture Behaviour of Shear-Critical Reinforced HPFRCC Members, Proceeding of the Workshop on HPFRCC in structural applications, Honolulu, Hawaii, USA,

Kanda, T., 1998, Design of Engineered Cementitious Composites for Ductile Seismic Resistant Elements, Ph.D. thesis, Michigan University, USA.

Kanda, T. and Li, V. C., 1998, Multiple Cracking Sequence and Saturation in Fiber Reinforced Cementitious Composites, Concrete Research and Technology, JCI, 9(2), pp. 19-33.

Kani, G. N.T., 1966, Basic Facts Concerning Shear Failure, Journal of the American Concrete Institute, 63, pp. 675-692.

Kesner, K.E., and Billington, S.L., 2001, Investigation of Ductile Cement-Based Composites for Seismic Strengthening and Retrofit, in Fractural Mechanics of Concrete Structures, de Bost et al(eds), A.A Balkema, Netherlands, pp. 65-72.

Kong, F. K. and Evans, R. H., 1987, Reinforced and Prestressed Concrete, Publish by Chapman and Hall, 2-6 Boundary Row, London SE1 8HN.

Lankard, D. R., 1984, Properties, Applications: Slurry Infiltrated Fibre concrete (SIFCON), Concrete International: Design and Construction, 61(12), pp. 44-47.

Li, V.C., 2002, Advances in ECC research, ACI Special Publication on Concrete: Material Science to Applications, SP 206-23, pp. 373-400.

Li, V.C., and Maalej, M. 1996, Toughening in cement based composites, Part II: Fiber Reinforced Cementitious Composites, J. of Cement and Concrete Composites, 18(4), pp. 239 – 249.

Li, V.C., Mishra, D.K., Naaman, A.E., Wigh, J.K., LaFave, J.M., Wu, H.C. and Inada, Y., 1994, On the shear behavior of engineered cementitious composites, J. of Advanced Cement Based Materials, 1(3), pp. 142-149.

Li, V. C., and Wang, S., 2002, Failure Mode and Structural Ductility of GFRP Reinforced Engineered Cementitious Composite Beams, ACI Materials J., 99(1), pp. 11-21.

Li, V.C., Ward, R., Hamza, A.M., 1992, ACI J. of Materials, 89 (5), pp. 499-508.

Lim, Y.M., and Li, V. C., 1997, Durable Repair of Aged Infrastructures Using Trapping Mechanism of Engineered Cementitious Composites Journal of Cement and Concrete Composites, 19(4), pp. 373-385.

Marshall, D.B and Cox. B.N., 1988, A J-integral method for calculating steady-state matrix crack stress in composite, Mechanics of materials, 7, pp. 127-133.

Morton, J., Ho, H., Tsai, M. and Farley, G. L., 1992, A Materials Shear Property Measurement, Journal of Composite Materials, 26.

Narayanan, R. and Darwish, I.Y.S., 1987, Use of Steel Fibers as Shear Reinforcement, ACI-JOURNAL, Proceedings, 69(10), pp. 216-226.

Nobuhiro, H., Isamu, Y., Hiroshi, T., and Sumio, H., 2005, Mechanical Behavior of Fiber Reinforced Concrete Element Subjected to Pure Shearing Stress, Proceeding of the Workshop on HPFRCC in structural applications, Honolulu, Hawaii, USA.

Parra-Montesinos, G. J., and Weight, J. K., 2000, Seismic Response of Exterior RC Column-to-Steel Beam Connections, ASCE J. Structural Engineering, pp. 1113-1121.

Paul, S.L., and Sinnamon, G.K., 1975, Concrete Tunnel Liners: Structural Testing of Segmented Liners, Final Report No. FRA-ORD-75-93, U.S. Department of Transportation/University of Illinois, Urbana.

Richards, G. L., Airhart, T. P., and Ashton, J.E., 1969, J. of Composite Materials, 3(7), 202.

Shah. SP., Kuder, K. G. and Mu, B., 2004, Fibre-reinforced cement-based composite: A forty year odyssey, corresponding paper in proceedings of BEFIB, pp. 3-30.

Shimizu, K., Kanakubo, T., Kanda, T. and Nagai, A., 2003, Experimental research of shear behavior of PVA-ECC beam element, in Proc. of JCI Symposium on Ductile Fiber Reinforced Cementitious Composites(in Japanese), Tokyo, (JCI, Tokyo, 2003), pp. 87-100.

Soroushian., Parviz and Lee, Cha-Don, 1990, Distribution and orientation of fibers in steel fiber reinforced concrete, ACI Materials Journal, 87(5), Sep-Oct 1990, pp. 433-532.

Sullivan, J.L., Kao, B.G and Van Oene, H., 1984, Shear properties and a stress analysis obtained from vinyl-ester Iosipescu specimen. Experimental Mechanics, 24(3), pp. 223-232.

Swamy, R. N., and Stavrides, H., 1979, Influence of Fibre Reinforcement on Restrained Shrinkage and Cracking, ACI JOURAL, 76(3), pp. 443-460.

Taylor, H. P. J., 1974, The fundamental behaviour of reinforced concrete beams in bending and shear. Proceedings ACI-ASCE Shear Symposium, Ottawa, American Concrete Institute, Detroit, pp. 43-77.

The ACI committee 544, 1988, Design Considerations for Steel Fibre Reinforced Concrete, American Concrete Institute, pp. 563-579.

Van Dyk,W.D., 2004, Development of thin fibre reinforced cementious plates and investigating influence of sand on ECC Behaviour, Final year BEng thesis, University of Stellenbosch, South Africa.

Vecchio, F., J. and Collins, M., P., 1986, The Modified Compression-Field Theory for Reinforced Concrete Elements Subjected to Shear, ACI Journal, 83(2).

Wall, J. D. and Card, M. F., 1971, Torsional Shear Strength of Filament-Wound Glass-Epoxy Tubes, Report NASA TN D-6140, NASA Lansearch Center, Hampton, VA.

Whitney, J. M., 1968, Application of the Plate Twist Test to Laminated Composites, Report AFML-TR-67-407, Air Force Materials Laboratory, Wright-Patterson Air Force Base.

Whitney, J. M., 1985, Composites Science and Technology, 22,167.

Walrath, D. E. and Adams, D. F., 1985, Iosipescu Shear Properties of Graphite Fabric/Epoxy Composite Laminates, University of Wyoming, Department Report UWME-DR-501-103-1.

Walrath, D.E. and Adams, D.F., 1981, Test Methods Development for 3-D cylindrical – Weave Carbon-Carbon Composite Materials, Report UWME-DR-104-104-1, Department of Mechanical Engineering, University of Wyoming, Laramie, Wyoming.